UNIVERSITY OF CALIFORNIA SAN DIEGO

The biological role and enzymatic source of extracellular reactive oxygen species in marine phytoplankton

A Dissertation submitted in partial satisfaction of the requirements
for the degree Doctor of Philosophy

in

Oceanography

by

Sydney Plummer

Committee in charge:

Professor Julia Diaz, Chair
Professor Andrew Allen
Professor Katherine Barbeau
Professor Jeff Bowman
Professor Sara Jackrel

2022

The Dissertation of Sydney Plummer is approved, and it is acceptable in quality and form for publication on microfilm and electronically.

University of California San Diego

2022

DEDICATION

This work is dedicated to my mentors and to the pursuit of excellence in mentorship.

TABLE OF CONTENTS

LIST OF FIGURES

LIST OF TABLES

LIST OF ABBREVIATIONS

ROS	reactive oxygen species
eROS	extracellular reactive oxygen species
eO_2^-	extracellular superoxide (O_2^-)
eH_2O_2	extracellular hydrogen peroxide (H_2O_2)
SOD	superoxide dismutase
MCLA	methyl *Cypridina* luciferin analog
DPI	diphenyl iodonium
DMSO	dimethyl sulfoxide

ACKNOWLEDGEMENTS

Chapter 1, in full, is a reprint of the material as it appears in Frontiers in Microbiology 2019, Plummer, Sydney; Taylor, Alexander E.; Harvey, Elizabeth L., Hansel, Colleen M.; Diaz, Julia M., Frontiers Media SA, 2019. The dissertation author was the primary investigator and author of this paper. The authors wish to thank Dee King for her assistance with literature searches and reference indexing, Dr. Patricia Yager and Dr. Brian Hopkinson for use of their labs, and Rachel Steffen for assistance in the lab.

Chapter 2 is currently being prepared for submission for publication of the material, Plummer, Sydney; Diaz, Julia M. The authors thank the Palenik lab, the Bowman lab, the Allen lab, and the Chisholm lab for supplying phytoplankton cultures. Allison Coe from the Chisholm lab is thanked for guidance in culturing *Prochlorococcus*. Susan Garcia is thanked for conducting initial growth and physiology experiments on *Prochlorococcus*. Finally, Whitney King is thanked for assisting in troubleshooting equipment.

Chapter 3 has been submitted for publication of the material as it may appear in Journal of Plankton Research, 2022, Plummer, Sydney; Holland, Alisia R.; Anderson, Sean R.; Duffy, Patrick I.; Diou-Cass Quintin P.; Bulski, Karrie; Bittar, Thais B.; Talmy, David; Harvey, Elizabeth L.; Diaz, Julia M., Oxford University Press, 2022. The dissertation author was the primary researcher and author of this paper. The authors thank the captain and crew of the *R/V Savannah* for facilitating research cruise sampling, thereby making the study possible.

VITA

2014	Bachelor of Arts in Biology, Valdosta State University
2014 – 2016	Undergraduate & Post-Baccalaureate Research Assistant, Valdosta State University
2016 – 2019	Graduate Research Assistant and National Science Foundation Graduate Research Fellow, University of Georgia – Skidaway Institute of Oceanography
2019 – 2022	Graduate Research Assistant, National Science Foundation Graduate Research Fellow, and UC President's Dissertation Year Fellow, University of California San Diego – Scripps Institution of Oceanography
2022	Doctor of Philosophy in Oceanography, University of California San Diego

PUBLICATIONS

Wangpraseurt, D., Sun, Y., You, S., Chua, S. T., Noel, S. K., Willard, H. F., Berry, D. B., Clifford, A. M., Plummer, S., Xiang, Y., Hwang, H. H., Kaandorp, J., Diaz, J. M., La Jeunesse, T. C., Pernice, M., Vignolini, S., Tresguerres, M., Chen, S. (2022). Bioprinted Living Coral Microenvironments Mimicking Coral-Algal Symbiosis. *Adv Funct Mater, n/a*(n/a), 2202273. doi:10.1002/adfm.202202273

Sutherland, K. M., Grabb, K. C., Karolewski, J. S., Plummer, S., Farfan, G. A., Wankel, S. D., Diaz, J. M., Lamborg. C. H., Hansel, C. M. (2020). Spatial heterogeneity in particle-associated, light-independent superoxide production within productive coastal waters. *J Geophys Res Oceans, 125*(10), e2020JC016747. doi:10.1029/2020JC016747

Sutherland, K. M., Coe, A., Gast, R. J., Plummer, S., Suffridge, C. P., Diaz, J. M., Bowman, J. S., Wankel, S. D., Hansel, C. M. (2019). Extracellular superoxide production by key microbes in the global ocean. *Limnology and Oceanography, 64*(6), 2679-2693. doi:10.1002/lno.11247

Plummer, S., Taylor, A. E., Harvey, E. L., Hansel, C. M., & Diaz, J. M. (2019). Dynamic regulation of extracellular superoxide production by the coccolithophore *Emiliania huxleyi* (CCMP 374). *Frontiers in Microbiology, 10*(1546), 1546. doi:10.3389/fmicb.2019.01546

Diaz, J. M., Plummer, S., Hansel, C. M., Andeer, P. F., Saito, M. A., & McIlvin, M. R. (2019). NADPH-dependent extracellular superoxide production is vital to photophysiology in the marine diatom *Thalassiosira oceanica*. *Proc Natl Acad Sci USA, 116*(33), 16448-16453. doi:10.1073/pnas.1821233116

Hansel, C. M., Diaz, J. M., & Plummer, S. (2019). Tight regulation of extracellular superoxide points to its vital role in the physiology of the globally relevant Roseobacter clade. *mBio, 10*(2), e02668-02618. doi:10.1128/mBio.02668-18

Diaz, J. M., Plummer, S., Tomas, C., & Alves-de-Souza, C. (2018). Production of extracellular superoxide and hydrogen peroxide by five marine species of harmful bloom-forming algae. *J Plankton Res, 40*(6), 667-677. doi:10.1093/plankt/fby043

Diaz, J. M., & Plummer, S. (2018). Production of extracellular reactive oxygen species by phytoplankton: past and future directions. *J Plankton Res, 40*(6), 655-666. doi:10.1093/plankt/fby039

Manning, T., Plummer, S., Woods, R., Wylie, G., Phillips, D., & Krajewski, L. (2017). Cell line studies and analytical measurements of three paclitaxel complex variations. *Bioorg Med Chem Lett, 27*(12), 2793-2799. doi:https://doi.org/10.1016/j.bmcl.2017.04.070

Plummer, S., Manning, T., Baker, T., McGreggor, T., Patel, M., Wylie, G., & Phillips, D. (2016). Isolation, analytical measurements, and cell line studies of the iron–bryostatin-1 complex. *Bioorg Med Chem Lett, 26*(10), 2489-2497. doi:https://doi.org/10.1016/j.bmcl.2016.03.099

Manning, T., Plummer, S., Baker, T., Wylie, G., Clingenpeel, A. C., & Phillips, D. (2015). Development of a three component complex to increase isoniazid efficacy against isoniazid resistant and nonresistant Mycobacterium tuberculosis. *Bioorg Med Chem Lett, 25*(20), 4621-4627. doi:10.1016/j.bmcl.2015.08.046.

ABSTRACT OF THE DISSERTATION

The biological role and enzymatic source of extracellular reactive oxygen species in marine phytoplankton

by

Sydney Plummer

Doctor of Philosophy in Oceanography

University of California San Diego, 2022

Professor Julia Diaz, Chair

Within the marine environment, reactive oxygen species (ROS) are abundant and participate in geochemical reactions that shape the fate and availability of metals, carbon, and oxygen due to their reactive nature. Phytoplankton are major sources of the ROS superoxide (O_2^-) and hydrogen peroxide (H_2O_2). Indeed, by exporting electrons to surrounding oxygen via enzymes, phytoplankton generate extracellular O_2^- (eO_2^-) which can then dismutate to

extracellular H_2O_2 (eH_2O_2). ROS are commonly associated with stress; however, they also serve beneficial biological functions. Despite the environmental importance of eROS, their enzymatic source and ecophysiological role in phytoplankton has remained mysterious. In phytoplankton, several biological functions have been proposed for eROS production, yet a consensus has not been reached. Additionally, a class of enzymes that catalyzes electron transfers called flavoenzymes mediates production of eROS in many organisms. However, pathways of eROS production by phytoplankton are poorly understood. Here, I interrogate the ecophysiological role(s) of eROS production and its enzymatic source in a diversity of phytoplankton in laboratory and field settings. In Chapter I, results demonstrate that eO_2^- production is stress-independent and dynamically regulated as a function of cell abundance and growth phase consistent with a signaling role, as well as light availability in the globally-relevant coccolithophore *E. huxleyi*. Chapter II reveals that eO_2^- production is light-driven, regulated by flavoenzymes, and promotes health by serving a photoprotective role in many phytoplankton. Further, results support my hypothesis that many phytoplankton form eO_2^- to dissipate excess energy from light stress. Also, I estimate that light-driven eO_2^- production by phytoplankton will increase in future ocean conditions where mixing layer light levels are predicted to increase due to climate change. In Chapter III, field results demonstrate that eH_2O_2 production is dynamically regulated consistent with a signaling role and influences phytoplankton growth and microzooplankton grazing. Indeed, eH_2O_2 production, phytoplankton growth, and grazing were inversely correlated. Moreover, incubations show that increasing eH_2O_2 production decreases phytoplankton growth and grazing. Overall, my work helps illuminate the ecophysiological role and enzymatic source of eROS production by phytoplankton, thereby advancing understanding of biogeochemical cycling, redox states, plankton web dynamics, and health of current and future oceans.

INTRODUCTION

Reactive oxygen species (ROS) are intermediates in the reduction of molecular oxygen to water. These species include superoxide (O_2^-), which is generated by the single electron reduction of molecular oxygen. Superoxide is further reduced to hydrogen peroxide (H_2O_2), and finally the hydroxyl radical (•OH). In aerobic organisms, ROS are inevitably produced as metabolic byproducts. Their overproduction and accumulation can lead to oxidative stress and damage to biomolecules; however, ROS also serve beneficial functions. Indeed, ROS serve a range of functions from growth promotion to innate immunity across biological systems from bacteria to humans (Aguirre and Lambeth, 2010, Hansel et al., 2019, Weinberger, 2007, Hansel and Diaz, 2021). Thus, a balance between ROS and antioxidant production must be maintained (Mittler, 2017).

ROS are present everywhere in aquatic systems. Indeed, ROS measurements have been conducted across the globe in freshwater, brackish, and marine waters ranging from inland lakes to open ocean sites (Roe et al., 2016, Vermilyea et al., 2010a, Vermilyea et al., 2010b, Rose et al., 2008, Zhang et al., 2016b). These efforts have revealed that H_2O_2 has a typical half-life of hours to days with concentrations typically in the nanomolar range and sometimes reaching micromolar (10^{-9} – 10^{-6} M) in aquatic environments. On the other hand, O_2^- has a shorter half-life of seconds to minutes with concentrations being ~ 1000-fold lower (10^{-12} – 10^{-9} M) (Zinser, 2018, Diaz and Plummer, 2018). In these aquatic systems, ROS help drive biogeochemical cycling of both toxic (e.g., mercury) (Siciliano et al., 2002) and nutrient metals (e.g., iron, manganese) (Wuttig et al., 2013, Rose, 2012), oxygen (Sutherland et al., 2020), and carbon (Heller and Croot, 2010b) due to their ability to act as oxidants and reductants.

Aquatic ROS originate from abiotic processes and directly from organisms. For example, abiotic processes include photochemical production of ROS. Photochemical ROS production begins with the excitation of chromophoric dissolved organic matter (CDOM), which reduces molecular oxygen to form O_2^-. Additionally, ROS can result from reactions with reduced or oxidized metals including manganese, iron, and copper (Zinser, 2018). More recently, biologically-derived ROS have been recognized as a significant source of marine ROS pools and can even dominate abiotic sources (Rose et al., 2008, Cory et al., 2016, Dixon et al., 2013, Hansard et al., 2010). Biological sources of ROS include both active and passive microbial processes. For instance, intracellular O_2^- can be released upon lysis of planktonic cells (passive), however, these rates cannot account for the steady state concentrations that have been measured in natural waters (Rose, 2012, Hansard et al., 2010). Additionally, O_2^- cannot readily cross intact biological membranes due to its negative charge, short intracellular lifetime (μsec), and limited diffusive distance (~100s nm) (Lesser, 2006, Brown and Griendling, 2009, Diaz and Plummer, 2018). Therefore, intracellular processes are not a direct source of biologically derived O_2^- in natural waters, and extracellular production must be involved (Diaz and Plummer, 2018). Indeed, enzymatically-driven extracellular O_2^- (eO_2^-) production by microbes (active) contributes the majority of biologically derived O_2^- concentrations in natural waters (Rose, 2012).

The ability to produce extracellular ROS (eROS) has been documented among heterotrophic bacteria (Diaz et al., 2013) and phytoplankton, including cyanobacteria, diatoms, dinoflagellates, nontoxic phytoplankton, and harmful phytoplankton (Diaz and Plummer, 2018, Sutherland et al., 2019). Despite advancements in identifying the extensive presence and environmental relevance of eROS production by marine microorganisms, the mechanisms of production as well as its biological roles are not well understood. A number of functions have

been proposed for eROS production ranging from interactions with other microbes to baseline physiological functioning (Hansel and Diaz, 2021). Production of eROS may be involved in antagonistic biological interactions such as ichthyotoxicity in harmful algal bloom (HAB)-forming species, predatory grazing, and/or bacterial allelopathy (Hansel and Diaz, 2021). For instance, much research has focused on the role of eROS production in ichthyotoxicity of HAB species. Many cases support this eROS production as having a synergistic or indirect effect with organic toxins, rather than the eROS directly causing damage themselves (Diaz and Plummer, 2018). Also, eROS may be involved in phytoplankton predator-prey interactions (Martel, 2009, Flores et al., 2012), similar to the oxidative bursts observed in macroalgae that deter grazers (McDowell et al., 2016, McDowell et al., 2014). Production of eO_2^- has also been implicated as a means to acquire metal nutrients such as iron (Rose, 2012). O_2^- can both oxidize and reduce iron, thereby potentially changing its bioavailability to phytoplankton; however, eO_2^--mediated iron uptake among phytoplankton species appears inconsistent (Middlemiss et al., 2001, Rose et al., 2005, Roe and Barbeau, 2014, Fujii et al., 2010, Garg et al., 2007, Liu et al., 2007, Kustka et al., 2005). Production of eROS may be important for processes essential in phytoplankton baseline physiology rather than being exclusively associated with stress (Diaz and Plummer, 2018). From bacteria to humans, eROS can act as a signaling molecule that regulates cell development (Hansel et al., 2019, Aguirre and Lambeth, 2010, Bhattacharjee, 2012, Mittler et al., 2011). In fact, the presence of eROS is essential for normal development in at least one species of phytoplankton (Oda et al., 1995). Also, eROS may serve as an autocrine growth promoter in other phytoplankton species as well. Alternatively, eROS production may indirectly affect growth or overall health of phytoplankton. For example, light stimulates eO_2^- production in several phytoplankton (Hansel et al., 2016, Kim et al., 2000, Saragosti et al., 2010, Schneider et

al., 2016, Milne et al., 2009, Marshall et al., 2002, Yuasa et al., 2020a, Plummer et al., 2019, Diaz et al., 2019), suggesting a possible connection to photophysiological processes such as photosynthesis. Overall, eROS production may not only be part of, but *necessary* for, normal physiological functioning and vitality in phytoplankton.

Clarifying the cellular mechanisms and biological function of eROS production by phytoplankton is critical to understand the effects of ROS on ocean redox balance and biogeochemical cycling in marine waters. Furthermore, given the potential effects eROS can have on phytoplankton physiology (e.g., growth promotion) and ecological interactions among various trophic levels (e.g., allelopathy, defense), these reactive species can impact health and functioning of marine microbial communities, and thereby the ecosystem services they provide. Thus, the goal of my PhD research is to illuminate the ecophysiological role(s) and enzymatic source of eROS production by marine phytoplankton.

ROS are commonly associated with stress; however I demonstrate that production of eROS is *beneficial* for normal physiological functioning and vitality in phytoplankton. Specifically in Chapter I, I characterized patterns of eO_2^- production and its physiological effects on the globally relevant phytoplankton species, *Emiliania huxleyi*. Through this work, I found that eROS influences growth and overall health of *E. huxleyi*. Further, I discovered that production of eO_2^- by *E. huxleyi* is stress-independent, tightly regulated as a function of cell abundance and light, and critically tied to its photosynthetic lifestyle (Plummer et al., 2019).

Based on results of Chapter I and other research (Diaz et al., 2019), in Chapter II I investigated whether photosynthetic processes and a certain group of enzymes called flavoenzymes regulate eO_2^- production as a mechanism to prevent damage by excess light (i.e.,

photoprotection) among several model phytoplankton. By applying established mathematical models of photosynthesis, I show that eO_2^- production is driven by light and photosynthesis in all species tested. Further, application of the flavoenzyme inhibitor DPI shows that flavoenzymes are essential for eO_2^- production in most phytoplankton tested. Moreover, blocking eO_2^- production with these flavoenzyme inhibitors is catastrophic for photosynthetic health and vitality in most phytoplankton. These findings support the hypothesis that eO_2^- production is photosynthetically driven and benefits phytoplankton physiology through a photoprotective mechanism. Moreover, flavoenzymes are not only involved in eO_2^- production but are critical to the photosynthetic health and functioning of diverse phytoplankton. In future oceans, mixing layer depths are predicted to change, where shallowing of the mixed layer depth would trap phytoplankton in surface layers thereby exposing phytoplankton to higher light levels (Gao et al., 2012). Because eO_2^- production is light-dependent, future eO_2^- production may also shift. Therefore, I estimated eO_2^- production rates in future conditions of the North Pacific Gyre and found that eO_2^- production rates will increase in the future, potentially impacting ROS driven biogeochemical cycling.

Once eO_2^- forms in the proposed photoprotective mechanism discussed in Chapter II, it may go on to elicit biological responses as a signaling molecule, either as eO_2^- or perhaps its more stable product extracellular H_2O_2 (eH_2O_2). In fact, eROS are well known signaling molecules in many organisms (Sies and Jones, 2020, Gough and Cotter, 2011, Mittler et al., 2011) and have been proposed to serve as signals in addition to other biological functions in phytoplankton (Hansel and Diaz, 2021). Production of eROS may influence phytoplankton growth and ecological interactions (see above) possibly through signaling pathways. Therefore, Chapter III investigates whether eROS influence phytoplankton growth and microzooplankton

grazing in natural plankton communities of the South Atlantic Bight. Our results reveal that biological eH_2O_2 production is dynamically regulated, and therefore corroborates the view of eH_2O_2 acting as a signal in phytoplankton. Further, biological eH_2O_2 production was inversely correlated with phytoplankton growth rates and microzooplankton grazing rates. Consistent with in situ observations, ROS-manipulated field incubations demonstrate that eH_2O_2 production decreases phytoplankton growth and microzooplankton grazing rates. Overall, Chapter III shows that eROS may control phytoplankton populations through bottom-up (i.e., growth) and top-down processes (i.e., grazing), thereby directly shaping health and functioning of marine microbial communities.

CHAPTER 1: DYNAMIC REGULATION OF EXTRACELLULAR SUPEROXIDE PRODUCTION BY THE COCCOLITHOPHORE *EMILIANIA HUXLEYI* (CCMP 374)

Abstract

In marine waters, ubiquitous reactive oxygen species (ROS) drive biogeochemical cycling of metals and carbon. Marine phytoplankton produce the ROS superoxide (O_2^-) extracellularly and can be a dominant source of O_2^- in natural aquatic systems. However, the cellular regulation, biological functioning, and broader ecological impacts of extracellular O_2^- production by marine phytoplankton remain mysterious. Here, we explored the regulation and potential roles of extracellular O_2^- production by a noncalcifying strain of the cosmopolitan coccolithophorid *Emiliania huxleyi*, a key species of marine phytoplankton that has not been examined for extracellular O_2^- production previously. Cell-normalized extracellular O_2^- production was highest under presumably low-stress conditions during active proliferation and inversely related to cell density during exponential phase. Removal of extracellular O_2^- through addition of the O_2^- scavenger superoxide dismutase (SOD), however, increased growth rates, growth yields, cell biovolume, and photosynthetic efficiency (F_v/F_m) indicating an overall physiological improvement. Thus, presence of extracellular O_2^- does not directly stimulate *E. huxleyi* proliferation, as previously suggested for other phytoplankton, bacteria, fungi, and protists. Extracellular O_2^- production decreased in the dark, suggesting a connection with photosynthetic processes. Taken together, the tight regulation of this stress independent production of extracellular O_2^- by *E. huxleyi* suggests that it could be involved in fundamental photophysiological processes.

Introduction

Ubiquitous reactive oxygen species (ROS) within marine waters help drive global biogeochemical cycling. ROS include intermediates in the reduction of molecular oxygen (O_2) to water (H_2O), which consist of superoxide (O_2^-), hydrogen peroxide (H_2O_2), and hydroxyl radical (OH•). These ROS shape the transformation of metal nutrients including iron (Rose, 2012) and manganese (Wuttig et al., 2013), as well as carbon (Heller and Croot, 2010b) due to their ability to act as both oxidants and reductants. Within aquatic environments, ROS are produced through both abiotic (e.g., via photodegradation of organic matter) and biotic means (Zinser, 2018). Biotic mechanisms include active extracellular production by marine microorganisms, which can be a dominant source of O_2^- in natural waters (Rose et al., 2008, Hansard et al., 2010).

While ROS are formed intracellularly within all aerobic organisms as metabolic by-products, a plethora of marine microorganisms actively produce ROS extracellularly as well. Although intracellular O_2^- can be released into the marine environment upon cell lysis, these rates cannot account for the steady-state concentrations that have been measured in natural waters (Rose, 2012). Furthermore, within cells, O_2^- exists in equilibrium with its conjugate acid, the hydroperoxyl radical (HOO•), however, with a pK_a of 4.8 the O_2^- anion is the dominant form at physiological pH (Bielski et al., 1985). Unlike H_2O_2, O_2^- cannot readily diffuse across membranes due to its negative charge, short lifetime (~10^{-5} s), and limited diffusive distance (~10^{-7} m) (Lesser, 2006, Brown and Griendling, 2009, Diaz and Plummer, 2018). Thus, the majority of microbially-derived O_2^- within the extracellular environment must be created on or near the cell surface via active extracellular O_2^- production mechanisms (Diaz and Plummer, 2018).

The ability to produce extracellular O_2^- has been documented among heterotrophic bacteria (Diaz et al., 2013) and phytoplankton, including cyanobacteria (Hansel et al., 2016, Godrant et al., 2009, Rose et al., 2008, Rose et al., 2005), diatoms (Schneider et al., 2016, Kustka et al., 2005, Hansel et al., 2016), dinoflagellates (Saragosti et al., 2010, Zhang et al., 2016a), nontoxic microalgae (Marshall et al., 2005a), and harmful microalgae (Oda et al., 1997, Portune et al., 2010, Marshall et al., 2005b, Marshall et al., 2005a, Diaz and Plummer, 2018). Despite advancements in identifying the extensive presence and environmental relevance of extracellular O_2^- production by marine microflora, the mechanisms of extracellular O_2^- production and its biological roles are not well understood. The freshwater chlorophyte *Chlamydomonas reinhardtii* (Anderson et al., 2016) and marine raphidophytes *Chattonella marina* and *Chattonella ovata* (Kim et al., 2007, Kim et al., 2000) are either confirmed or thought to produce extracellular O_2^- via cell membrane associated enzymes known as NADPH oxidases (Nox). These enzymes transfer electrons from cytosolic NADPH pools across cell membranes to reduce O_2 in the surrounding aqueous environment, thus creating extracellular O_2^-. The presence of these enzymes has been implicated in diatoms and dinoflagellates as well (Saragosti et al., 2010, Kustka et al., 2005, Kim et al., 2000, Hervé et al., 2006). Extracellular O_2^- production is light dependent in several phytoplankton taxa (Milne et al., 2009, Schneider et al., 2016, Hansel et al., 2016, Kim et al., 1999, Marshall et al., 2002, Saragosti et al., 2010), which has led to speculation that photosynthesis may serve an indirect role in extracellular O_2^- production by supplying NADPH to cell surface-associated NADPH-oxidizing enzymes such as Nox (Saragosti et al., 2010, Schneider et al., 2016, Marshall et al., 2002).

Proposed biological roles of phytoplankton-derived extracellular O_2^- are diverse (Diaz and Plummer, 2018). For instance, extracellular O_2^- production has been implicated in harmful

algal bloom toxicity (Marshall et al., 2003, Kim and Oda, 2010, Mardones et al., 2015, Tanaka et al., 1992, Dorantes-Aranda et al., 2013, Kim et al., 1999, Yang et al., 1995, Dorantes-Aranda et al., 2015), metal nutrient acquisition (Rose, 2012, Rose et al., 2005, Roe and Barbeau, 2014, Garg et al., 2007, Liu et al., 2007), allelopathy(Oda et al., 1992, Oda et al., 1997, Marshall et al., 2005b), and defense against grazing (Flores et al., 2012, Martel, 2009). Model phytoplankton species generate abundant extracellular O_2^- even under ideal growth conditions in the absence of any obvious stressors (Diaz et al., 2013, Hansel et al., 2016, Godrant et al., 2009, Rose et al., 2005, Kustka et al., 2005, Schneider et al., 2016, Marshall et al., 2005a, Marshall et al., 2005b, Portune et al., 2010), suggesting an association with basal functioning. For example, extracellular O_2^- regulates growth and morphology in the prolific ROS producer, *C. marina* (Oda et al., 1995), as well as growth in bacteria (Saran, 2003, Hansel et al., 2019) and differentiation in microbial eukaryotes (Aguirre et al., 2005). In these microorganisms, extracellular O_2^- production rates are highest during active growth and at low cell densities consistent with beneficial cell signaling and autocrine growth regulation, as also seen in plants (Mittler et al., 2011) and animals (Brown and Griendling, 2009, Aguirre and Lambeth, 2010). The accumulation of studies showing that extracellular O_2^- production by diverse phytoplankton is similarly dependent on cell density (Marshall et al., 2005a, Diaz et al., 2018, Hansel et al., 2016) and growth phase (Oda et al., 1995, Portune et al., 2010, Kim et al., 1999) has spurred speculation that extracellular O_2^- production may be involved in phytoplankton cell signaling and/or growth regulation in species other than *C. marina*, although this possibility remains largely untested (Hansel et al., 2016, Diaz and Plummer, 2018).

Clarifying the cellular regulation and biological function of active extracellular O_2^- production by phytoplankton is critical to understanding the effects of ROS on ocean redox

balance, biogeochemical cycling, and ecological interactions in marine waters. Among phytoplankton, coccolithophores are one of the most prevalent groups in the global ocean. Further, the original report of extracellular H_2O_2 production by the coccolithophorid species *Pleurochrysis carterae* pioneered the recognition of microorganisms as significant sources of ROS in aquatic systems (Palenik et al., 1987). Despite this discovery, however, coccolithophorids are understudied in terms of extracellular ROS production. Therefore, this study was conducted to investigate the dynamics, cellular regulation, and biological function of extracellular O_2^- production by a noncalcifying strain of *Emiliania huxleyi* (CCMP 374), the most prevalent coccolithophore species in modern oceans (Westbroek et al., 1989, Brown and Yoder, 1994).

Materials and Methods

Cultivation of *E. huxleyi*, growth tracking, and cell counts

Axenic cultures of *E. huxleyi* CCMP 374 were obtained from the National Center for Marine Algae and Microbiota (NCMA) at Bigelow Laboratory for Ocean Sciences (East Boothbay, ME). Cultures of *E. huxleyi* were inoculated into f/2 growth media prepared without the addition of silicic acid (Guillard and Ryther, 1962) using 0.2 μm filtered natural seawater collected from the South Atlantic Bight. Media were prepared and autoclaved (121°C, 20 min) at least one day prior to inoculating cultures. Cultures were begun with exponential phase inocula, unless otherwise stated. Cultures were either grown in borosilicate culture tubes with caps or Erlenmeyer flasks of various sizes with aluminum foil or an acid washed plastic beaker covering the mouth of the flask at 18°C under cool, white light (~130 μmol photons m^{-2} s^{-1}, 14:10 light dark cycle). Growth was monitored by observing *in vivo* chlorophyll fluorescence using an AquaFluor® handheld fluorometer (Turner Designs, San Jose, CA) or a 10-AU™ fluorometer

(Turner Designs, San Jose, CA). *In vivo* fluorescence values were normalized to measurements taken on day 0. Exponential growth phase was defined as the log-linear portion of the *in vivo* fluorescence data versus time ($R^2 \geq 0.98$ in all cultures). Stationary phase was determined to be the time between the end of the log linear portion of the growth curve and until the end of the growth curve. Specific growth rates during exponential growth phase were found by calculating the slope of the regression of the natural log-normalized *in vivo* fluorescence versus time. Culture pH was monitored using an Accumet AB 15/15+ pH meter (Thermo Fisher Scientific, Waltham, MA) in cultures grown from stationary phase inocula in 25 mm borosilicate tubes (Thermo Fisher Scientific, 14-961-34). *E. huxleyi* cell abundances (cells mL^{-1}) were obtained using a Guava® easyCyte flow cytometer (Millipore Sigma, Merck KGaA, Dermstadt, Germany) and analyzed with Guava InCyte™ 3.1 software. Flow cytometry samples were preserved with a final concentration of 0.5% glutaraldehyde, as well as 1% peptone to prevent cell adsorption to sample tubes. Flow cytometry samples were stored at -80°C prior to processing. To process samples, 50-200 μL of each sample was pipetted into 96-well plates, diluted with filtered seawater as needed, and run at a low flow rate (0.24 μL s^{-1}) for 3 min. For analysis, concentrations of healthy cell populations (cells mL^{-1}) were determined based on gates of red fluorescence and forward scatter signals from previously run samples of exponentially growing cultures.

In two separate experiments, extracellular O_2^- was removed from *E. huxleyi* cultures by adding superoxide dismutase (SOD, Millipore Sigma 574594-50KU), an enzyme that specifically degrades O_2^-. To begin this experiment, 7.5 mL of media were inoculated with 300 μL stationary phase culture to give an initial concentration of ~ 2.3×10^5 cells mL^{-1} and grown under the conditions above in 13 mm borosilicate glass tubes (Thermo Fisher Scientific, 14-962-

26D). Treatments included three different concentrations of SOD added at three different volumes and a deionized water (DI) control. A 10 kU mL^{-1} stock of SOD was prepared using DI. Then, treatments were performed on triplicate cultures, where each tube received daily additions of 20.25 µL, 37.5 µL, or 75 µL of the 10 kU mL^{-1} SOD stock, or 75 µL DI to give final concentrations of 27 U mL^{-1} SOD, 50 U mL^{-1} SOD, 100 U mL^{-1} SOD, or 0 U mL^{-1} SOD, respectively. A subsequent control experiment was performed with diafiltered SOD to ensure that SOD was responsible for potential changes observed in the cultures. For this control experiment, 7.5 mL of media were inoculated with 300 µL stationary phase culture to give an initial concentration of ~1.8×10^5 cells mL^{-1} and grown under the conditions above in 13 mm borosilicate glass tubes. To create the dialyzed SOD, a 10 kU mL^{-1} SOD stock prepared with DI was diafiltered by passing the SOD solution through an Amicon ultrafiltration device (10 kDa molecular weight cut-off, Millipore) at 3200 × g for 20 minutes at 4ºC, thereby removing the enzyme from the solution. Treatments were performed on triplicate cultures, where each tube received daily additions of 75 µL dialyzed SOD, 75 µL DI, and 75 µL SOD (100 U mL^{-1} SOD final concentration).

Cell imaging and analysis

Individual *E. huxleyi* cells were imaged using a FlowCam® (Fluid Imaging Inc., Scarborough, ME), a continuous flow-through microscope fitted with a color and monochromatic camera. To calibrate the FlowCam® for imaging, dilutions of *E. huxleyi* cultures from 0% to 95% using 0.2 µm filtered seawater were analyzed in varying context settings. Final settings (Table 1.1) were chosen based on their ability to differentiate cell shape and color and provide useable images for morphological and volume assessments. Culture samples of 100 µL

were diluted with 500 µL of 0.2 µm filtered seawater prior to analysis on the FlowCam®. Images were analyzed with VisualSpreadsheet® (Fluid Imaging Inc., Scarborough, ME).

To filter out all non-*E. huxleyi* particles, two universal sort functions were applied to every sample. First, each sample was sorted for filled pixel area. The area of the smallest and largest *E. huxleyi* cell in each sample was noted. Then, each sample was sorted for Hu Circularity. Hu Circularity assigns a value from 0 to 1 for how well the edge trace of the particle fits a perfect circle (Žunić et al., 2010). Since *E. huxleyi* is spherical and appears circular in two dimensions, this was deemed an effective method for removing pieces of contaminants such as transparent exopolymer particles (TEP). The value of the lowest and highest *E. huxleyi* Hu Circularity in each sample was noted. Then, each sample was filtered for these two parameters (i.e., filled pixel area, Hu Circularity). Particles that did not fit the parameters were binned and not included in further analysis. The sample was then scanned visually for extraneous particles and any found were removed.

Biovolume was calculated with 3 different measurements of cell diameter: Area Based Diameter (ABD), Filled or Full Diameter (FD), and Equivalent Spherical Diameter (ESD). ABD is found by measuring the number of pixels within a circular-traced cell, determining the area of the cell from the measured number of pixels, and finding diameter from this calculated area. ESD is calculated by taking the average value of 36 feret measurements, where a feret measurement is the distance between two parallel lines touching either side of the cell. FD is the diameter determined from a cell that has an area equal to the maximum filled intracellular area.

Table 1.1: FlowCam® context parameters for *E. huxleyi* imaging

FlowCam® Context Parameter	Setting
Objective	20x Olympus
Collimator	10x/20x Collimator Installed
Sample Volume	500 µL
Flow Rate	0.02 mL min^{-1}
Dilution	0.2
Distance Between Cells	0 µm
Filter	Use equivalent spherical diameter (ESD), from 2 µm to 20 µm.
Laser	Enable
Channel 1 and 2	ON, threshold 400, measure ON
Scatter	ON, measure
Fluorescence Scale	Linear
Sample Width	4
Flash Duration	100 µsec
Flash Delay	1 µsec

Photophysiology

Photophysiological health of *E. huxleyi* was monitored using the Satlantic fluorescence induction and relaxation (FIRe) fluorometer system (Sea-bird Scientific, Halifax, NS Canada). Prior to analysis, samples were allowed to dark adapt for approximately 30 minutes and were then diluted using 0.2 µm filtered seawater as necessary to avoid detector saturation. Samples were illuminated with a single turnover flash of blue excitation for a duration of 80 µsec. The measured fluorescence response was used to calculate the maximum efficiency of photosystem II (PSII), or F_v/F_m, using the equation:

$$F_v/F_m = \frac{(F_m - F_o)}{F_m}$$

where F_m is the maximum fluorescence yield, and F_o is the minimum fluorescence yield. For each sample, 20 acquisitions were obtained.

Extracellular O_2^- production

Net extracellular O_2^- production by *E. huxleyi* was measured using the flow-through FeLume (II) analytical system (Waterville Analytical, Waterville, ME) by detecting chemiluminescence emitted through the reaction of O_2^- and the specific probe methyl *Cypridina* luciferin analog (MCLA), as previously described (Diaz et al., 2013, Schneider et al., 2016). This method allows for manipulation of experimental settings (e.g., light levels, increasing cell density) during analysis to detect changes in O_2^- on immediate timescales (i.e., seconds). It has been used to measure O_2^- production in pure cultures (Kustka et al., 2005, Schneider et al., 2016, Diaz et al., 2013, Hansel et al., 2019, Zhang et al., 2016a) and natural waters (Hansel et al., 2016, Zhang et al., 2016b, Diaz et al., 2016). Following the procedures of Diaz et al. (2013), MCLA blanks generated in the absence of SOD were used to determine biologically-derived O_2^- concentrations, in order to avoid overestimation of biological O_2^- production rates due to MCLA

auto-oxidation. Briefly, cells were deposited onto an inline filter (0.22 μm), continuously rinsed (2 mL min^{-1}) with a phosphate buffer (20 mM; pH = 7.6) that matched the salinity of the seawater media base (38 psu), and O_2^- was quantified in the cell-free effluent upon reaction with the MCLA reagent (4 μM MCLA, 0.1 M MES, 75μM diethylenetriamine pentaacetic acid [DTPA], pH = 6) in a spiral flow cell adjacent to a photomultiplier tube. Chemiluminescent signals from the phosphate buffer and MCLA baselines as well as biological samples were allowed to stabilize (≤ 4% CV) for at least 1 minute, allowing calculation of a steady-state O_2^- concentration. In this way, obtaining a stable chemiluminescent signal from the MCLA reacting with effluent from biological samples demonstrated that the O_2^- being detected was not a rapid, short-lived release of intracellular O_2^- due to cell rupture. SOD was added at the end of each analysis (final concentration of ~ 800 U L^{-1}) to confirm the signal acquired on the FeLume (II) system was due to O_2^-. In comparison to the aforementioned study by Diaz et al. (2013), the following exceptions were implemented here. First, cells deposited on the filter were exposed to ambient light (~ 5 μmol photons m^{-2} s^{-1}) unless they were covered in a dark photography film-changing bag to obtain dark (0 μmol photons m^{-2} s^{-1}) measurements, as indicated. Second, only net production rates were determined, and finally, calibration was performed using standard additions of potassium superoxide (KO_2) by the method of Schneider et al. (2016). A preliminary cell concentration was obtained by microscopy using a hemocytometer counting chamber to help ensure that the same number of cells were loaded onto the in-line filter from each biological replicate and on each day within an experiment. The biotic steady-state O_2^- concentration was calculated by subtracting blank signals generated from the mixture of MCLA and phosphate buffer with a syringe filter inline and in the absence of SOD. Then, net O_2^- production rates were calculated by multiplying the biotic steady-state O_2^-concentration (pM) by the flow rate (2 mL

min^{-1}), dividing that value by the number of cells loaded onto the inline filter (either found using microscopy or flow cytometry), and converting to final units of amol $cell^{-1}$ hr^{-1}. All chemicals used to measure O_2^- were obtained from Millipore Sigma, except for MCLA, which was obtained from Tokyo Chemical Industry Co., Ltd.

Statistical analyses

All statistical analyses were performed using JMP Pro 13.0.0 (SAS Institute Inc., Cary, NC). Regression analyses of cell-normalized O_2^- production rates as a function of time across the growth curve of *E. huxleyi* and cell density were performed using Spearman's rank-order correlation. This regression analysis indicates presence or absence of monotonic relationships based on the correlation coefficient (ρ) and its p-value. An independent two sample student's t-test was used to determine potential differences between mean F_v/F_m values measured on various days throughout the growth curve of *E. huxleyi*. To determine the effect of SOD additions on *in vivo* fluorescence, a mixed factor repeated measures ANOVA was used. To determine the effect of dilution on per-cell O_2^- production and the effect of SOD addition on growth rates, cell abundances, cell biovolume, and F_v/F_m values, a comparison of means using an independent two sample student's t-test was employed for each parameter interrogated. A one-sample student's t-test was used to determine the potential difference between *E. huxleyi* O_2^- production in the presence and absence of light. For all statistical analyses, the significance threshold (alpha) was set to 0.05.

Results

Extracellular O_2^- production as a function of growth phase

To assess per-cell extracellular O_2^- modulation across different average metabolic states, cell-normalized extracellular O_2^- production by *E. huxleyi* was measured throughout the growth

curve of batch cultures. To rule out potential cell density effects, the number of cells analyzed at each timepoint was kept constant (average ± SE was $8.32 \times 10^5 \pm 5.98 \times 10^4$ cells (n = 30)). The highest per-cell net extracellular O_2^- production rates were observed during early exponential growth when F_v/F_m values were highest (Figure 1.1) and significantly declined as *E. huxleyi* grew over time (Spearman's $\rho = -0.58$; $p < 0.0001$) (Figure 1.2). For example, *E. huxleyi* produced maximum amounts of O_2^- (average ± SE) at the first time point measured in early exponential phase (4478 ± 611 amol $cell^{-1}$ hr^{-1}, n=3; day 2). These maximal rates were nearly 78 times higher than net production rates measured between day 8 and day 25, when average production declined to 58 ± 55 amol $cell^{-1}$ hr^{-1} (n = 30). Flow cytometry analyses revealed this decline was not due to an increase in senescent cells (i.e., cells with low chlorophyll). After day 8, net cell-normalized O_2^- production rates were occasionally negative, fluctuating between -253 ± 167 (day 22; n = 3) and 209 ± 360 (day 17; n = 3). Net per-cell O_2^- production rates account for the simultaneous production and decay of O_2^- at the cell surface. Because auto-oxidation of the MCLA probe results in a small amount of O_2^- production (Fujimori et al., 1993), the negative net per-cell O_2^- production rates between day 8 and day 25 reflect degradation of O_2^- originating from the MCLA reagent.

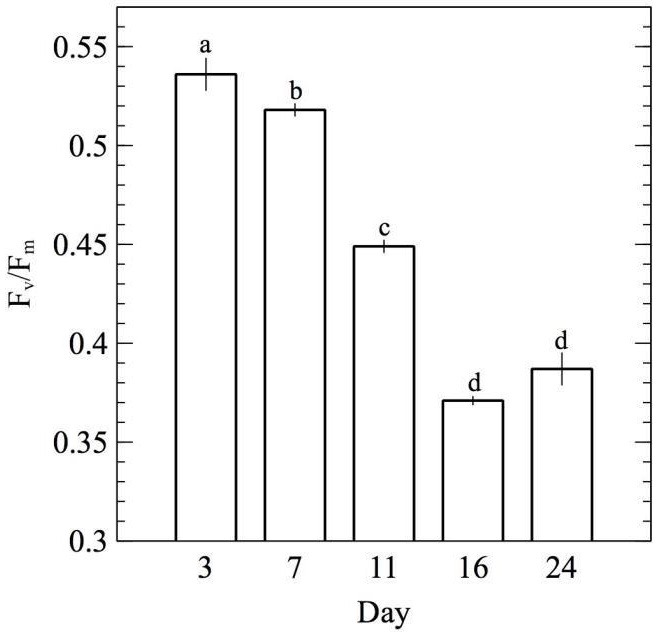

Figure 1.1: Fv/Fm values measured at various points along the growth curve of *E. huxleyi*. Significant differences (comparison of the means, two sample student's t-test) between average Fv/Fm values on each day are indicated by different letters. Error bars represent one standard error of the mean of biological replicates (n = 3).

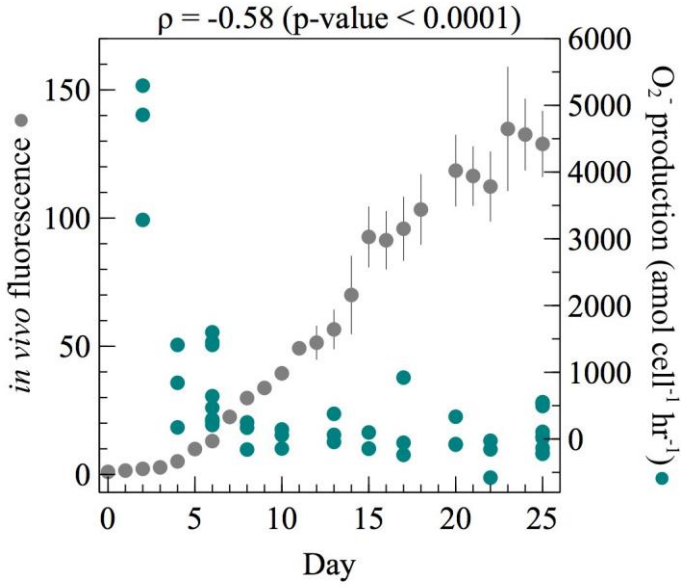

Figure 1.2: At each time point throughout the growth curve of *E. huxleyi*, net per-cell O_2^- production rates were measured from ~ 10^6 cells (n = 3 biological replicates for each day except day 6 and day 25 where 3 separate measurements were made on 3 biological replicates giving n = 9). Regression analysis on per-cell O_2^- production as a function of time was performed using Spearman's rank-order correlation. The correlation coefficient (ρ) and its level of significance (p-value) are provided. *In vivo* fluorescence was normalized to the value on day 0. Error bars indicate one standard error of the mean of 3 biological replicates.

Extracellular O_2^- production as a function of cell density

Two approaches were undertaken to determine the potential effect of cell density on extracellular O_2^- production. First, short-term effects (sec-min) were tested by measuring cell-normalized O_2^- production rates and total O_2^- concentrations while increasing the number of cells loaded on the FeLume filter in both exponential and stationary growth phase. The total O_2^- concentration increased significantly with increasing cell density during both exponential (Spearman's $\rho = 0.92$; $p < 0.0001$) and stationary phase (Spearman's $\rho = 0.89$; $p < 0.0001$). Conversely, net per-cell O_2^- production rates decreased significantly with increasing cell density during exponential phase (Spearman's $\rho = -0.74$; $p < 0.001$) but not during stationary phase (Spearman's $\rho = -0.20$; $p = 0.45$) (Figure 1.3). In exponential phase, average net per-cell O_2^- production rates decreased by 235% from the highest (9.2×10^6) to lowest (4.6×10^5) number of cells analyzed.

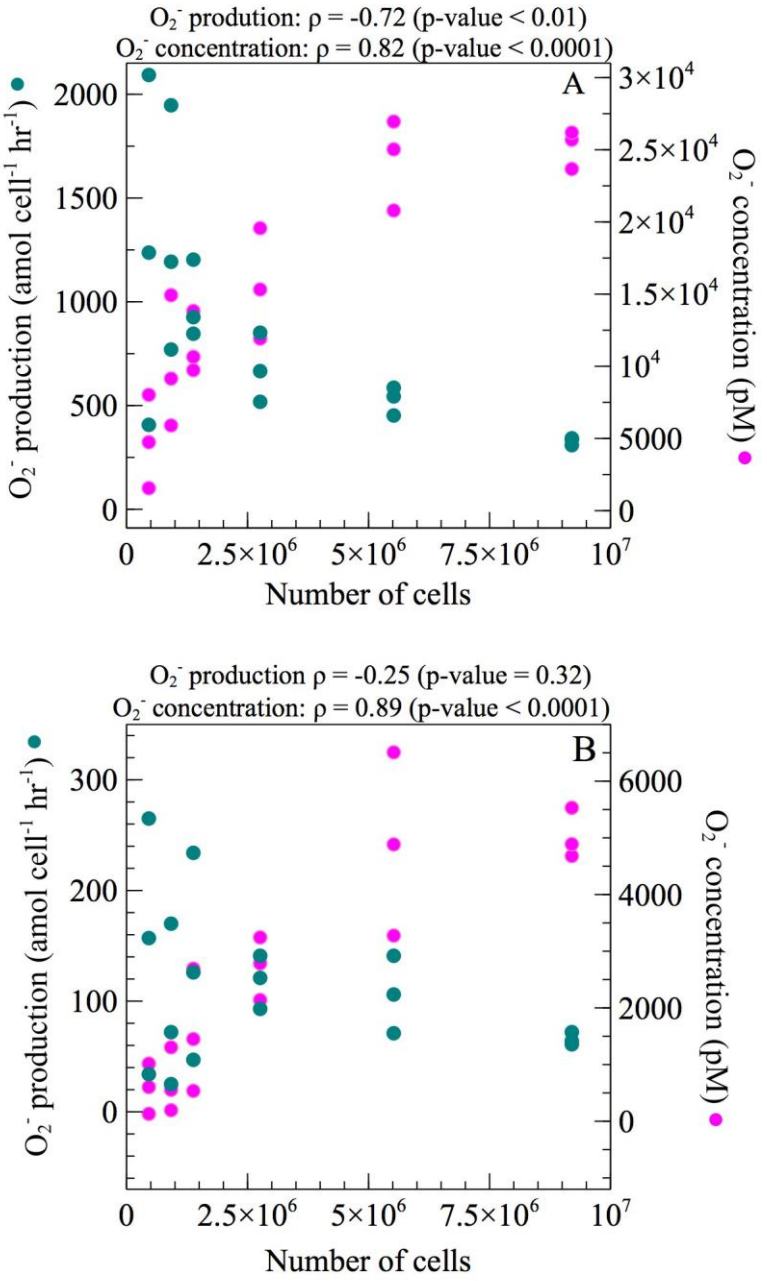

Figure 1.3: Net per-cell O_2^- production rates and total steady-state O_2^- concentrations were measured across a range of increasing cell numbers during (A) exponential and (B) stationary growth phases of *E. huxleyi*. Regression analysis was performed using Spearman's rank-order correlation. Correlation coefficients (ρ) and their level of significance (p-value) are provided.

To assess longer-term effects (min-hr) of cell density on extracellular O_2^- production, exponentially growing cells were preconditioned to lower cell densities by diluting cultures with 0.22 µm filtered, autoclaved seawater and incubating for 0 – 6.5 hours prior to conducting O_2^- measurements. In this experiment, the number of cells loaded on the FeLume filter at each dilution level were kept constant (average ± SE was $1.32 \times 10^6 \pm 8.47 \times 10^4$ cells (n = 26). A 10- and 100-fold dilution of *E. huxleyi* resulted in a 51% and 172% increase in cell-normalized net extracellular O_2^- production rates, respectively. Although average rates increased at both dilution levels, only the 100-fold dilution resulted with significantly more extracellular O_2^- per cell than the undiluted control (t-test; $p < 0.05$) (Figure 1.4). The 0.22 µm filtered, autoclaved seawater diluent was also measured for O_2^- to ensure the O_2^- measured in the diluted samples was not due to the seawater diluent. At maximum, O_2^- produced in the seawater diluent could only account for 3.0-4.6% of the total steady-state O_2^- concentrations measured in experiments with *E. huxleyi*, confirming that the contribution from the diluent was negligible.

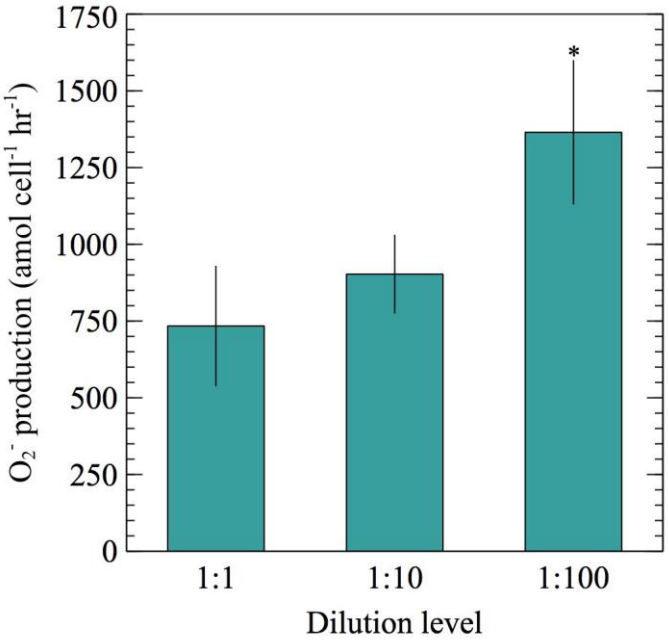

Figure 1.4: Net per-cell O_2^- production rates were measured from ~ 10^6 *E. huxleyi* cells during exponential growth phase post no dilution (1:1), 10-fold dilution (1:10), or 100-fold dilution (1:100) with 0.22 µm filtered, autoclaved seawater for 0-6.5 hours. Significant differences (two sample student's t-test) relative to the undiluted control (1:1) are indicated by asterisks, where a p-value of < 0.05 is represented by one asterisk symbol. Error bars depict one standard error of the mean of replicates (n = 8 for 1:100 and 9 for 1:1 and 1:10 dilutions).

SOD addition experiments

To assess how extracellular O_2^- influences growth and physiology, *E. huxleyi* cultures were grown with a range of SOD concentrations and monitored until the end of exponential phase. Since SOD is a large enzyme (>31 kDa) (Cass, 1985), it cannot passively cross cell membranes and therefore selectively targets O_2^- within the extracellular milieu. Overall, the addition of SOD stimulated growth (Figure 1.5 – 1.6). For example, *in vivo* fluorescence was significantly different in cultures with various SOD concentrations (mixed factor repeated measures ANOVA; $p < 0.001$) and became more significant over time (mixed factor repeated measures ANOVA; $p < 0.0001$) (Figure 1.5A). In addition, specific growth rates were between 15% and 22% higher (t-test; $p < 0.05$) in the presence of SOD (Figure 1.5B). Cell abundances from cultures grown with 100 U mL^{-1} SOD were significantly higher (t-test; $p < 0.05$) than cell abundances from cultures grown without SOD beginning on day 7 (Figure 1.5C), when cell concentrations in the highest SOD addition were 41% higher than the unamended treatment.

To confirm whether these results were specifically due to SOD, a control experiment was performed in which SOD was removed via diafiltration and only the low molecular weight fraction (< 10 kDa) of the SOD suspension was added to cultures. *In vivo* fluorescence was significantly different between treatments (mixed factor repeated measures ANOVA; $p < 0.05$) with significance increasing over time (mixed factor repeated measures ANOVA; $p < 0.0001$) (Figure 1.6A). Cultures grown with SOD grew significantly faster (t-test; $p < 0.05$) than those grown with dialyzed SOD (Figure 1.6B). By the end of the control experiment (day 12), cell abundances from cultures grown with dialyzed SOD were significantly lower (t-test; $p < 0.05$) than those grown with SOD by about 32% (Figure 1.6C). Thus, the effect of SOD addition on

growth rates and growth yields could not be accounted for by the dialyzed SOD control (Figure 1.6).

In addition to growth yields and growth rates, the cellular biovolume of *E. huxleyi* was monitored in SOD addition experiments. Biovolume was calculated using 3 different methods, but regardless of the calculation method used, cellular biovolume was larger in cultures grown with SOD (t-test; $p < 0.0001$) (Figure 1.7A, Figure1.8A). Adding SOD increased biovolume between 6.3% and 22.1%, depending on the SOD concentration and calculation method used. In the control experiment with dialyzed SOD, biovolume of cells grown with SOD were significantly larger (t-test; $p < 0.0001$) than those grown with dialyzed SOD by at least 19% (Figure 1.8A) confirming the response was due to the presence of SOD.

In addition to stimulating growth, SOD improved photophysiological health, as evidenced by increased F_v/F_m values, which indicated more efficient light assimilation by PSII in the presence of SOD. By day 10, adding SOD at each concentration increased F_v/F_m between 11% and 18% compared to the 0 U mL^{-1} SOD control (t-test; $p < 0.05$) (Figure 1.7B). A similar trend was seen in the control experiment with dialyzed SOD, where F_v/F_m values from cultures grown with SOD were significantly higher than those from cultures grown with dialyzed SOD starting on day 7 (t-test; $p < 0.05$) (Figure 1.8B). Therefore, improvements in photophysiological health are attributed to the effects of SOD.

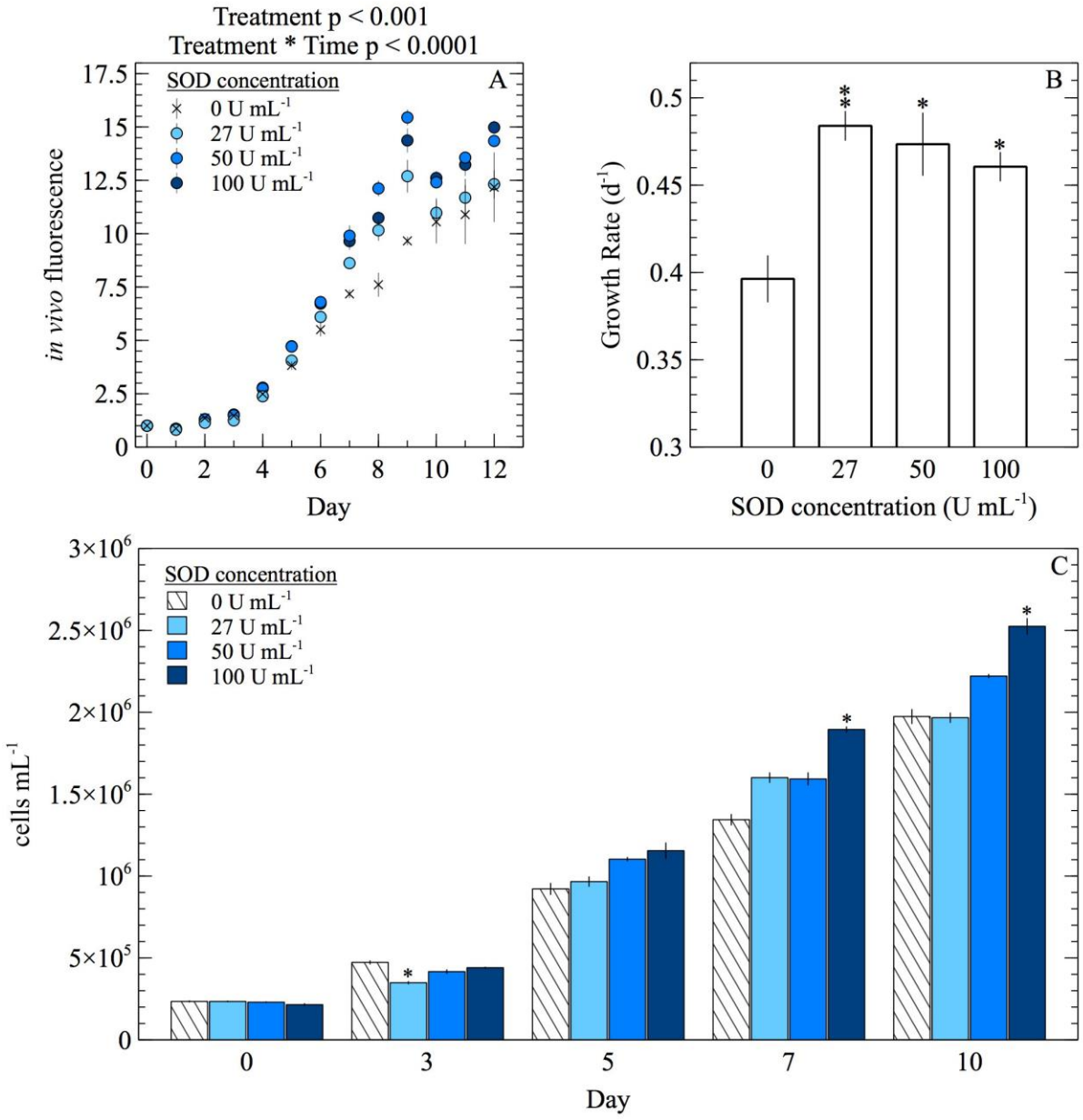

Figure 1.5: The effect of daily SOD additions on (A) average *in vivo* fluorescence, (B) specific growth rate during exponential growth phase, and (C) cell abundance of *E. huxleyi*. Significant differences in *in vivo* fluorescence between SOD additions were found using a mixed factor repeated measures ANOVA. Significant differences (two sample student's t-test) in specific growth rate and cell abundances relative to the control (0 U mL^{-1} SOD) are indicated by asterisks, where a p-value of < 0.05 and < 0.01 are represented by one and two asterisk symbols, respectively. Error bars depict one standard error of the mean of biological replicates (n = 3).

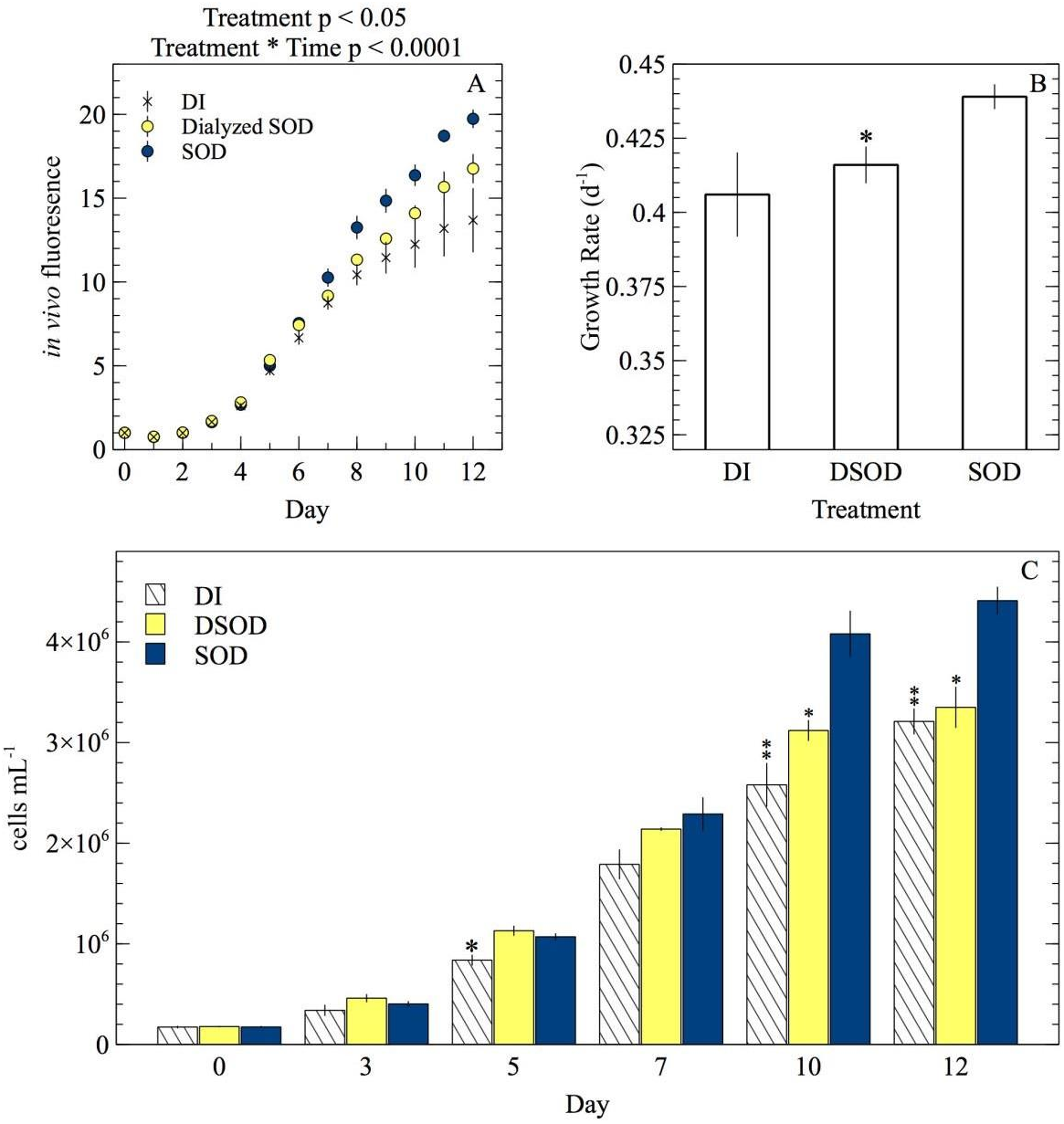

Figure 1.6: The effect of daily additions of DI, dialyzed SOD (DSOD), and 100 U mL^{-1} SOD on (A) average *in vivo* fluorescence, (B) specific growth rate, and (C) cell abundance of *E. huxleyi*. Significant differences in *in vivo* fluorescence between SOD additions were found using a mixed factor repeated measures ANOVA. Significant differences (two sample student's t-test) in specific growth rate and cell abundances relative to the 100 U mL^{-1} SOD treatment are indicated by asterisks, where a p-value of < 0.05, < 0.01, and < 0.0001 are represented by one, two, and three asterisk symbols, respectively. Error bars depict one standard error of the mean of biological replicates (n = 3).

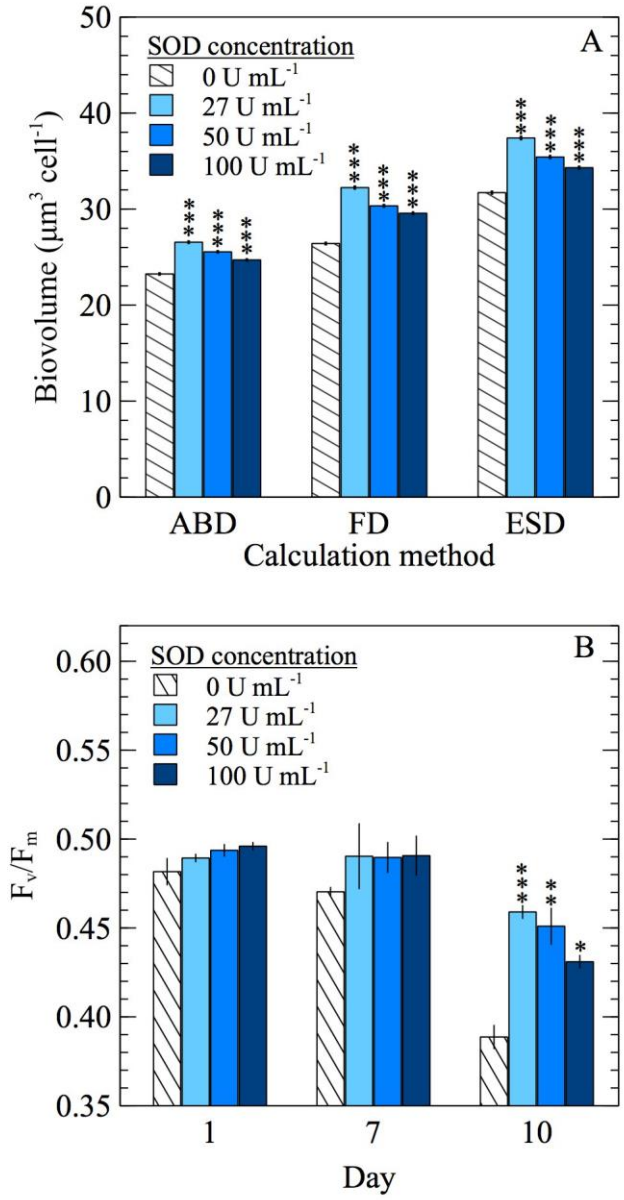

Figure 1.7: The effect of daily SOD additions on *E. huxleyi* (A) cellular biovolume (n = 19041, 17344, 24902, and 33006 individual cells for 0, 27, 50, and 100 U mL^{-1} SOD, respectively) sampled on day 10 and calculated using 3 different measurements of cell diameter (Area Based Diameter (ABD), Filled or Full Diameter (FD), and Equivalent Spherical Diameter (ESD)) and (B) F_v/F_m values (n = 3 biological replicates). Significant differences (two sample student's t-test) relative to the control (0 U mL^{-1} SOD) are indicated by asterisks, where a p-value of < 0.05, < 0.01, and < 0.0001 are represented by one, two, and three asterisk symbols, respectively. Error bars represent one standard error of the mean.

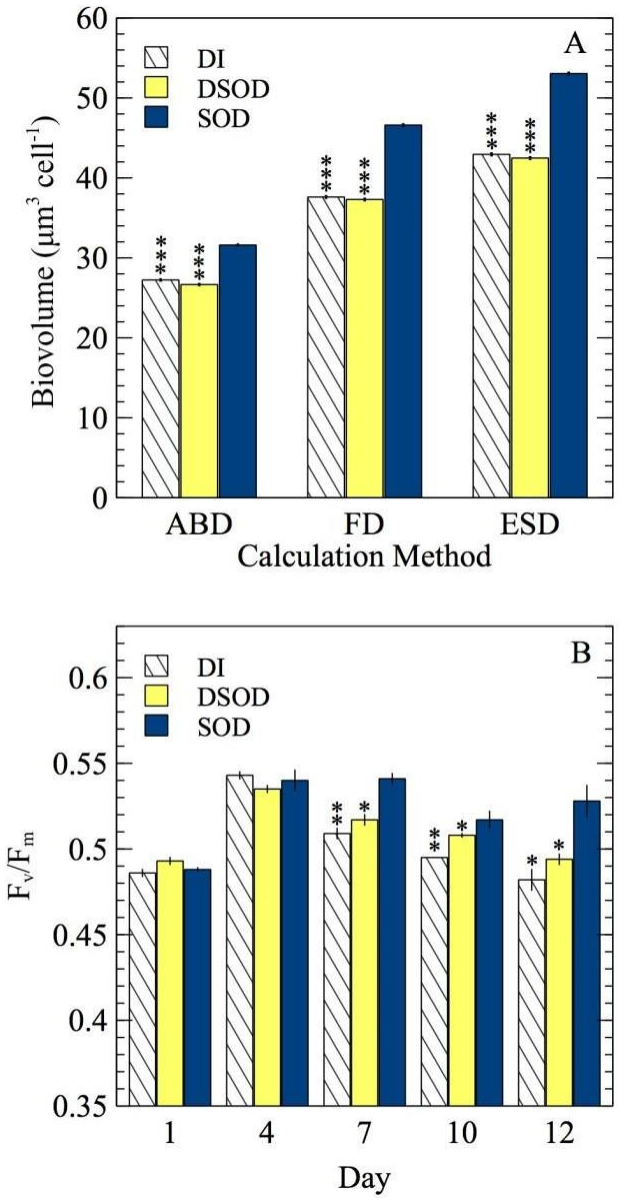

Figure 1.8: The effect of daily additions of dialyzed SOD (DSOD), DI, and 100 U mL^{-1} SOD on *E. huxleyi* (A) average cellular biovolume (μm^3 $cell^{-1}$; n = 49007, 61757, and 96758 for DI, dialyzed SOD, and 100 U mL^{-1} SOD, respectively) sampled on day 10 and calculated using 3 different measurements of cell diameter (Area Based Diameter (ABD), Filled or Full Diameter (FD), and Equivalent Spherical Diameter (ESD)) and (B) Fv/Fm values (n = 3 biological replicates). Significant differences (two sample student's t-test) relative to the 100 U mL^{-1} SOD are indicated by asterisks, where a p-value of < 0.05, < 0.01, and < 0.0001 are represented by one, two, and three asterisk symbols, respectively. Error bars represent one standard error of the mean.

Extracellular O_2^- production in the presence and absence of light

To investigate whether extracellular O_2^- production by *E. huxleyi* is dependent on light, extracellular O_2^- production was measured in ambient light and dark conditions. A representative FeLume time series measurement of O_2^- concentration showed that extracellular O_2^- production by *E. huxleyi* under ambient light reached and stabilized at 2395 ± 27 pM (Figure 1.9). Upon removal of light, there was an immediate decline in production, which stabilized at 1085 ± 29 pM after ~160 s in dark conditions. This result could not be accounted for by abiotic factors, as the removal of light had insignificant effects on O_2^- production in the absence of *E. huxleyi* cells. The drawdown of signal below the abiotic O_2^- baseline by SOD confirmed that the biogenic signal was indeed due to O_2^- production (Figure 1.9). All biological replicates produced less O_2^- in dark compared to ambient light conditions (t-test; $p < 0.0001$), indicating a connection with photophysiological processes (Figure 1.10). Dark conditions inhibited O_2^- production by an average of 70%.

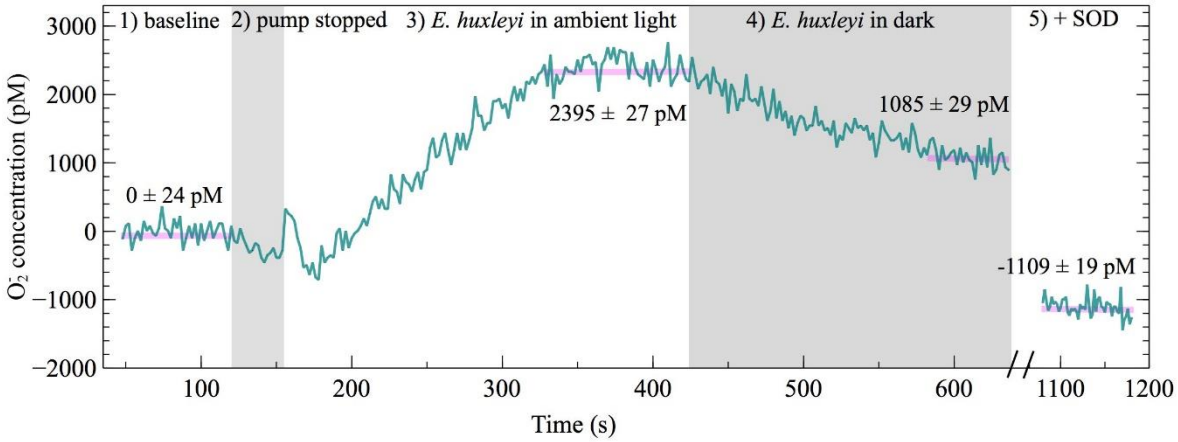

Figure 1.9: FeLume time-series of O_2^- measurements under different light conditions on day 2 of *E. huxleyi* growth (biological replicate B) split into five regions: 1) phosphate buffer solution and MCLA reagent baseline (which is subtracted from the biogenic O_2^- concentration in regions 3 and 4), 2) shaded region showing loading of *E. huxleyi* cells while the pump was stopped, 3) *E. huxleyi* in ambient light, 4) the second shaded region showing *E. huxleyi* in the dark, and 5) drawdown of the O_2^- signal below the baseline after addition of SOD (negative O_2^- concentrations account for SOD driven degradation of O_2^- originating from auto-oxidation of the MCLA reagent). The average ± SE of stable steady-state O_2^- concentration measurements are indicated by horizontal grey lines.

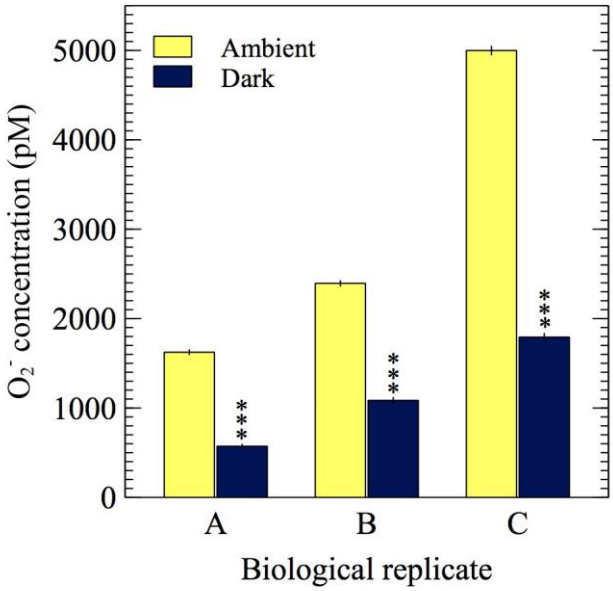

Figure 1.10: O_2^- measurements from 3 biological replicates of *E. huxleyi* in the presence of ambient light (~ 5 μmol photons m^{-2} s^{-1}) and in the dark (0 μmol photons m^{-2} s^{-1}). Asterisks show significant difference ($p < 0.0001$) between the average dark and average ambient light steady-state O_2^- concentration for each biological replicate. Error bars represent one standard error of the mean ($n \geq 31$ chemiluminescent counts).

Discussion

Here, we investigated the cellular regulation and potential physiological roles of extracellular O_2^- production in a noncalcifying strain (CCMP 374) of the cosmopolitan marine coccolithophore *E. huxleyi* to approach a broader understanding of the potential ecological and environmental impacts of phytoplankton-derived extracellular O_2^-. The ability to produce extracellular O_2^- is widespread among phytoplankton, yet production rates can vary substantially within and between species (Diaz and Plummer, 2018). For example, compared to *Chattonella* spp., the most prolific microbial ROS producers, maximal extracellular O_2^- production rates by *E. huxleyi* were about 100 to 10,000 times lower. Indeed, *E. huxleyi* produced O_2^- at a rate more similar to nonharmful algae such as *Symbiodinium* spp. and *Thalassiosira* spp. (Diaz and Plummer, 2018).

The extracellular O_2^- concentrations and production rates by *E. huxleyi* were not due to the release of intracellular O_2^-. First, the release of intracellular O_2^- through cell lysis would have been detected as a rapidly decaying pulse of O_2^-, but this can be ruled out because O_2^- signals were stable for at least 1-2 min (see Materials and Methods), a significant timeframe compared to the typical half-life of O_2^- in our analysis (~2 min) (Diaz et al., 2013). Second, the physiochemical nature of the O_2^- anion prevents it from passively crossing intact cell membranes (Bielski et al., 1985, Brown and Griendling, 2009, Lesser, 2006). Therefore, the production rates measured in this study reflect active production of O_2^- on or near the surface of *E. huxleyi*. The reported rates of extracellular O_2^- production reflect the balance of gross production and decay at the cell surface, thus giving a net production rate. Therefore, any change in the net production rate of extracellular O_2^- could result from a change in gross production, decay, or both. Several abiotic and biotic factors have the potential to degrade extracellular O_2^- at or near the cell

surface, such as interactions with trace metals including soluble and mineral-bound iron (Heller and Croot, 2010a, Fujii et al., 2006) and expression of cell surface SODs (Aguirre et al., 2005, Oshikawa et al., 2010, Bauer, 2014).

ROS production is commonly associated with stress, however, *E. huxleyi* produced extracellular O_2^- without any added stressors. In fact, cell-normalized O_2^- production by *E. huxleyi* was highest in early exponential phase under presumably the least taxing culture conditions when nutrient concentrations were highest (Figure 1.2) and when photosynthetic efficiency was at a maximum (Figure 1.1). These results reflect the rates of extracellular O_2^- production by cells that were removed from the prevailing culture conditions and analyzed *ex situ*. The *ex situ* analytical conditions were identical across culture samples of all ages, such as pH (7.6), yet differed from *in situ* levels (Figure 1.11). These results therefore show that as cultures age, there is a shift towards lower O_2^- production when cells are analyzed under the same conditions. The potential effect of pH on extracellular O_2^- production by *E. huxleyi* is unknown, but an increase in pH stimulates extracellular ROS production by *C. marina* (Liu et al., 2007), which is opposite to the trend reported here (Figure 1.1; Figure 1.2). The observed decline in extracellular O_2^- production with culture age therefore suggests that extracellular O_2^- production is physiologically driven and unlikely related to a stress response, as levels of stress would presumably increase with time in batch culture due to the depletion of resources. These findings do not rule out the potential for *E. huxleyi* to upregulate extracellular O_2^- under stressful conditions, as seen with extracellular H_2O_2 (Evans et al., 2006) and intracellular ROS (Evans et al., 2006, Vardi et al., 2012) during viral infection, but do demonstrate a physiological investment in the production of extracellular O_2^- under ideal growth conditions, which suggests some role in basal metabolism. In order to clarify if and how *E. huxleyi* regulates extracellular

O_2^- in response to biogeochemical variability and stress, future work should consider the influence of factors such as viral infection and pH.

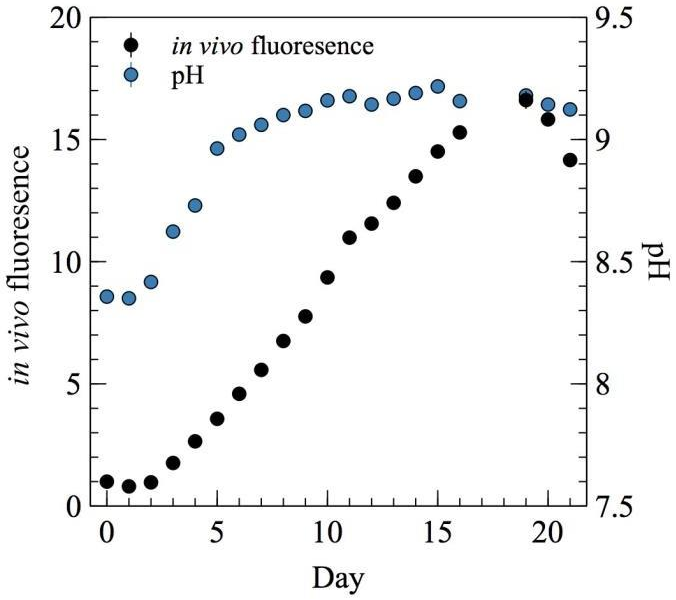

Figure 1.11: The average pH and *in vivo* fluorescence of *E. huxleyi* cultures (n=3) were measured throughout the growth curve. Most of the error bars, representing one standard error of the mean, are hidden by the data symbols.

In addition to having growth phase dependence (Figure 1.2) similar to other phytoplankton (Oda et al., 1995, Portune et al., 2010, Kim et al., 1999), cell-normalized net extracellular O_2^- production rates by *E. huxleyi* were also inversely dependent on cell density over a range of timescales during exponential growth phase. For example, this trend occurred when cell density increased on time scales of seconds to minutes (Figure 1.3A) and when cells were preconditioned to lower cell densities on timescales of minutes to hours (Figure 1.4). This tight regulation may suggest a dynamic cell density-dependent signaling role for O_2^- production in *E. huxleyi*. For instance, extracellular O_2^- deriving from one cell may act as a signal between other cells or within the same cell to provide information on surrounding population density (Diaz and Plummer, 2018). Similar cell density dependent trends in extracellular O_2^- production have been demonstrated in other phytoplankton (Marshall et al., 2005a, Diaz et al., 2018, Hansel et al., 2016), including *C. marina* (Marshall et al., 2005b).

Although evidence has been accumulating that extracellular O_2^- production is directly involved in growth promotion in a range of microbial cell types (Oda et al., 1995, Aguirre et al., 2005), our results show that the presence of extracellular O_2^- does not directly stimulate growth of *E. huxleyi*. The potential role of extracellular O_2^- in *E. huxleyi* growth was addressed through selective removal of extracellular O_2^- from the local environment of cells using SOD. Scavenging O_2^- promoted growth (Figure 1.5), increased cell biovolume (Figure 1.7A), and improved photosynthetic efficiency (Figure 1.7B). Conversely, removal of extracellular O_2^- from cultures of *Chattonella* spp. attenuates growth (Oda et al., 1995, Tanaka et al., 1992). Specifically, in one prior study, *C. marina* growth was significantly hampered under similar SOD concentrations used in the present study, and the morphological state of cells was altered (Oda et al., 1995). Recently, Hansel et al. (2019) revealed that the growth of common marine bacteria from the

Roseobacter clade was inhibited by SOD in a dose-dependent manner (Hansel et al., 2019). Similarly, the removal of extracellular ROS from fungi and the amoebozoan *Dictyostelium discoideum* is also detrimental to development (Aguirre et al., 2005). Taken together, extracellular O_2^- does not seem to directly stimulate growth in *E. huxleyi*. Rather, these results may highlight a different role for extracellular O_2^- in *E. huxleyi* that contrasts with the proposed growth-promoting role of extracellular O_2^- in *C. marina* (Oda et al., 1995), bacteria (Hansel et al., 2019), fungi, and protists (Aguirre et al., 2005). However, the addition of SOD not only removes O_2^- but produces H_2O_2, which may also have impacts on *E. huxleyi* physiology. For example, high concentrations of H_2O_2 are harmful to phytoplankton (Morris et al., 2011, Dupouy et al., 1985), but normal growth of *C. marina* is dependent on low levels of extracellular H_2O_2 (Oda et al., 1995). In fact, in a variety of cell types, the dismutation of Nox-derived O_2^- by cell surface SOD generates extracellular H_2O_2, which can diffuse into the cell, to elicit gene expression (Shapiguzov et al., 2012), morphogenesis (Rossi et al., 2017), and proliferation (Oshikawa et al., 2010, Bauer, 2014). It remains possible, yet speculative, that the addition of SOD in our experiments accelerated the dismutation of O_2^- to H_2O_2, which then may have acted as a growth promoter for *E. huxleyi*. Thus, the role of extracellular O_2^- in *E. huxleyi* may be contingent on its ability to give rise to H_2O_2, which should be interrogated in future work.

The fact that there are clear trends in extracellular O_2^- production as a function of growth phase and cell density, but that *E. huxleyi* growth was not shunted with removal of extracellular O_2^-, leaves the possibility open that extracellular O_2^- could be connected to other aspects of *E. huxleyi* physiology and health. To examine whether extracellular O_2^- production may be involved in photosynthetic physiology, we interrogated O_2^- production as a function of light and found that O_2^- production was attenuated within seconds upon transition from light to dark conditions

(Figure 1.9). This finding adds to a growing body of evidence linking modulation of extracellular O_2^- production by phytoplankton to light availability and therefore photophysiology. For instance, extracellular O_2^- production is light dependent in many phytoplankton including *Thalassiosira* spp. (Schneider et al., 2016, Milne et al., 2009), *Trichodesmium* (Hansel et al., 2016), *Symbiodinium* (modulated on same time scales shown here) (Saragosti et al., 2010), and *Chattonella* spp. (Marshall et al., 2002, Dorantes-Aranda et al., 2013, Kim et al., 1999). Thus, O_2^- production may somehow be involved with light dependent processes (e.g., photosynthesis, photoacclimation physiology), and this functionality may be conserved across phytoplankton taxa. Interestingly, in a previous study, when *C. marina* was treated with DCMU (3-(3,4-dichlorophenyl)-1,1-dimethylurea), an electron transfer inhibitor between photosystem I and II, extracellular O_2^- production was quenched to levels observed under dark conditions (Marshall et al., 2002), further illustrating a mechanistic link between extracellular O_2^- production and photophysiology.

Overall, this study reveals that the stress-independent production of extracellular O_2^- by *E. huxleyi* is dynamically regulated, and potentially part of a basal process involved with photophysiology. Extracellular O_2^- production by *E. huxleyi* is conceivably part of healthy cellular functioning for several reasons. First, the fact that cells diverted energy towards making O_2^- in the absence of a stressor suggests its production can be unassociated with stress and probably related to basal functioning. Indeed, *E. huxleyi* produced maximum amounts of extracellular O_2^- per cell under ideal growth conditions while cells were most metabolically active (Figure 1.2) and when efficiency of photosynthetic processes was highest (Figure 1.1). Further, the steady-state concentrations of O_2^- generated by *E. huxleyi* cells are not consistent with concentrations that would be damaging ($> 10^{-6}$ M) but are consistent with concentrations of

biological signaling molecules (~10^{-12} M) (Saran, 2003). Additionally, *E. huxleyi* cells tightly controlled the production of extracellular O_2^- as a function of light, cell density, and growth phase, and on timescales as short as seconds, consistent with other phytoplankton (Oda et al., 1995, Kim et al., 1999, Portune et al., 2010, Milne et al., 2009, Schneider et al., 2016, Hansel et al., 2016, Saragosti et al., 2010, Marshall et al., 2002, Dorantes-Aranda et al., 2013, Diaz et al., 2018, Marshall et al., 2005a, Marshall et al., 2005b), suggesting a potential dynamic role in signaling and photophysiology. Indeed, stress-independent extracellular O_2^- production by *E. huxleyi* is in agreement with several other microorganisms such as phytoplankton and bacteria where its production is prolific under ideal growth conditions (Kustka et al., 2005, Marshall et al., 2005a, Marshall et al., 2005b, Rose et al., 2005, Godrant et al., 2009, Portune et al., 2010, Hansel et al., 2016, Diaz et al., 2013, Schneider et al., 2016, Oda et al., 1995). The fact that *E. huxleyi* still produces extracellular O_2^- in the absence of light suggests there could be additional and/or alternative purposes for this production beyond photophysiology. Indeed, extracellular O_2^- production can be produced through a variety of subcellular mechanisms, and could be produced for a combination of ecophysiological functions (Diaz and Plummer, 2018). Contrasting with other diverse microorganisms (Hansel et al., 2019, Oda et al., 1995, Tanaka et al., 1992, Saran, 2003, Aguirre et al., 2005), the presence of extracellular O_2^- does not promote growth in *E. huxleyi*. This finding underscores a potentially unprecedented role for the presence and/or production of extracellular O_2^-, which should be investigated among other phytoplankton. Finally, non-calcifying *E. huxleyi* cells coexist with calcareous varieties in nature but typically are not dominant (Frada et al., 2012).Several ecological and physiological processes are variable within (Strom et al., 2003, Strom and Bright, 2009, Harvey et al., 2015, Poulson-Ellestad et al., 2016, Sunda and Hardison, 2010), and between (Paasche, 2002, Harvey et al., 2015, Poulson-

Ellestad et al., 2016, Suggett et al., 2007) calcifying and noncalcifying strains. Whether the rates, regulation, and roles of extracellular O_2^- production are different in calcifying versus noncalcifying strains of *E. huxleyi* has yet to be determined but should be considered in future work.

Acknowledgements

Chapter 1, in full, is a reprint of the material as it appears in Frontiers in Microbiology 2019, Plummer, Sydney; Taylor, Alexander E.; Harvey, Elizabeth L., Hansel, Colleen M.; Diaz, Julia M.2019, Frontiers Media SA, 2019. The dissertation author was the primary investigator and author of this paper.

The authors wish to thank Dee King for her assistance with literature searches and reference indexing, Dr. Patricia Yager and Dr. Brian Hopkinson for use of their labs, and Rachel Steffen for assistance in the lab.

CHAPTER 2: LIGHT-DEPENDENT EXTRACELLULAR SUPEROXIDE PRODUCTION SERVES A PHOTOPROTECTIVE ROLE AND IS DRIVEN BY FLAVOENZYMES IN PHYTOPLANKTON

Abstract

In the marine environment, reactive oxygen species (ROS), or intermediates in the reduction of O_2 to H_2O, are widespread. ROS influence biogeochemical cycles by driving reactions with toxic and nutrient metals, carbon, and oxygen due to their reactive nature. Phytoplankton are a major source of marine ROS. In aquatic systems, phytoplankton export electrons to O_2 outside of the cell to create extracellular superoxide (eO_2^-), an important ROS. Phytoplankton derived eO_2^- production may shift in the future due to climate change impacts, which may have impacts on ROS-driven biogeochemical cycling. Despite the environmental relevance of phytoplankton-derived ROS, the ecophysiological role(s) and cellular mechanism of extracellular ROS (eROS) production by phytoplankton remain mysterious. Here, we surveyed a broad diversity of model phytoplankton including prokaryotic, eukaryotic, and harmful bloom forming species to understand the enzymatic source and potential photophysiological role of eO_2^- production. We found that light stimulates eO_2^- production in all phytoplankton assessed, and that its production is linked to photosynthesis. Additionally, application of the flavoenzyme inhibitor, DPI, inhibits eO_2^- production, photosynthetic efficiency, and vitality in most phytoplankton. Taken together, eO_2^- production is regulated by flavoenzymes and serves a photoprotective mechanism in diverse phytoplankton species. Further, this research highlights the importance of eROS in current and future ocean redox conditions and biogeochemical cycling by estimating the future change in eO_2^- production rates by *Prochlorococcus* in brighter, shallower mixing layer depths in the North Pacific Gyre.

Introduction

Reactive oxygen species (ROS) form during the reduction of oxygen to water. These transient species are prevalent in aqueous environments including the oceans (Zinser, 2018). The reactive nature of ROS such as hydrogen peroxide (H_2O_2), superoxide (O_2^-), and the hydroxyl radical (OH•) means these species can transform important elements in aquatic systems. Indeed, ROS react with harmful metals (e.g., Hg) (Siciliano et al., 2002), metal nutrients (e.g., Fe, Cu) (Wuttig et al., 2013, Rose, 2012), carbon (Heller and Croot, 2010b), and oxygen (Sutherland et al., 2020) in the marine environment via redox reactions, thereby influencing biogeochemical cycling.

In the marine environment, phytoplankton are major sources of ROS (Morris et al., 2022). While some ROS such as H_2O_2 can diffuse out of cells to contribute to the dissolved ROS pool (Diaz and Plummer, 2018), others such as O_2^- cannot cross biological membranes due to physiological constraints (i.e., negative charge, short intracellular lifetime, limited diffusive distance) (Korshunov and Imlay, 2002, Lesser, 2006). Also, the majority of microbially-derived O_2^- in the marine environment does not originate from ruptured cells. Rather, the dominant biological O_2^- source is active production via cell membrane associated or extracellular enzymes, which export electrons to O_2 outside of the cell to produce extracellular superoxide (eO_2^-) (Diaz and Plummer, 2018, Rose, 2012). Despite the environmental importance and abundance of extracellular ROS (eROS) production by marine phytoplankton, the enzymatic source and biological role of this production remains unclarified.

Flavoenzymes are a large class of electron transferring enzymes (i.e., oxidoreductases) that have been implicated in eO_2^- production in phytoplankton. Indeed, diphenyl iodonium (DPI), which blocks electron transfer activity in flavoenzymes (O'Donnell et al., 1993), inhibits eO_2^-

production in several taxonomic groups of eukaryotic phytoplankton (Anderson et al., 2016, Kustka et al., 2005, Laohavisit et al., 2015, Park et al., 2009, Saragosti et al., 2010, Diaz et al., 2019). In these phytoplankton, inhibition of eO_2^- production via DPI has been associated with inhibition of NADPH oxidases (Nox) (Kustka et al., 2005, Park et al., 2009, Saragosti et al., 2010, Laohavisit et al., 2015, Anderson et al., 2016), which are well-known O_2^- producing enzymes in many organisms (Aguirre and Lambeth, 2010, Bedard et al., 2007). However, DPI is a broad inhibitor of flavoenzymes and not just an inhibitor of Nox. Therefore, other flavoenzymes besides Nox may be responsible for DPI-inhibitable O_2^- production. For example, DPI inhibits O_2^- production in another flavoenzyme, glutathione reductase (Diaz and Shi, Submitted).

Biological ROS are typically thought of as damaging byproducts of aerobic metabolism. However, ROS also serve a diversity of beneficial roles throughout biological systems ranging from pathogen defense to growth and development (Aguirre and Lambeth, 2010, Saran, 2003, Hansel et al., 2019, Weinberger, 2007). In phytoplankton, eROS production appears to serve beneficial roles in ecological interactions, innate physiology, and homeostasis (Hansel and Diaz, 2021). For example, many phytoplankton produce eO_2^- as a function of cell density, which has been attributed to a potential cell signaling function (Sutherland et al., 2019, Marshall et al., 2005b, Hansel et al., 2016, Diaz and Plummer, 2018, Plummer et al., 2019). Production of eO_2^- by phytoplankton has also been linked to photophysiology. Indeed, the photosynthetic electron transport inhibitor DCMU (3-(3,4-dichlorophenyl)-1,1-dimethylurea) inhibits eO_2^- production in the prolific eROS producer *Chattonella marina* (Yuasa et al., 2020a, Marshall et al., 2002). Further, light stimulates eO_2^- production in several phytoplankton (Diaz et al., 2019, Plummer et al., 2019, Saragosti et al., 2010, Schneider et al., 2016, Yuasa et al., 2020a, Hansel et al., 2016,

Dorantes-Aranda et al., 2013), and the photosynthate NADPH stimulates eO_2^- production in cellular exudates (Kim et al., 2000, Diaz et al., 2019). These findings have led to the hypothesis that NADPH from photosynthesis supplies reducing power to transplasma membrane enzymes to form eO_2^- (Diaz and Plummer, 2018, Saragosti et al., 2010).

Recent evidence points to production of eO_2^- by a putative glutathione reductase being a coping mechanism against excess light stress in the diatom *Thalassiosira oceanica*. Intriguingly, bioinformatics analyses revealed homologs of this *T. oceanica* glutathione reductase in diverse phytoplankton genomes and throughout the global ocean (Diaz et al., 2019). This finding led us to conduct a survey of model phytoplankton species to determine if this flavoenzyme-driven, photoprotective role for eO_2^- production is in fact widespread. Here, we find that light drives eO_2^- production in all phytoplankton tested. Further, flavoenzymes appear involved in eO_2^- production and maintaining health in most phytoplankton surveyed. Like *T. oceanica* (Diaz et al., 2019), flavoenzyme-driven eO_2^- production appears to be an essential photoprotective mechanism in many phytoplankton, which has implications for redox states and biogeochemical cycling of future oceans.

Methods

Phytoplankton cultivation

All phytoplankton were obtained from the National Center for Marine Algae and Microbiota (NCMA) at Bigelow Laboratory for Ocean Sciences except for the following strains: *Karenia brevis* ARC5 from the Algal Resources Collection at the University of North Carolina Wilmington (www.algalresourcescollection.com), *Ostreococcus tauri* OTH95 from the Palenik lab (Scripps Institution of Oceanography), *Dunaliella* sp. 15-1a from the Bowman lab (Scripps Institution of Oceanography), *Phaeodactylum tricornutum* CCAP 1055/1 from the Allen lab (J.

Craig Venter Institute), and *Prochlorococcus marinus* NATL2A and MIT9312 from the Chisholm lab (Massachusetts Institute of Technology). Phytoplankton were grown in autoclaved (121°C, 20 min) SN (Waterbury, 1987), L1 with the addition of silicic acid (Guillard and Hargraves, 1993), f/2, f/2 with the addition of silicic acid (Guillard and Ryther, 1962), or Pro99 (Moore et al., 2007) media using 0.2 µm filtered natural seawater as a base (Table 2.1). All experimental cultures were begun with stationary phase inoculum except for *P. marinus* strains, which were begun with exponential phase inoculum. Cultures were maintained in borosilicate culture tubes with caps at 18°C or 23°C under cool, white light (14:10 light dark cycle) (Table 2.1). Growth was monitored by observing *in vivo* chlorophyll fluorescence using a handheld *Aqua*fluor® fluorometer (Turner Designs) or cell abundance (cells mL^{-1}) using a Guava® easyCyte flow cytometer (Luminex). Flow cytometry samples were analyzed by running live samples in a 96-well plate at a low flow rate of 0.24 µL s^{-1} for 3 minutes or until at least 1000 particles were counted. Instrument performance was validated daily using instrument specific beads. For analyses, gates of cell populations were created based on diagnostic red fluorescence and forward scatter signals of healthy, exponentially growing cells. Aside from cultivation experiments, all experiments were conducted on exponentially growing cells.

Table 2.1: Growth conditions, sources, and ecotypes of the 16 model phytoplankton strains selected for the study. Strains are marine unless otherwise stated.

Class	Genus species	Strain	Media	~ Irradiance ($\mu mol\ m^{-2}\ s^{-1}$)	Temperature (°C)	Ecotype Notes
Prymnesiophyceae	*Emiliania huxleyi*	CCMP 374	f/2	100-130	18	non-calcifying
	Emiliania huxleyi	CCMP 371	f/2	100-130	18	calcifying
Chlorophyceae	*Ostreococcus tauri*	OTH95	f/2	100-130	18	
	Micromonas pusilla	CCMP 1545	f/2	100-130	18	
	Dunaliella sp.	15-1a	L1 + Si (120 ppt)	100-130	18	hypersaline
Bacillariophyceae	*Thalassiosira pseudonana*	CCMP 1335	f/2 + Si	100-130	18	coastal
	Thalassiosira weissflogii	CCMP 1336	f/2 + Si	100-130	18	coastal
	Thalassiosira oceanica	CCMP 1005	f/2 + Si	100-130	23	oligotrophic
	Phaeodactylum tricornutum	CCAP 1055/1	L1 + Si	100-130	18	
Dinophyceae	*Symbiodinium* sp.	CCMP 3364	L1 + Si	100-130	23	coral symbiont
	Karenia brevis	ARC 5	L1 + Si	100-130	23	HAB-forming
Pelagophyceae	*Aureococcus anophagefferens*	CCMP 1984	L1 + Si	100-130	18	HAB-forming
Cyanophyceae	*Synechococcus* sp.	WH 8102	SN	70-80	23	oligotrophic
	Synechococcus sp.	WH 5701	L1 + Si	70-80	23	coastal
	Prochlorococcus marinus	MIT9312	Pro99	70	23	high light adapted
	Prochlorococcus marinus	NATL2A	Pro99	40	23	low light adapted

In a set of cultivation experiments, cultures were grown with the addition of the flavoenzyme inhibitor DPI, which irreversibly binds to the flavin adenine dinucleotide (FAD)/ flavin mononucleotide (FMN) sites and consequently blocks the electron transfer activity of the flavin cofactors (O'Donnell et al., 1993), or the solvent control DMSO. Treatments included DPI dissolved in 10% DMSO (2 µM and 0.02 µM final concentrations), 10% DMSO (0.03% v/v final concentration), or no treatment (unamended). The DPI and DMSO treatments (75 µL each) were added once after exponential growth phase had begun. In these experiments, growth was monitored by obtaining daily fluorescence for *P. marinus* strains or by obtaining daily cell abundance for all other strains as detailed above. Specific growth rate (d^{-1}) was calculated by finding the slope of the regression of the natural log-normalized cell abundance or fluorescence over time during exponential phase. Exponential phase was defined as the natural log-linear ($R^2 \geq 0.98$) portion of cell abundance or fluorescence over time.

Production of eO_2^-

Production of eO_2^- by phytoplankton cells was measured using the flow-through FeLume (II) analytical system (Waterville Analytical) via reaction with the O_2^--specific chemiluminescent probe methyl *Cypridina* luciferin analog (MCLA), as previously described (Diaz et al., 2013, Schneider et al., 2016, Plummer et al., 2019). To do so, cells were gently deposited onto an inline filter (0.22 µm for most strains, except 0.1 µm for cyanobacteria and smaller picoeukaryotes, polyethersulfone membrane, 13 mm diameter) using a syringe and continuously washed (2 mL min^{-1}) with artificial seawater (20 mM phosphate; pH = 7.6) that matched the salinity of the culture media. The eO_2^- within this cell-free effluent reacted with the MCLA reagent [4 µM MCLA, 0.1 M MES, 75 µM diethylenetriamine pentaacetic acid (DTPA); pH = 6] at the center of a spiral flow cell sitting below a photomultiplier tube housed within a light-tight box.

Chemiluminescent data emitted from the reaction between eO_2^- and MCLA were collected in real time using Waterville Analytical software. Autooxidation of the MCLA reagent generates O_2^-. Therefore, chemiluminescence was measured from cell-free blanks (i.e., MCLA reagent + artificial seawater) just prior to depositing phytoplankton cells onto the inline syringe filter for each analysis. These blank chemiluminescent signals were subtracted from the subsequent biological chemiluminescent signals (i.e., MCLA reagent + artificial seawater + cells). A steady-state signal was obtained by allowing chemiluminescent signals of both blanks and cells to stabilize (≤ 5% CV) for at least 1 min. Superoxide dismutase (SOD; final concentration of ~800 U L^{-1}) was added at the end of each analysis to confirm chemiluminescent signals were due to O_2^-.

FeLume calibrations were performed with standard additions of potassium superoxide (KO_2), as previously described (Schneider et al., 2016, Plummer et al., 2019). First, primary KO_2 stocks were prepared by dissolving in a basic solution (0.03 N NaOH, pH=12.5; 90 μM DTPA). Then, absorbance of primary KO_2 stocks was measured at 240 nm before immediately being added into artificial seawater. The decay of O_2^- was measured in this solution. The primary KO_2 stocks were again measured at an absorbance of 240 nm after addition of SOD (~ 800 U L^{-1}, final concentration). Absorbance measurements of KO_2 primary stocks before and after SOD addition were used to quantify the O_2^- concentrations by applying the extinction coefficient of O_2^- corrected for production of H_2O_2 at 240 nm and a pH of 12.5 (2183 L mol^{-1} cm^{-1}) (Bielski et al., 1985). Biological chemiluminescent signals were converted to steady-state eO_2^- concentrations by dividing the chemiluminescent signals by the sensitivity of the analysis (chemiluminescent counts pM^{-1}) obtained through standard addition calibrations. Then eO_2^- concentrations (pM) were converted to production rates by multiplying by the flow rate (1 or 2

mL min^{-1}), dividing that number by the number of cells loaded on the inline syringe filter, and converting final units to amol $cell^{-1}$ h^{-1} or amol μm^{-2} h^{-1} to normalize to cell surface area. To ensure the same number of healthy cells was analyzed between replicates during an experiment, a cell concentration was first obtained via flow cytometry as detailed above. These production rates account for simultaneous production and decay of eO_2^- and are therefore net production rates.

Production of eO_2^- by phytoplankton cells was measured in the presence of DPI or the solvent control, DMSO. To do so, the artificial seawater (20 mM phosphate; pH = 7.6) that continuously washes cells during analysis was amended daily by heating and stirring for one hour, adding 20 µM DPI dissolved in 0.3% DMSO or 0.3% DMSO (final concentration), and allowing the solution to cool to room temperature. For these experiments, eO_2^- measurements were collected at the growth irradiance of each phytoplankton stain (Table 2.1). Irradiance was emitted from a dimmable soft white LED light bulb controlled with a manual dimmer and placed directly above the sample. A standard light bulb, which emits light in the visible range and little ultraviolet irradiation compared to natural sunlight (Klein et al., 2009), rather than a full spectrum light source was used to minimize abiotic ROS production while stimulating photosynthesis (Morris et al., 2022). Irradiance was monitored with a micro quantum photosynthetically active radiation (PAR) sensor (Walz). Data analysis and calculation of eO_2^- production rates in the presence of DPI followed that of Plummer et al. (2019) and is detailed above.

In another set of experiments, eO_2^- production was measured as a function of increasing plirradiance from ambient light levels (3-6 µmol m^{-2} s^{-1}) to ~2250 µmol m^{-2} s^{-1} as previously described (Diaz et al., 2019). Then, these eO_2^- production rates and irradiance data were fit to an

equation modified from the double exponential photosynthesis-irradiance (PI) model by Platt et al. (1980) which was adapted for eO_2^- production by Diaz et al. (2019). Data analysis and calculation of eO_2^- production rates as a function of irradiance followed that of Diaz et al. (2019).

Photophysiology

Photophysiology was monitored using either a Satlantic fluorescence induction and relaxation (FIRe) fluorometer system (Sea-bird Scientific) or a pulse amplitude modulation (WATER-PAM) fluorometer (Walz) similar to Diaz et al. (2019). Prior to measurements, phytoplankton were incubated with 2 µM DPI dissolved in 0.2% DMSO or 0.2% DMSO (final concentration) for at least 30 min either at their growth irradiance (Table 2.1) or in dark conditions. Photochemical efficiency of photosystem II (PSII) was determined by calculating photosynthetic efficiency (F_v/F_m) in the dark-adapted or light adapted state using the equation:

$$F_v/F_m = \frac{F_m - F_o}{F_m}$$

where F_m is the maximum fluorescence yield, and F_o is the minimum fluorescence yield. Decreases in F_v/F_m correspond to increases in photoinhibition (Murchie and Lawson, 2013, Mackey et al., 2008).

Statistical analyses

All statistical analyses were performed in JMP Pro statistical software (SAS Institute Inc.,) or Microsoft excel. A paired, two-sample Student's t-test and an unpaired, two-sample Student's t-test were used to determine the effect of DPI on eO_2^- production rates and phytoplankton growth rates, respectively. A Tukey-Honest Significance Difference (HSD) test was used to determine the effect of DPI on efficiency of PSII in light adapted and dark adapted states. The significance threshold (alpha) was set to 0.05 for all statistical analyses.

Results and Discussion

eO_2^- production rates

Here, we measured eO_2^- production rates among 16 strains of prokaryotic and eukaryotic phytoplankton spanning a diversity of taxonomic groups and ecotypes (Table 2.1). Several studies have shown that cell size influences eO_2^- production rates (Oda et al., 1997, Diaz et al., 2013, Marshall et al., 2005a). Therefore, we normalized production rates to surface area in a set of eO_2^- measurements. Production rates of eO_2^- spanned $10^{-3} – 10^{2}$ amol μm^{-2} h^{-1} (Figure 2.1), however, the majority of phytoplankton strains produced eO_2^- in the $10^{-1} – 10^{1}$ amol μm^{-2} h^{-1} range (Figure 2.1B-C). The two highest eO_2^- producers were the harmful algae *K. brevis* ARC 5 and *Aureococcus anophagefferens* CCMP 1984. While *A. anophagefferens* CMMP 1984 produced similar amounts of eO_2^- to many non-harmful strains (10^{1} amol μm^{-2} h^{-1}), *K. brevis* ARC 5 produced an order of magnitude more eO_2^-. Similar to our findings for *K. brevis* ARC 5, Kustka et al. (2005) observed that harmful algal species can produce more eO_2^- relative to non-harmful species even when accounting for cell size (Kustka et al., 2005). The cyanobacteria *P. marinus* were among the lowest eO_2^- producers (Figure 2.1A; $10^{-3} – 10^{-2}$ amol μm^{-1} h^{-1}), generating ~100-1000 fold less eO_2^- than the cyanobacteria *Synechococcus* sp. (Figure 2.1B-C). Similarly, Sutherland et al. (2019) found that *P. marinus* produced substantially less eO_2^- than *Synechococcus* sp. (Sutherland et al., 2019). Intraspecific variation in eO_2^- production was observed as well. Indeed, the low light adapted *P. marinus* strain NATL2A produced 10-fold more eO_2^- than the high-light adapted *P. marinus* strain MIT9312 (Figure 2.1A).

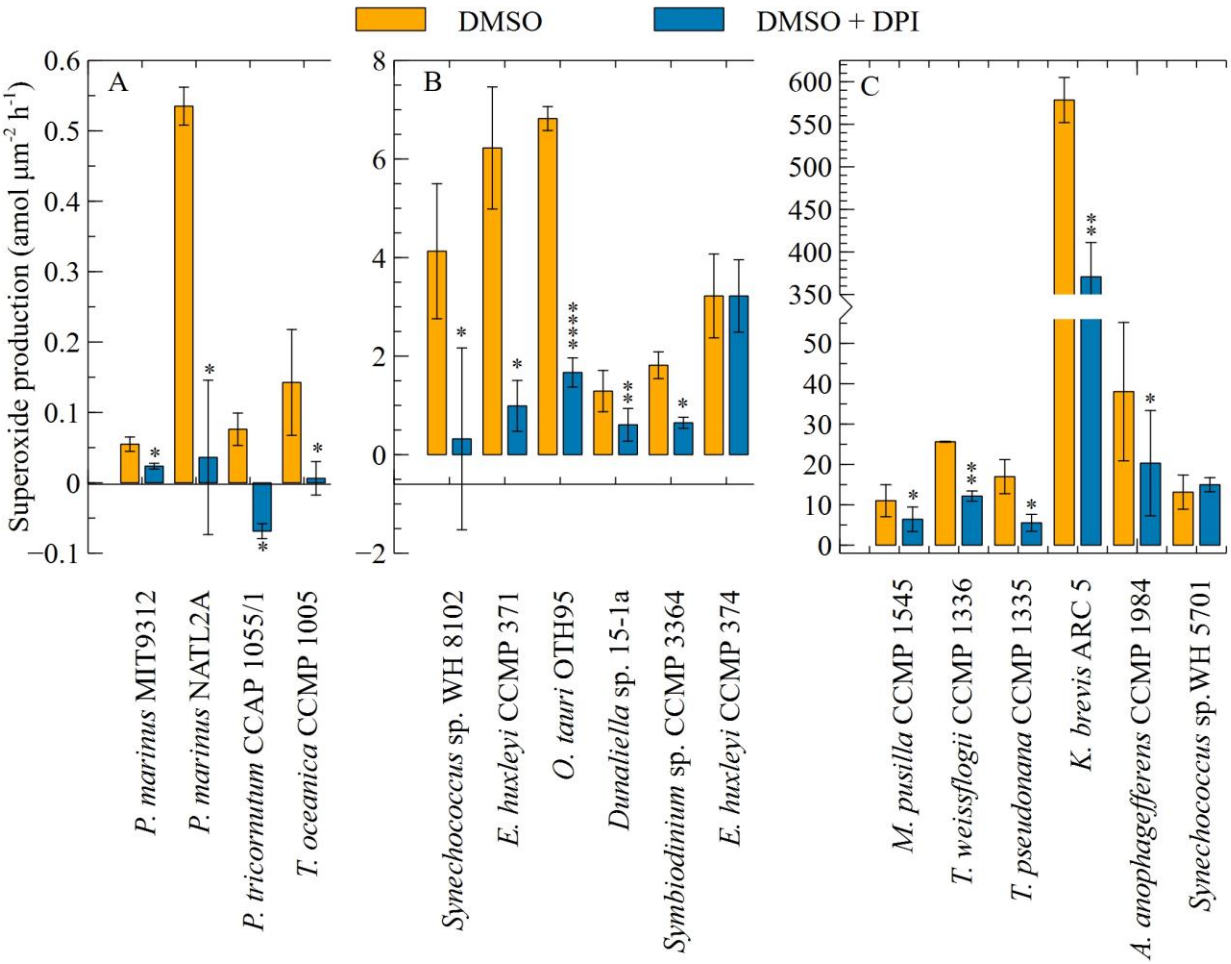

Figure 2.1: Rates of eO_2^- production in the presence and absence of the flavoenzyme inhibitor DPI. All measurements were conducted in 0.3% DMSO. Production rates were normalized to cell surface area (Table 2.2). Significant differences of mean eO_2^- production rates (n = 3 biological replicates) versus the DMSO control were found with a Student's t-test (paired, two sample). P-values are indicated by asterisks, where *, **, and **** signifies a p-value of <0.05, <0.01, and <0.0001, respectively. Error bars represent one standard deviation of the mean. Data from *T. oceanica* CCMP 1005 were taken from Diaz et al. 2019.

Table 2.2: Cell size and morphology data for surface area calculations of phytoplankton strains. Radius was calculated as $\frac{width}{2}$. For prolate spheroids surface area calculations, $A = \frac{length}{2}$, $B = \frac{width}{2}$, and $m = \sqrt{1 - (\frac{B}{A})^2}$. NCMA = National Center for Marine Algae and Microbiota

Phytoplankton strain	Length (µm)	Width (µm)	Radius (µm)	Shape	Surface Area Formula	Surface Area (µm²)	Source
Emiliania huxleyi CCMP 374	6	5	2.5	sphere	$4\pi r^2$	78.5	NCMA
Emiliania huxleyi CCMP 371	7	7	3.5	sphere	$4\pi r^2$	153.9	NCMA
Ostreococcus tauri OTH95	1	0.7	0.35	sphere	$4\pi r^2$	3.1	(Courties et al., 1994)
Micromonas pusilla CCMP 1545	3	2.5	-	prolate spheroid	$2\pi B^2(1 + \frac{Asin^{-1}(m)}{mB})$	22.3	NCMA
Dunaliella sp. 15-1a	8.3	3.3	-	prolate spheroid	$2\pi B^2(1 + \frac{Asin^{-1}(m)}{mB})$	71.6	Microscopy measurements
Thalassiosira pseudonana CCMP 1335	-	-	-	cylinder	$2\pi rh + 2\pi r^2$	51.0	(Kustka, Shaked, Milligan, King, & Morel, 2005)
Thalassiosira weissflogii CCMP 1336	-	-	-	cylinder	$2\pi rh + 2\pi r^2$	460.0	(Kustka et al., 2005)
Thalassiosira oceanica CCMP 1005	-	-	-	cylinder	$2\pi rh + 2\pi r^2$	122.0	(Lommer et al., 2012)
Phaeodactylum tricornutum CCAP 1055/1	22	2.5	-	pennate	-	368.0	(Leblanc et al., 2012)
Symbiodinium sp. CCMP 3364	13.5	11.5	-	prolate spheroid	$2\pi B^2(1 + \frac{Asin^{-1}(m)}{mB})$	464.4	(Zhang et al., 2016)
Karenia brevis ARC5	25	28	14	sphere	$4\pi r^2$	2461.8	(Novoveská & Robertson, 2019)
Aureococcus anophagefferens CCMP 1984	-	-	1.1	sphere	$4\pi r^2$	15.2	(Sieburth & Johnson, 1989)
Synechococcus sp. WH 8102	1.5	1.5	0.75	sphere	$4\pi r^2$	7.1	NCMA
Synechococcus sp. WH 5701	1	1	0.5	sphere	$4\pi r^2$	3.1	NCMA

Irradiance and photosynthesis drive eO_2^- production in phytoplankton

To test the hypothesis that eO_2^- production is dependent on photophysiology, we measured eO_2^- production as a function of increasing irradiance. In all phytoplankton tested, irradiance and photosynthesis drive eO_2^- production (Figure 2.2 – 2.3). In most phytoplankton tested, eO_2^- production as a function of light behaved similarly to the expected response of photosynthesis as a function of light. Specifically, low light levels increased eO_2^- production followed by saturation and inhibition of production at higher light levels (Figure 2.2A). However, a different response was observed in the oligotrophic *Synechococcus* strain (WH 8102), where eO_2^- production was not inhibited with increasing light (Figure 2.2B). To further test the proposed photophysiological role for eO_2^- production, we applied an equation modified from a photosynthesis-irradiance (PI) model to describe the relationship between irradiance and eO_2^- production (Diaz et al., 2019). The model fit well in all phytoplankton tested (Table 2.3; avg. ± SD of R^2 in all strains = 0.95 ± 0.05). These findings support the hypothesis that eO_2^- production is involved in photosynthetic processes either indirectly or directly, as previously proposed (Diaz and Plummer, 2018, Saragosti et al., 2010, Diaz et al., 2019), and that this characteristic is widespread in phytoplankton.

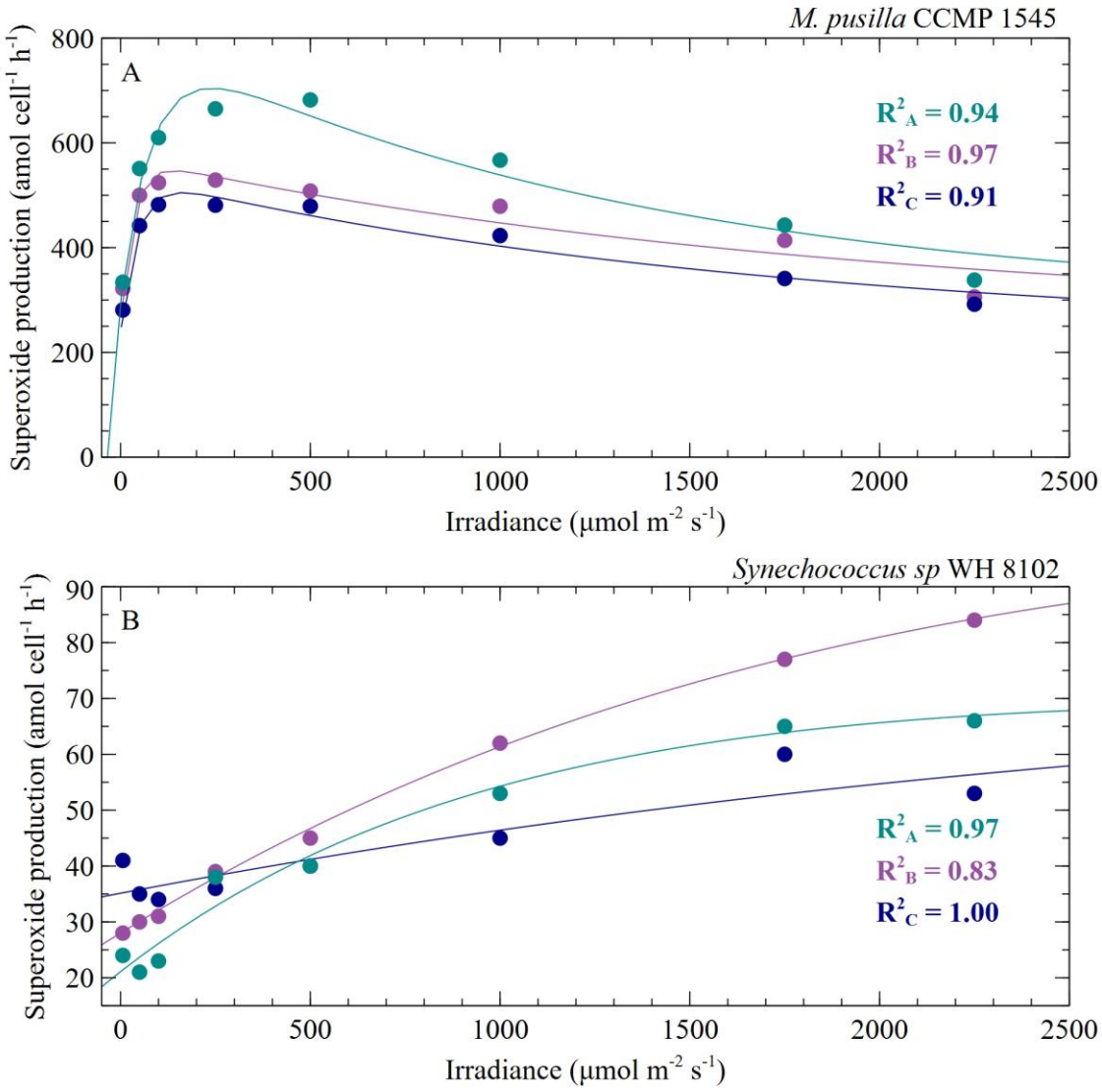

Figure 2.2: eO_2^- production rates (circles) measured at increasing irradiances from triplicate batch cultures of *M. pusilla* CCMP 1545 showing the typical photoinhibition response observed in other strains (A) and *Synechococcus* sp. WH 8102 (B) showing the non-photoinhibiting response observed only in this strain. Irradiance and eO_2^- production rate data were fit with a Photosynthesis-Irradiance model by Platt et al. (1980) that was adapted by Diaz et al. (2019) for eO_2^- production rates (lines). Each color represents a different biological replicate. R^2 values of the model fit for each biological replicate are provided. Model rates are presented in Table 2.3.

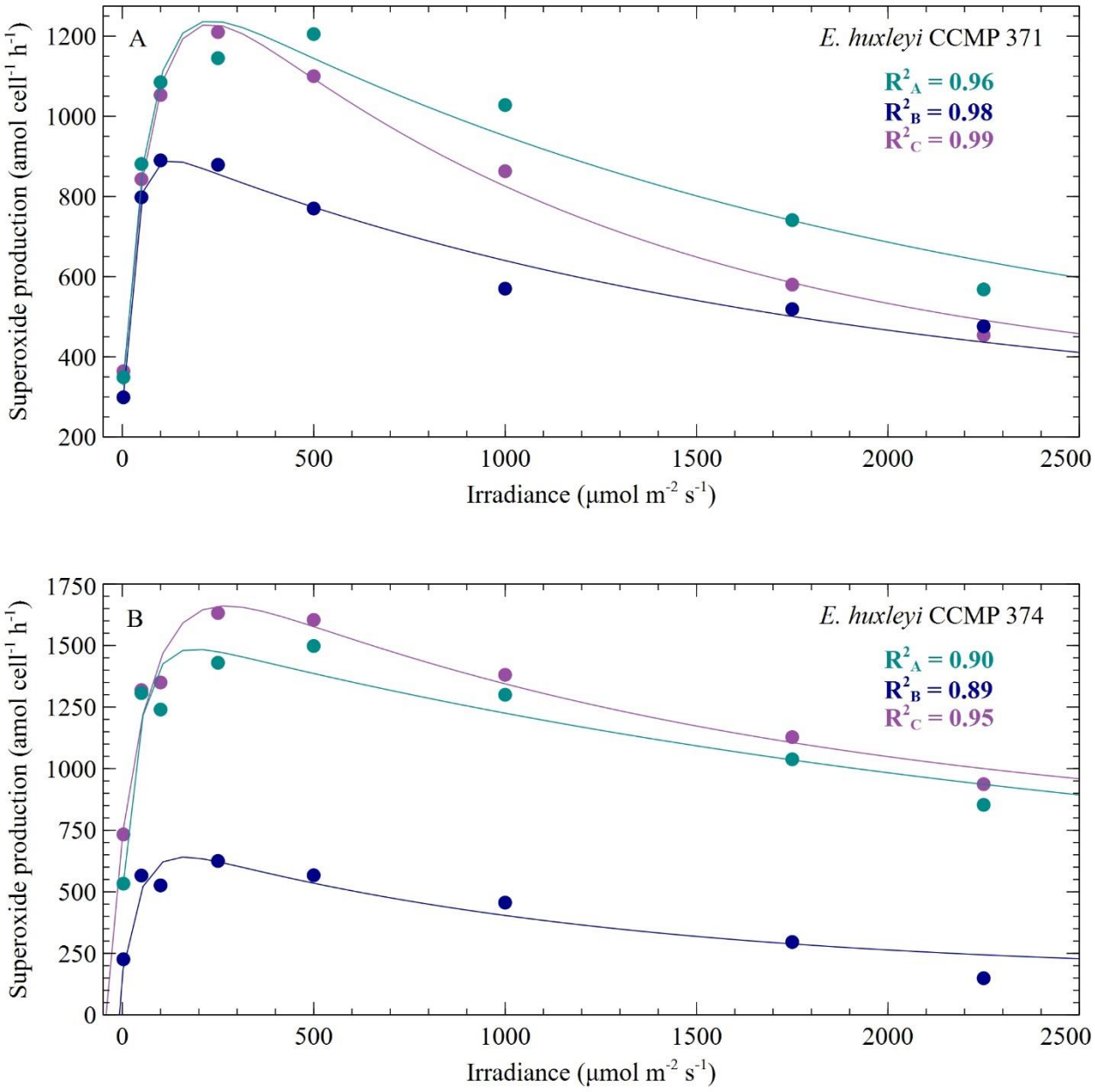

Figure 2.3: eO_2^- production rates (circles) measured at increasing irradiances from triplicate batch cultures of model phytoplankton strains (A-). Irradiance and eO_2^- production rate data were fit with a photosynthesis-irradiance model by Platt et al. (1980) that was adapted by Diaz et al. (2019) for eO_2^- production rates (lines). Each color represents a different biological replicate. R^2 values of the model fit for each biological replicate are provided. Model rates are presented in Table 2.3.

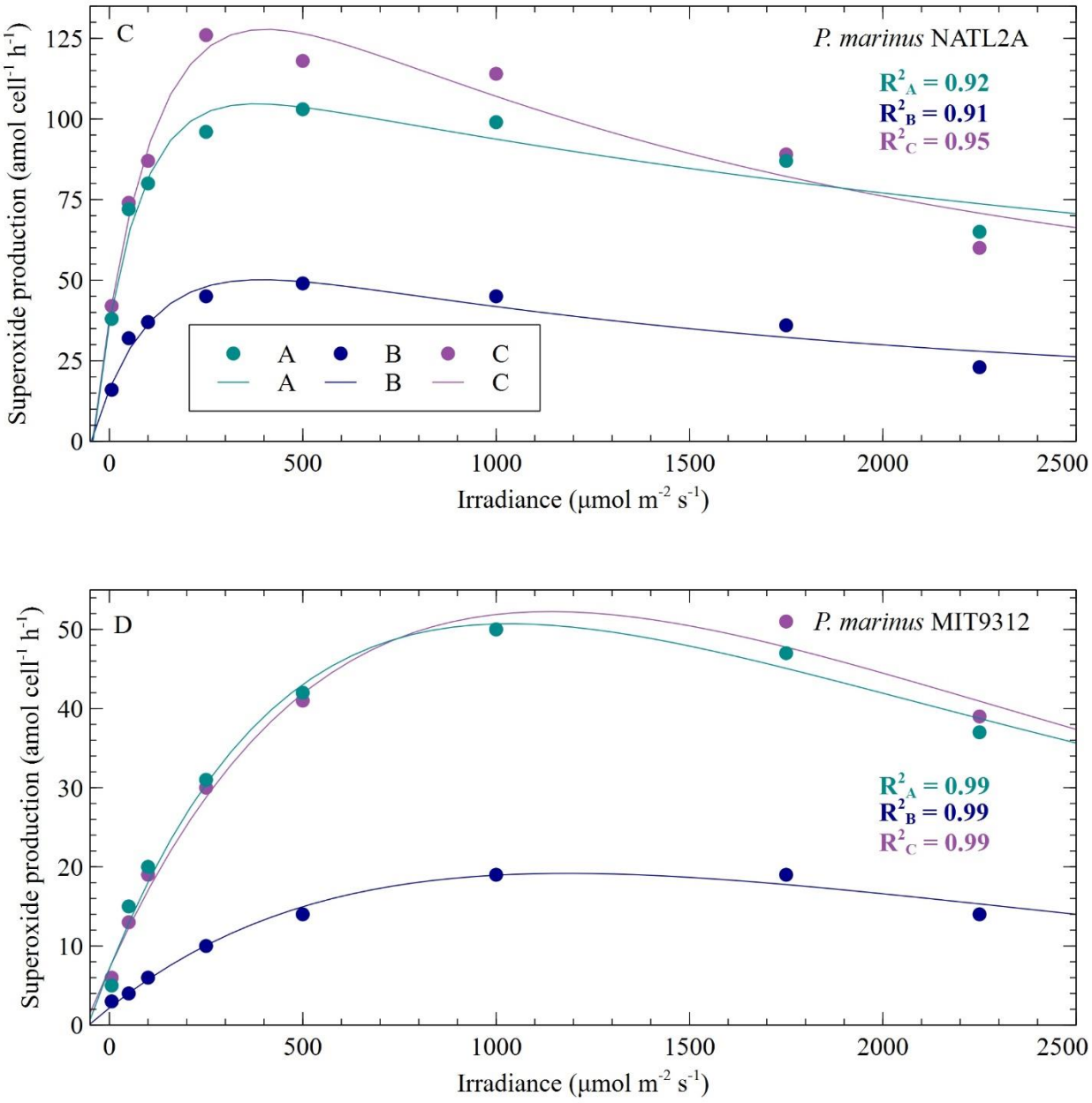

Figure 2.3 Continued: eO_2^- production rates (circles) measured at increasing irradiances from triplicate batch cultures of model phytoplankton strains (A-M). Irradiance and eO_2^- production rate data were fit with a photosynthesis-irradiance model by Platt et al. (1980) that was adapted by Diaz et al. (2019) for eO_2^- production rates (lines). Each color represents a different biological replicate. R^2 values of the model fit for each biological replicate are provided. Model rates are presented in Table 2.3.

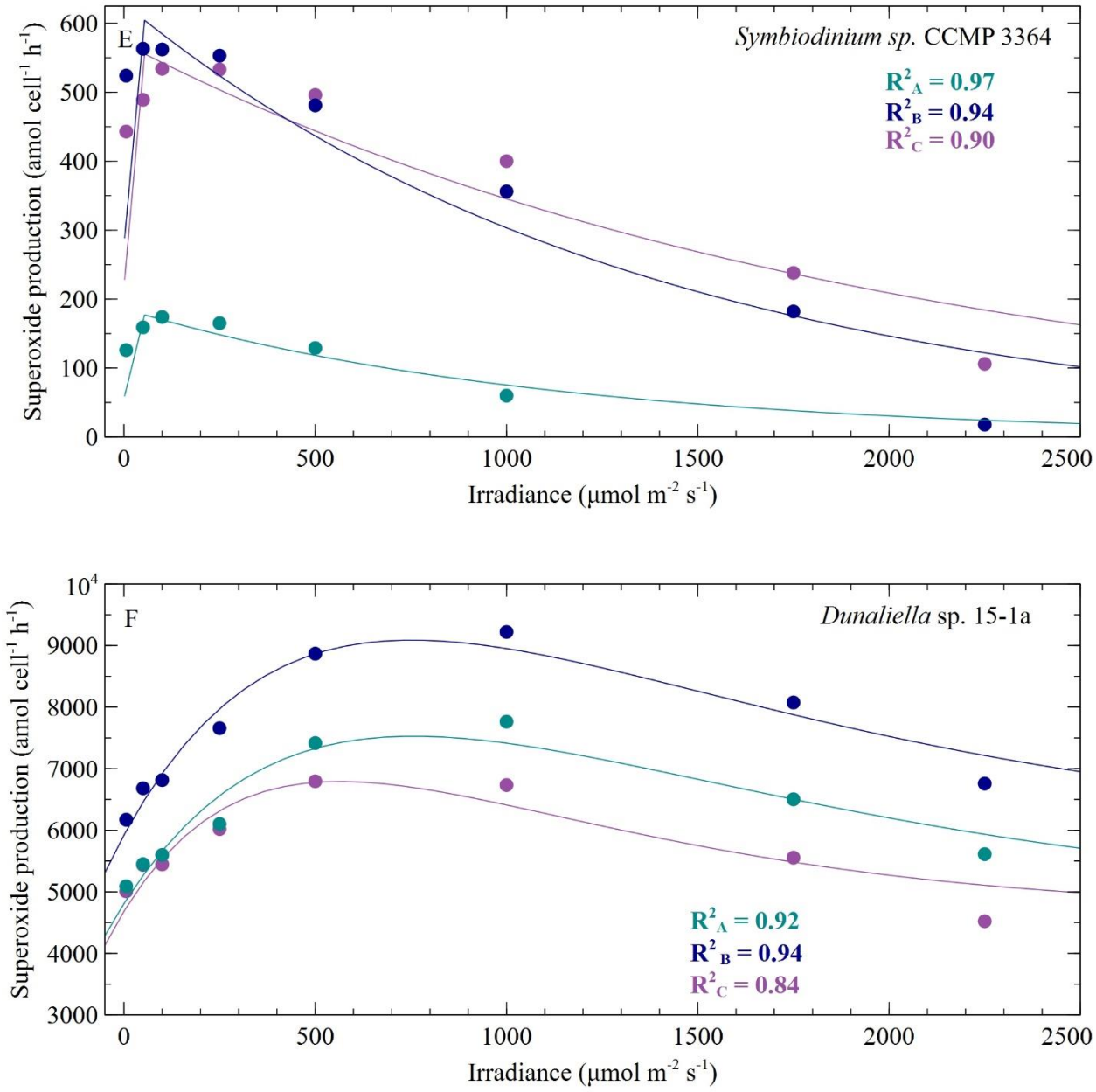

Figure 2.3 Continued: eO_2^- production rates (circles) measured at increasing irradiances from triplicate batch cultures of model phytoplankton strains (A-M). Irradiance and eO_2^- production rate data were fit with a photosynthesis-irradiance model by Platt et al. (1980) that was adapted by Diaz et al. (2019) for eO_2^- production rates (lines). Each color represents a different biological replicate. R^2 values of the model fit for each biological replicate are provided. Model rates are presented in Table 2.3.

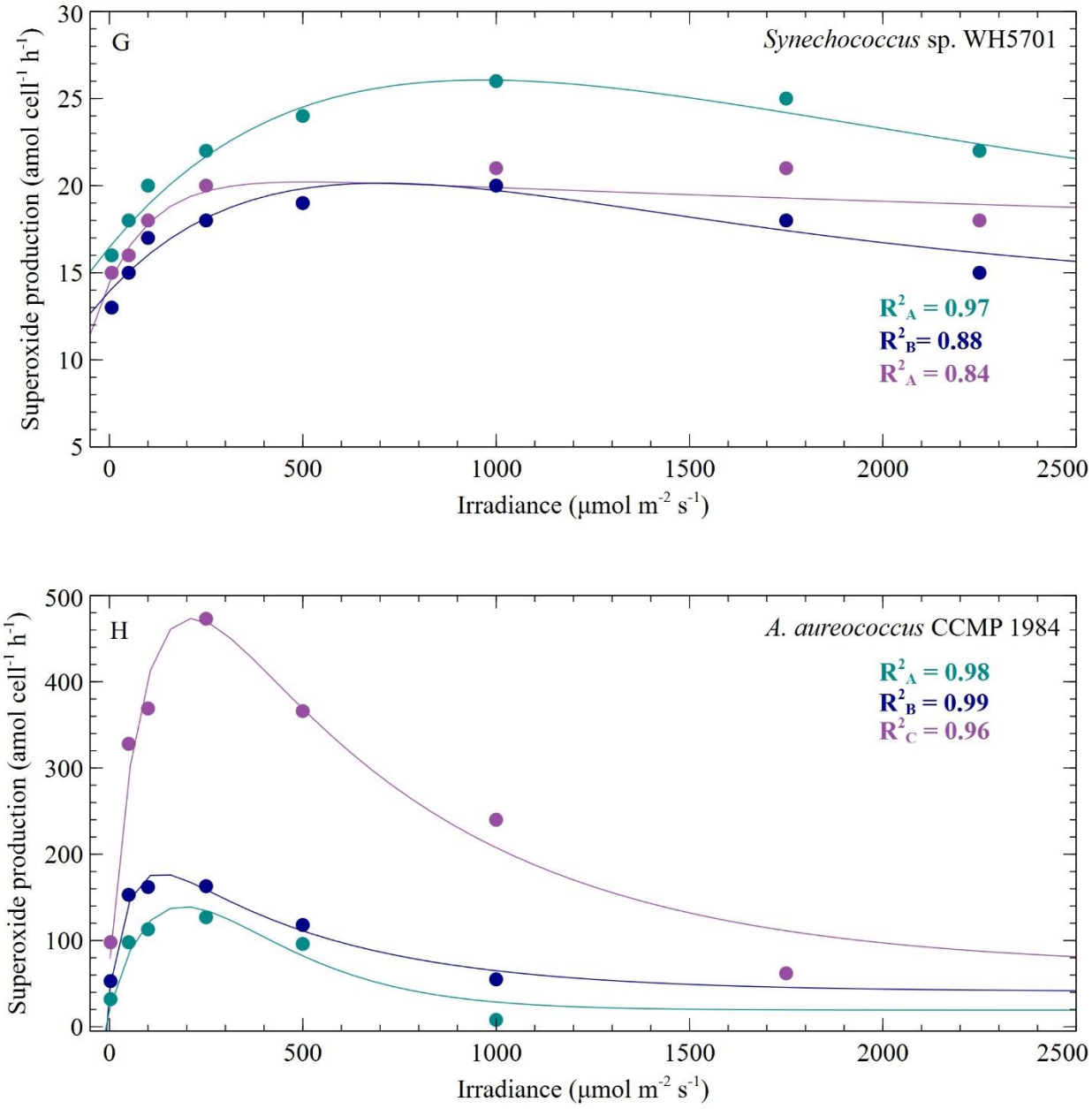

Figure 2.3 Continued: eO_2^- production rates (circles) measured at increasing irradiances from triplicate batch cultures of model phytoplankton strains (A-M). Irradiance and eO_2^- production rate data were fit with a photosynthesis-irradiance model by Platt et al. (1980) that was adapted by Diaz et al. (2019) for eO_2^- production rates (lines). Each color represents a different biological replicate. R^2 values of the model fit for each biological replicate are provided. Model rates are presented in Table 2.3.

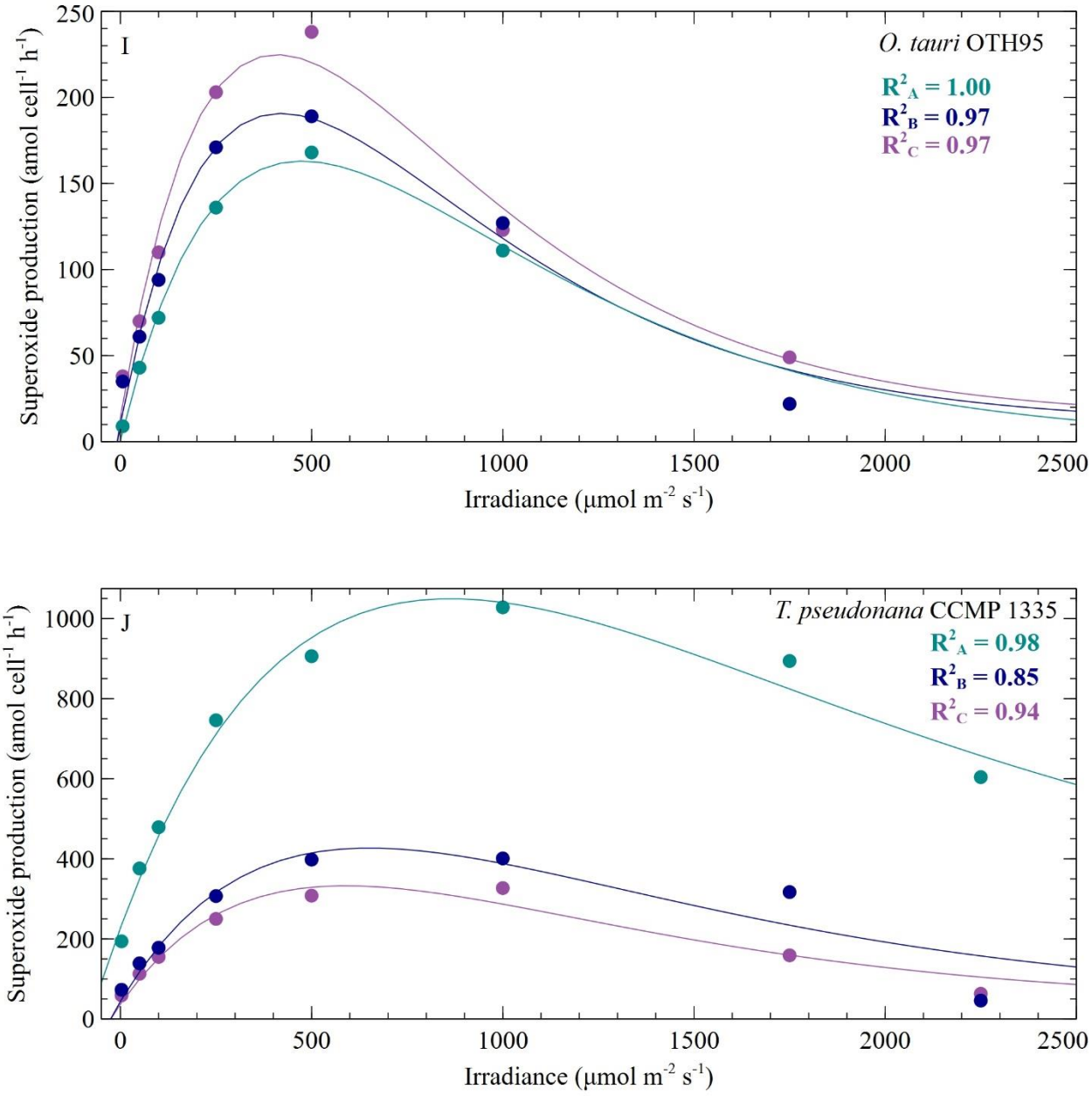

Figure 2.3 Continued: eO_2^- production rates (circles) measured at increasing irradiances from triplicate batch cultures of model phytoplankton strains (A-M). Irradiance and eO_2^- production rate data were fit with a photosynthesis-irradiance model by Platt et al. (1980) that was adapted by Diaz et al. (2019) for eO_2^- production rates (lines). Each color represents a different biological replicate. R^2 values of the model fit for each biological replicate are provided. Model rates are presented in Table 2.3.

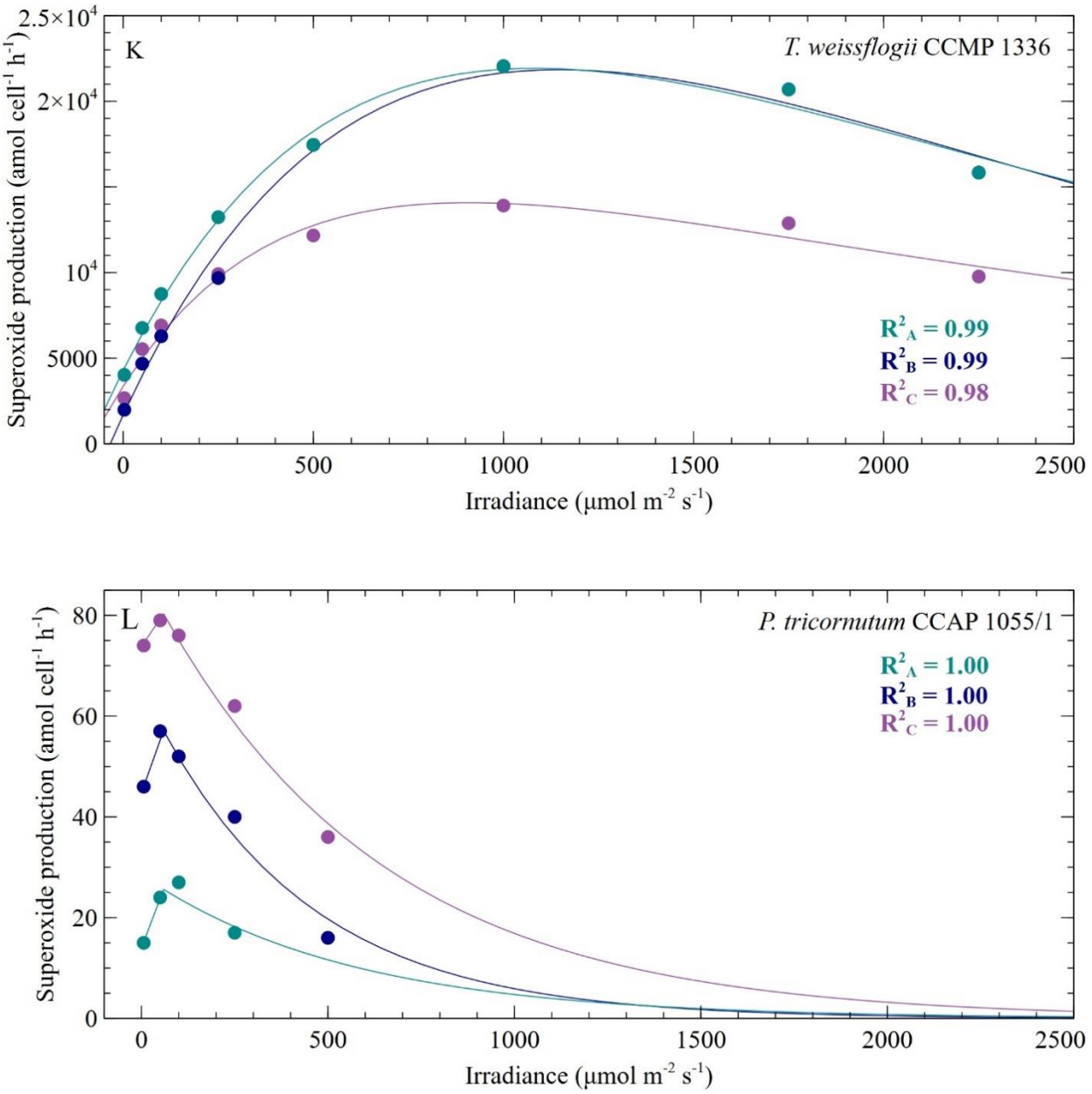

Figure 2.3 Continued: Extracellular superoxide (eO_2^-) production rates (circles) measured at increasing irradiances from triplicate batch cultures of model phytoplankton strains (A-M). Irradiance and eO_2^- production rate data were fit with a photosynthesis-irradiance model by Platt et al. (1980) that was adapted by Diaz et al. (2019) for eO_2^- production rates (lines). Each color represents a different biological replicate. R^2 values of the model fit for each biological replicate are provided. Model rates are presented in Table 2.3.

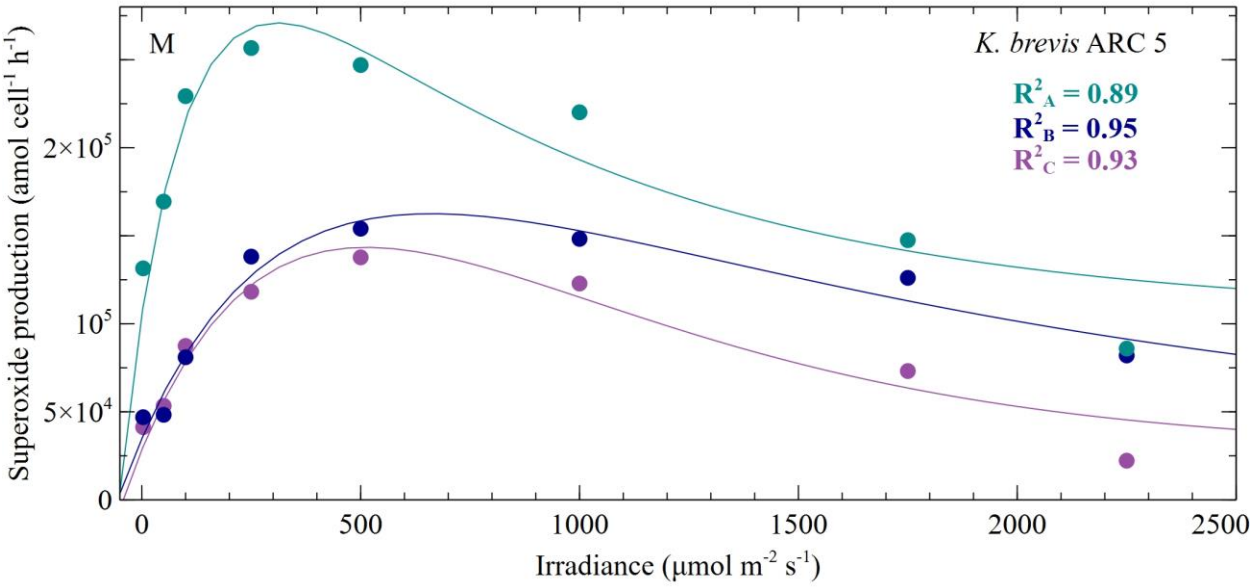

Figure 2.3 Continued: Extracellular superoxide (eO_2^-) production rates (circles) measured at increasing irradiances from triplicate batch cultures of model phytoplankton strains (A-M). Irradiance and eO_2^- production rate data were fit with a photosynthesis-irradiance model by Platt et al. (1980) that was adapted by Diaz et al. (2019) for eO_2^- production rates (lines). Each color represents a different biological replicate. R^2 values of the model fit for each biological replicate are provided. Model rates are presented in Table 2.3.

Table 2.3: eO_2^- irradiance curve parameters. eO_2^- production rates and irradiance data for each biological replicate were fit to a photosynthesis-irradiance model originally by Platt et al. (1980) and adapted for eO_2^- production by Diaz et al. (2019). * = data taken from Diaz et al. 2019 α = the initial linear slope of the best fit curve, β = parameter describing the decrease of eO_2^- at high irradiances, $P_D^{O_2^-}$ = eO_2^- under dark conditions, $P_S^{O_2^-}$ = the estimated light-saturated rate of eO_2^- production if β = 0, $P_M^{O_2^-}$ = light saturated rates of eO_2^- production, $E_k^{O_2^-}$ = minimum saturating irradiance of eO_2^- production

Phytoplankton Strain	Biological Replicate	P_D^{O2-}	P_S^{O2-}	P_m^{O2-}	α	β	E_k^{O2-}	R^2
		amol cell^{-1} h^{-1}			amol cell^{-1} h^{-1} / µmol m^{-2} s^{-1}		µmol m^{-2} s^{-1}	
Synechococcus sp. WH 8102	A	21.1	56.5	67.8	0.053	0.002	1271.2	0.97
	B	35.1	3267.3	69.8	0.013	0.457	5222.2	0.83
	C	28.0	983.3	94.9	0.042	0.206	2260.6	1.00
Synechococcus sp. WH 5701	A	16.5	1068.3	26.1	0.027	1.092	960.6	0.97
	B	13.9	208.6	20.2	0.024	0.285	837.2	0.88
	C	14.4	6.4	20.2	0.049	0.001	414.0	0.84
Prochlorococcus marinus MIT9312	A	7.1	100.9	50.7	0.122	0.049	414.4	0.99
	B	2.2	1864.4	19.2	0.039	1.554	491.8	0.99
	C	7.2	368.4	52.3	0.108	0.272	483.4	0.99
Prochlorococcus marinus NATL2A	A	36.8	80.6	104.7	0.689	0.028	151.9	0.92
	B	16.2	48.0	50.2	0.287	0.030	175.2	0.91
	C	38.5	125.8	127.7	0.738	0.076	173.2	0.95
Emiliania huxleyi CCMP 374	A	475.2	1107.0	1485.0	23.484	0.431	63.2	0.90
	B	162.5	574.9	641.2	11.282	0.499	56.8	0.89
	C	722.1	1185.5	1660.8	12.527	0.764	132.6	0.95
Emiliania huxleyi CCMP 371	A	298.2	1098.6	1238.0	15.891	0.572	77.9	0.96
	B	247.2	704.3	890.5	22.836	0.411	39.0	0.98
	C	314.7	1194.1	1229.5	13.907	1.014	88.4	0.99
Ostreococcus tauri OTH95	A	0.6	25286.4	163.0	0.930	52.801	175.3	1.00
	B	10.2	84543.1	190.6	1.169	200.841	163.1	0.97
	C	13.8	19863.4	224.9	1.401	47.809	160.5	0.97

Table 2.3: Continued: eO_2^- irradiance curve parameters. eO_2^- production rates and irradiance data for each biological replicate were fit to a photosynthesis-irradiance model originally by Platt et al. (1980) and adapted for eO_2^- production by Diaz et al. (2019). * = data taken from Diaz et al. 2019 α = the initial linear slope of the best fit curve, β = parameter describing the decrease of eO_2^- at high irradiances, $P_D^{O_2^-}$ = eO_2^- under dark conditions, $P_S^{O_2^-}$ = the estimated light-saturated rate of eO_2^- production if β = 0, $P_M^{O_2^-}$ = light saturated rates of eO_2^- production, $E_k^{O_2^-}$ = minimum saturating irradiance of eO_2^- production

Phytoplankton Strain	Biological Replicate	P_D^{O2-}	P_S^{O2-}	P_m^{O2-}	α	β	E_k^{O2-}	R^2
		amol cell^{-1} h^{-1}			amol cell^{-1} h^{-1} / µmol m^{-2} s^{-1}		µmol m^{-2} s^{-1}	
Micromonas pusilla CCMP1545	A	294.9	524.7	704.3	6.072	0.402	116.0	0.94
	B	235.3	304.6	504.9	6.958	0.182	72.6	0.97
	C	262.2	311.3	547.0	9.163	0.162	59.7	0.91
Dunaliella sp. 15-1a	A	4806.8	467192.0	7526.7	9.763	612.006	771.0	0.92
	B	5918.7	491118.2	9088.2	11.450	646.982	793.7	0.94
	C	4682.4	429379.0	6791.9	10.165	756.058	668.2	0.84
Symbiodinium sp. CCMP 3364	A	0.0	185.9	180.4	35.457	0.168	5.1	0.97
	B	0.0	628.6	618.0	190.099	0.458	3.3	0.94
	C	0.0	570.8	562.7	143.464	0.287	3.9	0.90
***Karenia brevis* ARC 5**	A	105103.3	289012.8	270949.5	1644.497	342.555	164.8	0.89
	B	34694.2	263581.3	162532.1	569.618	179.279	285.3	0.95
	C	28386.6	88440425.9	143429.3	610.110	172241.168	235.1	0.93
Thalassiosira weissflogii CCMP 1336	A	4298.0	1063152.3	21922.1	44.300	961.037	494.9	0.99
	B	1699.2	749719.2	21840.8	47.775	630.454	457.2	0.99
	C	3365.4	22666.5	14082.3	34.611	11.519	406.9	0.98
Thalassiosira pseudonana CCMP 1335	A	227.3	25891.4	1049.5	2.590	28.719	405.2	0.98
	B	44.1	64340.6	426.8	1.599	98.051	267.0	0.85
	C	37.3	15095.7	332.7	1.364	24.959	243.9	0.94
Thalassiosira oceanica CCMP 1005*	A	28.2	32.9	51.1	0.390	0.010	130.9	0.98
	B	16.7	42.4	57.7	0.340	0.002	167.6	1
	C	29.4	33.6	58.8	0.230	0.007	259.6	0.99

Table 2.3: Continued: eO_2^- irradiance curve parameters. eO_2^- production rates and irradiance data for each biological replicate were fit to a photosynthesis-irradiance model originally by Platt et al. (1980) and adapted for eO_2^- production by Diaz et al. (2019). * = data taken from Diaz et al. 2019 α = the initial linear slope of the best fit curve, β = parameter describing the decrease of eO_2^- at high irradiances, $P_D^{O_2^-}$ = eO_2^- under dark conditions, $P_S^{O_2^-}$ = the estimated light-saturated rate of eO_2^- production if β = 0, $P_M^{O_2^-}$ = light saturated rates of eO_2^- production, $E_k^{O_2^-}$ = minimum saturating irradiance of eO_2^- production

Phytoplankton Strain	Biological Replicate	P_D^{O2-}	P_S^{O2-}	P_m^{O2-}	α	β	E_k^{O2-}	R^2
		amol cell^{-1} h^{-1}			amol cell^{-1} h^{-1} / µmol m^{-2} s^{-1}		µmol m^{-2} s^{-1}	
Phaeodactylum tricornutum CCAP 1055/1	A	0.0	28.5	26.4	3.599	0.051	7.3	1
	B	0.0	65.9	61.7	13.292	0.159	4.6	1
	C	0.0	88.6	85.7	27.372	0.147	3.1	1
***Aureococcus anophagefferens* CCMP 1984**	A	19.3	9196.7	139.4	1.700	47.049	82.0	0.98
	B	40.8	204.9	177.6	3.358	0.438	52.9	0.99
	C	67.6	661.9	473.3	5.965	1.028	79.4	0.96

The light-dependent eO_2^- production results, which show that photoinhibition occurs with increasing light like photosynthesis, also support the hypothesis that eO_2^- production may serve a role in photoprotection. Specifically, the process of making eO_2^- may help phytoplankton cope with light stress by getting rid of excess energy, in the form of electrons, in order to maintain redox balance within the cell. During photosynthesis, light reactions create the compounds NADPH, a reducing compound, and ATP, which are then consumed in the Calvin cycle to fix carbon and in other processes such as biosynthesis. However, more NADPH is created than what is needed for these cellular processes (Behrenfeld et al., 2008). So, cells overcome this excess reducing power issue with a variety of mechanisms that involve forming more ATP or diverting electrons to other pathways (i.e., electron sinks) so that NADPH is not formed (Behrenfeld et al., 2008). For example, in cyclic electron flow, electrons are rerouted from NADP+ reductase back to a ferredoxin-plastoquinone oxidoreductase, which transfers electrons towards PSI again. Thus, cyclic electron flow produces ATP and avoids NADPH production (Behrenfeld et al., 2008). Another way cells divert electrons is through the Mehler reaction, where intracellular oxygen is reduced to O_2^-, which is dismutated to H_2O_2 by superoxide dismutase (SOD) (Cardol et al., 2011). We hypothesized another way cells divert electrons in order to recycle NADPH and maintain redox balance is through eO_2^- production. Specifically, we hypothesized that in *T. oceanica* CCMP 1005, a flavoenzyme with an intra- and extra- cellular side shuttles electrons from NADPH to O_2 on the outside of the cell, thereby making eO_2^- and recycling NADPH to NADP+ (Diaz et al., 2019). In further support of this hypothesis, additions of glycolaldehyde, which inhibit the Calvin-Benson cycle and lead to an accumulation of intracellular NADPH, stimulates eO_2^- production in *C. marina* (Yuasa et al., 2020a). The fact that homologs of this NADPH-oxidizing flavoenzyme found in *T. oceanica* were present in diverse phytoplankton

genomes and throughout the global ocean may mean that this photoprotective mechanism is widespread among phytoplankton (Diaz et al., 2019)

Flavoenzymes are involved in eO_2^- production and health in most phytoplankton

To test the hypothesis that eO_2^- is produced in order to cope with light stress, we first tested whether inhibiting flavoenzymes inhibits eO_2^- production. To do so, we measured eO_2^- production in our model phytoplankton strains with and without the presence of DPI, which blocks electron transfer of flavoenzymes, under each strain's growth irradiance (Table 2.1). In most phytoplankton such as *Thalassiosira pseudonana* CCMP 1335, DPI inhibited eO_2^- production significantly (Figure 2.1). Indeed, addition of DPI resulted in a substantial steady decrease of eO_2^- production on a minutes timescale until production stabilized at lower levels in many strains (Figure 2.4A), suggesting that flavoenzymes are involved in eO_2^- production at least partially. Here and in other studies (Anderson et al., 2016, Diaz et al., 2019, Park et al., 2009, Laohavisit et al., 2015, Saragosti et al., 2010), DPI does not completely eliminate eO_2^- production, potentially suggesting that additional enzymes outside of the flavoenzyme group also contribute to eO_2^- production. However, in *P. tricornutum* CCAP 1055/1, DPI inhibited eO_2^- production below baseline levels (i.e., overall net degradation of eO_2^-) (Figure 2.1A), suggesting that flavoenzymes were entirely responsible for eO_2^- production under these ambient conditions. DPI has been shown to inhibit eO_2^- in a number of phytoplankton species previously, including the diatoms *Thalassiosira weissflogii* (Kustka et al., 2005), *T. pseudonana* (Laohavisit et al., 2015), *T. oceanica* (Diaz et al., 2019), *P. tricornutum* (Laohavisit et al., 2015), the dinoflagellates *Symbiodinium* sp. (Saragosti et al., 2010) and *Procentrum minimum* (Park et al., 2009), and the green alga *Chlamydomonas reinhardtii* (Anderson et al., 2016). Our results and prior evidence of DPI inhibitable eO_2^- production demonstrates that flavoenzymes are involved

in eO_2^- production in many phytoplankton. It remains unclear which flavoenzyme may be regulating eO_2^- production, however, the O_2^- producing Nox (Anderson et al., 2016, Kim et al., 2000) and glutathione reductase (Diaz and Shi, Submitted, Diaz et al., 2019) are probable candidates. Further, both Nox and glutathione reductase could be generating eO_2^- simulataneously. For instance, eO_2^- production was inhibited but not eliminated in mutants of *C. reinhardti* lacking a putative Nox homolog in the respiratory burst oxidase homolog (Rboh) family. The DPI-inhibitable eO_2^- production by the mutant was attributed to another Rboh, however, involvement of other flavoenzymes besides Nox was not ruled out. Contrary to most phytoplankton we surveyed, DPI had no effect on eO_2^- production in the coccolithophore *E. huxley*i CCMP 374 and the coastal *Synechococcus* sp. strain WH5701 (Figure 2.1B-C and 2.4B). Therefore, flavoenzymes are not involved in eO_2^- production in these strains, and another enzyme type may be regulating eO_2^- production.

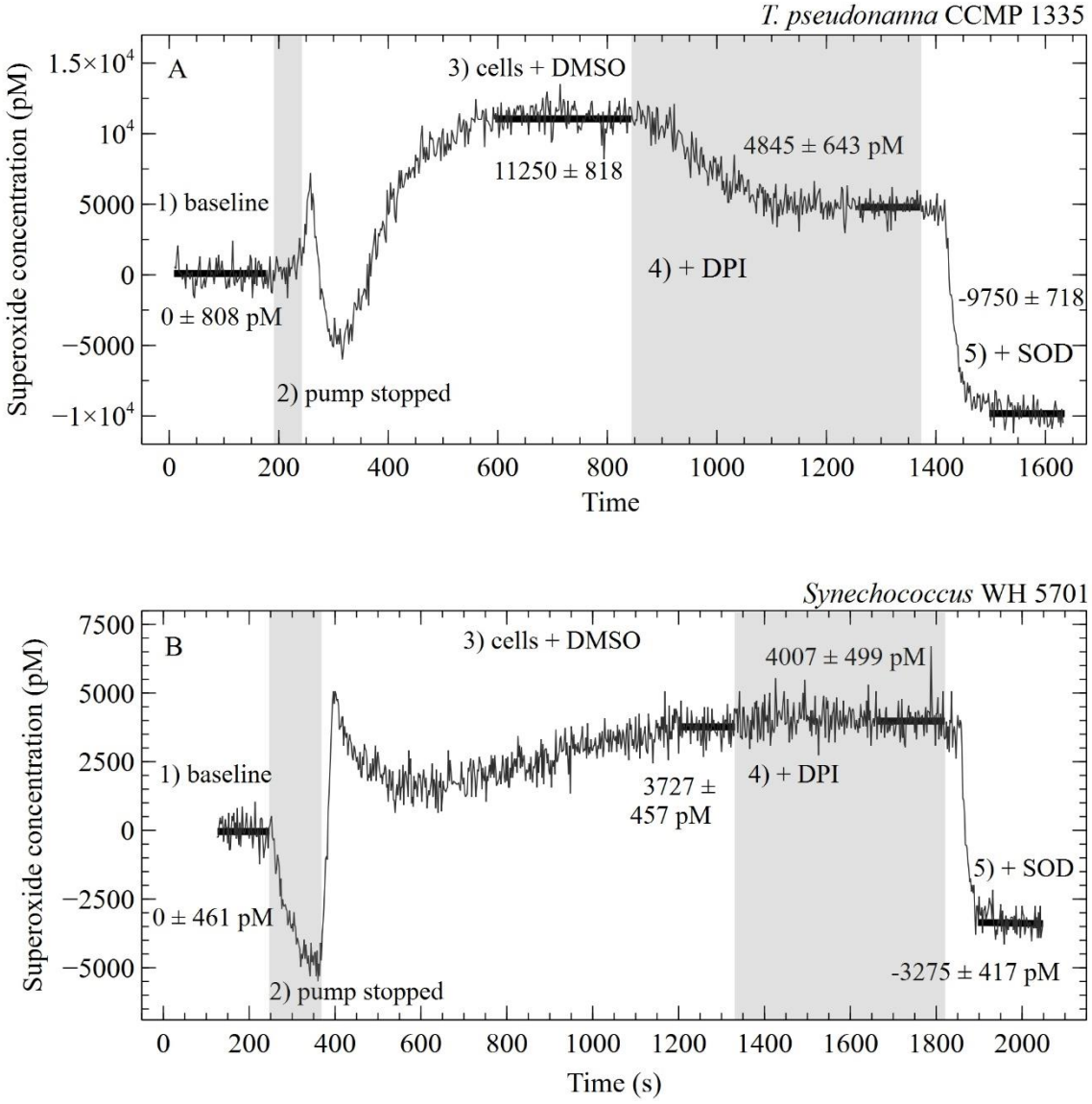

Figure 2.4: FeLume time series of eO_2^- production in the presence and absence of the flavoenzyme inhibitor DPI. All measurements were conducted in 0.3% DMSO. Traces depict the typical inhibiting effect of DPI exemplified by *T. pseudonana* CCMP 1335 (B) and the atypical lack of inhibition exemplified by *Synechococcus* sp. WH 5701. Traces are split into 5 regions: (1) artificial seawater solution and MCLA baseline (which is subtracted from the biological eO_2^- concentration in regions 3-5), (2) shaded region indicating where the pump was stopped to load cells, (3) cells in the presence of DMSO, (4) second shaded region indicating the addition of DPI, and (5) drawdown of the eO_2^- concentration due to addition of SOD (negative eO_2^- concentrations account for SOD degradation of O_2^- originating from autooxidation of the MCLA reagent). Horizontal black lines show the average ± SD of stable eO_2^- concentration measurements.

Next, we tested whether flavoenzymes are necessary for overall health and functioning. To do so, we measured efficiency of PSII and the growth of phytoplankton with and without DPI. Efficiency of PSII describes the efficiency at which light absorbed by PSII is used for electron transport from PSII to the primary quinone electron acceptor of PSII (Baker, 2008). A lower efficiency of PSII indicates higher levels of photoinhibition (Murchie and Lawson, 2013). In nearly all strains where DPI inhibits eO_2^- production, DPI also inhibits photosynthetic health (Figure 2.5) and growth (Figure 2.6). Indeed, incubation with DPI significantly decreased efficiency of PSII in most phytoplankton, especially in the presence of light (Figure 2.5 Group Ia). Some species were sensitive to DPI under dark conditions as well (Figure 2.5 Group Ib). In the diatom *P. tricornutum* CCAP 1055/1 and *O. tauri* CCMP OTH95, inhibiting flavoenzymes with DPI significantly increased photosynthetic efficiency under dark conditions. Yet under light conditions, DPI significantly decreased photosynthetic efficiency in these two strains (Figure 2.5 Group 1c). Therefore, shutting down flavoenzymes in the dark increased photosynthetic efficiency, further demonstrating a light-dependent connection to flavoenzymes. We also found that DPI was lethal to most phytoplankton, with vitality of some phytoplankton being more sensitive to DPI than others (Figure 2.6 Group Ib). Overall, these results (Figure 2.8) demonstrate that flavoenzymes are essential for eO_2^- production and health in most phytoplankton. Further, these findings are consistent with the hypothesis that eO_2^- production is essential for phytoplankton health and that photodamage may be prevented by eO_2^- production.

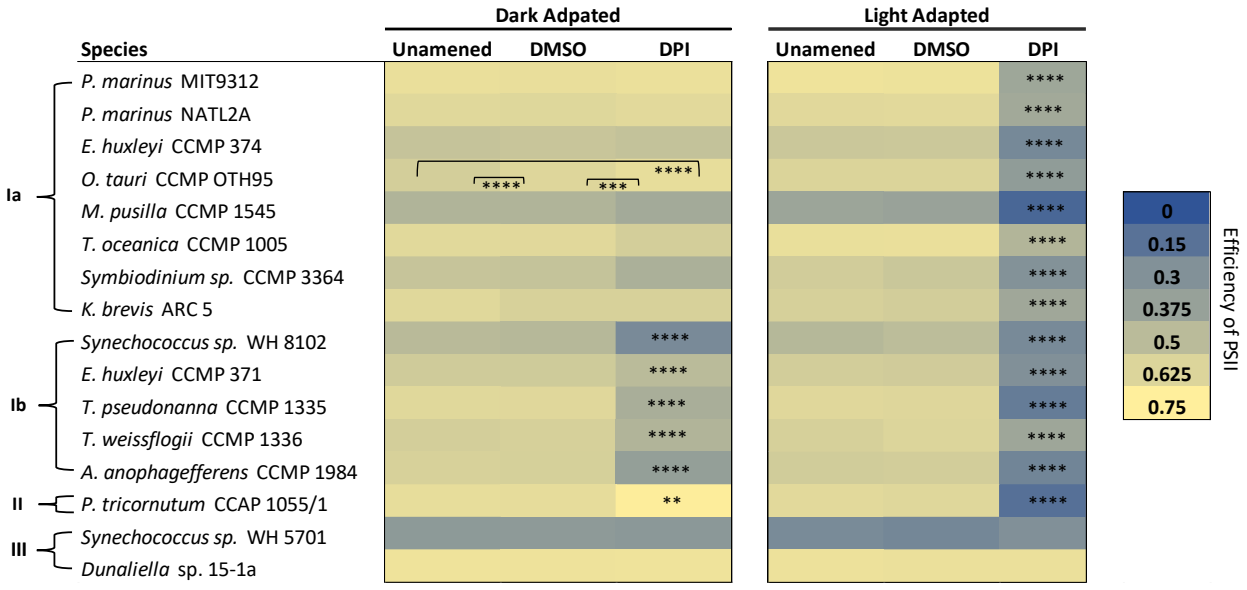

Figure 2.5: Efficiency of PSII (F_v/F_m) in phytoplankton acclimated to their growth irradiance (light adapted) or darkness (dark adapted) and after incubation with or without the flavoenzyme inhibitor DPI. All measurements were conducted in 0.2% DMSO, except the unamended control. Significant differences of the mean F_v/F_m (n = 3 biological replicates) between treatments were found using a Tukey-Honest Significance Difference (HSD) test. P-values are indicated by asterisks, where **, ***, and **** signifies a p-value of <0.01, <0.001, and <0.0001, respectively. Responses of efficiency of PSII to DPI are categorized into four groups: Ia, significant inhibition under light conditions; Ib, significant inhibition under both light and dark conditions; II, significant stimulation under dark conditions yet significant inhibition under light conditions; and III, no effect.

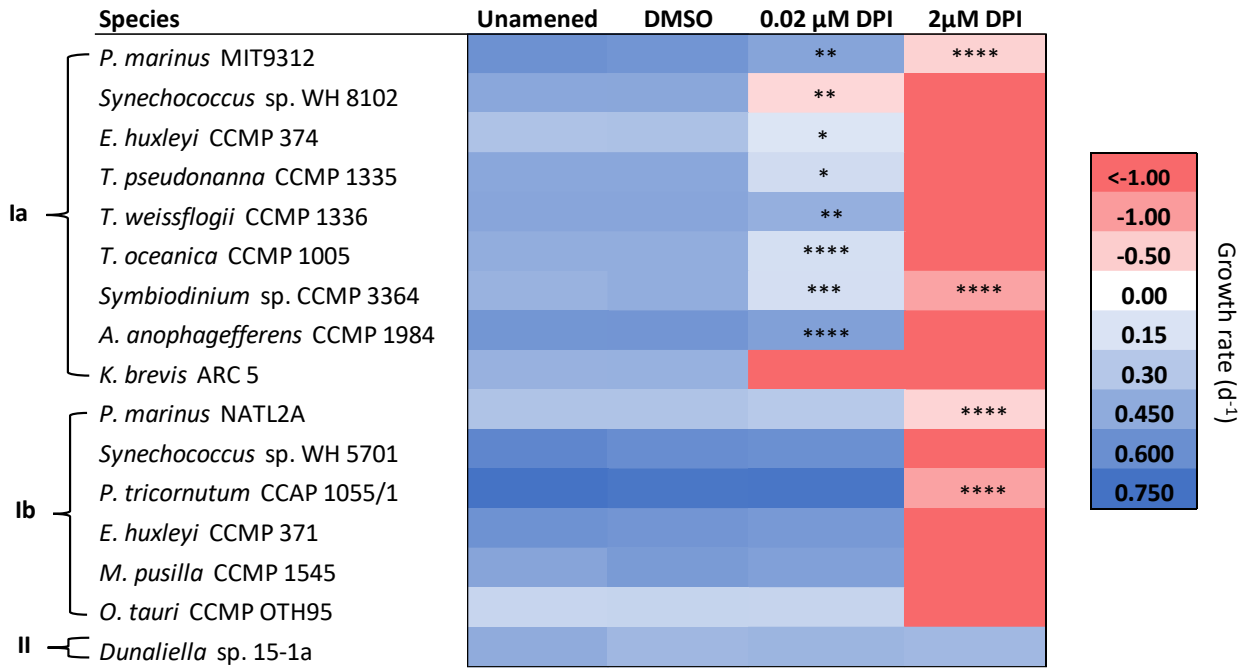

Figure 2.6: Specific growth rates (d^{-1}) of phytoplankton grown in the presence or absence of the flavoenzyme inhibitor DPI. All cultures were grown in 0.03% DMSO, except the unamended control. Growth rates < -1.00 d^{-1} indicate all cells died at a rate that was faster than our limit of detection. Significant differences of mean growth rates > -1.00 (n = 3 biological replicates) between the DPI and DMSO treatments were found using a Student's t-test (unpaired, two-sample). Statistical results between all treatments are shown in Figure 2.7. P-values are indicated by asterisks, where *, **, ***, and **** signifies a p-value of <0.05, <0.01, <0.001, and <0.0001, respectively. Responses of growth rates to DPI are categorized into 3 groups: Ia, declines in both the 0.02 µM DPI and 2 µM DPI treatments; Ib, declines in only the 2 µM DPI treatment; and II, no effect.

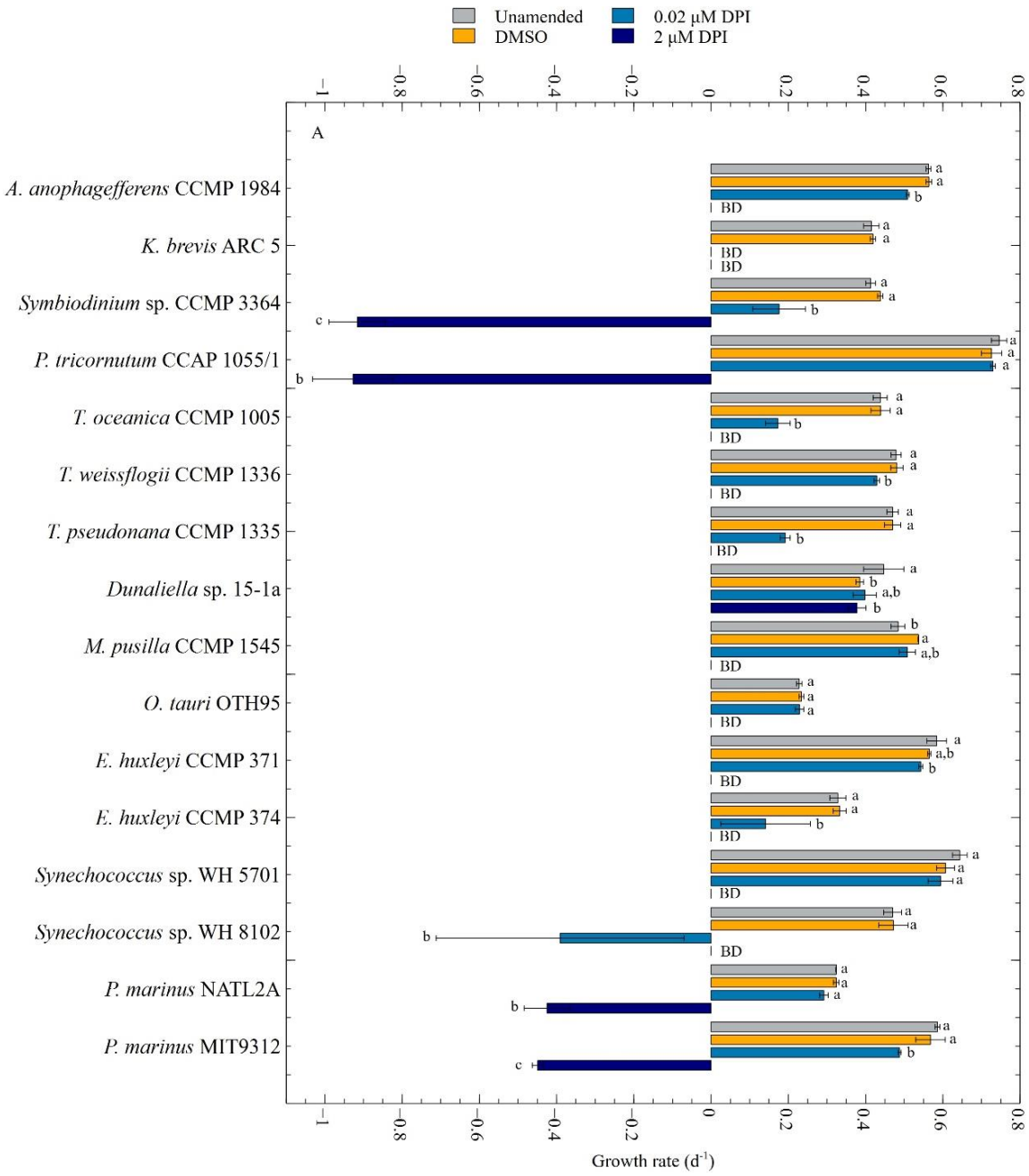

Figure 2.7: Specific growth rates (d^{-1}) of phytoplankton grown in the presence or absence of the flavoenzyme inhibitor DPI. All cultures were grown in 0.03% DMSO, except the unamended control. BD stands for below detection and indicates all cells died at a rate that was faster than our limit of detection. Significant differences of mean growth rates > -1.00 (n = 3 biological replicates) between treatments were found using a Student's t-test (unpaired, two-sample). Treatments not connected by the same letter within a strain are significantly different (p-value < 0.05). Error bars show the standard deviation of the mean of biological replicates (n=3).

However, in cases where DPI inhibits eO_2^- production, there may not be impairments to health from DPI treatments (Figure 2.8). For example, DPI inhibits eO_2^- production (Figure 2.1B) yet has no effect on photosynthetic health (Figure 2.5) or growth rate (Figure 2.6) in the extremophile *Dunaliella* sp. 15-1a (Figure 2.8). While growth rates were slightly lower in the DMSO treatment compared to the unamended (Figure 2.7, $p < 0.05$), there was no significant difference between the DMSO treatment and the two DPI treatments (Figure 2.7, $p > 0.6$). Therefore, it appears that *Dunaliella* sp. 15-1a does not need to produce eO_2^- via flavoenzymes, or perhaps any mechanism, to stay healthy. *Dunaliella* sp. is well to known to be able to grow under hypersaline conditions that limit most life (Boetius and Joye, 2009). Whether other extremophiles need to produce eO_2^- to maintain health remains an open question.

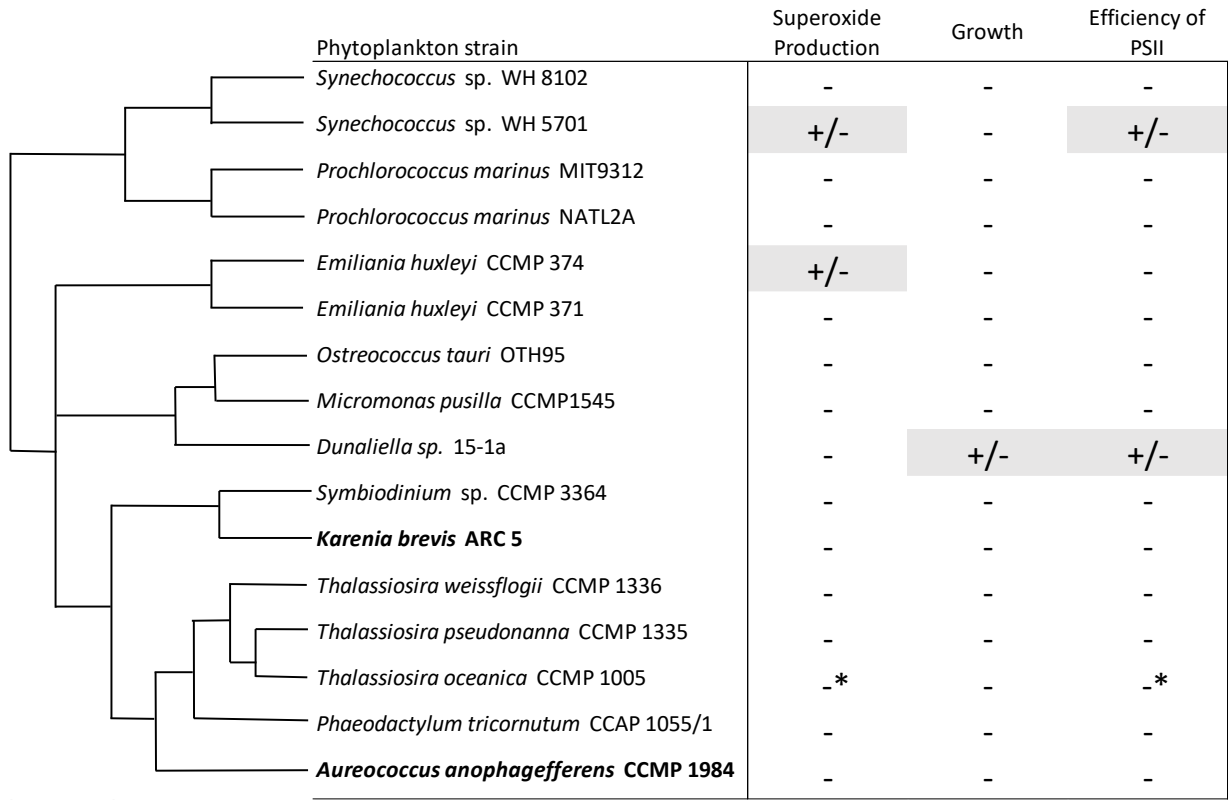

Figure 2.8: Summary of the effect of DPI on eO_2^- production, growth, and efficiency of PSII in 16 strains of prokaryotic and eukaryotic phytoplankton. The symbols - and +/- indicate inhibition and no effect by DPI, respectively. Phylogenetic tree branches show evolutionary relatedness of phytoplankton strains. Bold fond indicates a HAB forming species. * = taken from Diaz et al. 2019

We also found that in cases where DPI does not inhibit eO_2^- production, there may be impairments to health from DPI treatments (Figure 2.8). For instance, in only two species – *E. huxleyi* CCMP 374 and *Synechococcus* sp. WH 5701 – DPI had no effect on eO_2^- production (Figure 2.1B-C and 2.4B). However, in *E. huxleyi* CCMP 374 DPI inhibited both growth and photosynthetic health (Figure 2.5 – 2.6, Figure 2.8), whereas DPI only inhibited growth in *Synechococcus* sp. WH5701 (Figure 2.5 – 2.6, Figure 2.8). So, in *E. huxleyi* CCMP 374, flavoenzymes are essential for photophysiological health, which is essential for vitality. Contrarily, in *Synechococcus* sp. WH5701, flavoenzymes are involved in essential functions unrelated to photophysiology that ultimately impact vitality, consistent with the diverse physiological roles of flavoenzymes (Joosten and van Berkel, 2007). These results also demonstrate that flavoenzyme functions can vary between strains of the same phytoplankton species (Figure 2.8; *E. huxleyi* CCMP 371 and *E. huxleyi* CCMP 374).

Here, we find evidence to support the hypothesis that producing eO_2^- acts as a photoprotective mechanism in phytoplankton. Indeed, most of the phytoplankton surveyed with a few exceptions (*Dunaliella* sp. 15-1a, *Synechococcus* sp. WH5701, and *E. huxleyi* CCMP 374) behaved similarly to *T. oceanica* CCMP 1005. Specifically, eO_2^- production increased with light, and eO_2^- production, photosynthetic health, and growth declined when impairing flavoenzymes (Diaz et al., 2019). These results are consistent with the majority of phytoplankton tested producing eO_2^- via a transmembrane flavoenzyme as a mechanism to maintain redox homeostasis and photosynthetic health, like *T. oceanica* (Diaz et al., 2019).

Production of eO_2^- may serve additional biological functions outside of photoprotection. Indeed, there is much evidence to suggest that eO_2^- production is involved in additional biological purposes outside of photoprotection including physiological processes like growth

regulation and ecological interactions with other microbes (Hansel and Diaz, 2021). In many organisms, ROS are well known signaling molecules (Gough and Cotter, 2011, Bhattacharjee, 2012, Sies and Jones, 2020). Further, in phytoplankton, cell-density dependent production of eROS suggests this production may be involved in signaling as well (Plummer et al., 2019, Diaz et al., 2018, Sutherland et al., 2019, Hansel et al., 2016, Marshall et al., 2005b). Indeed, once eO_2^- forms in the proposed electron sink mechanism to maintain intracellular redox balance, eO_2^- may participate in other biological processes, as O_2^- or possibly its more stable product H_2O_2. In fact, H_2O_2 likely deriving from the Mehler reaction acts as a signal that induces high light dependent gene expression in plant chloroplasts (Exposito-Rodriguez et al., 2017). Further, alternative electron flows in microalgae have been proposed to be involved in signaling in addition to balancing production of ATP and NADPH (Curien et al., 2016). Additionally, previous studies (Saragosti et al., 2010, Diaz et al., 2019, Zhang et al., 2016b) and the present study with the exception of *P. tricornutum* CCAP 1055/1 and *Symbiodinium* sp. CCMP 3364 (Table 2.3), indicate many phytoplankton generate eO_2^- in the dark. Also, the photosynthetic electron transport inhibitor DCMU does not always inhibit eO_2^- production in phytoplankton (Oda et al., 1998, Yuasa et al., 2020b). These results support pathways and purposes for eO_2^- production in addition to photoprotection in many phytoplankton. However, light-independent production of eO_2^- may also help maintain intracellular redox balance and prevent reductive stress. Indeed, the oxidative pentose phosphate pathway is another metabolic pathway in many organisms including phytoplankton that creates NADPH and can lead to intracellular redox imbalance (Wu et al., 2015). Yuasa et al. posited that nutrient deficient cultures of *C. marina* produced elevated levels of eO_2^- to regulate imbalanced NADPH:NADP+ ratios produced by the oxidative pentose phosphate pathway (2020b). Enzyme purification as well as genetic

manipulation in model organisms of flavoenzymes implicated in eO_2^- production would definitively address the metabolic pathways and ecophysiological purposes of eO_2^- production in phytoplankton.

eO_2^- production rates in future oceans

The proposed role of eO_2^- production in photoprotection may have implications for redox conditions of future oceans. Impacts of climate change are predicted to decrease mixed layer depths in some areas of the ocean, potentially trapping phytoplankton in shallower layers of the ocean surface where light levels are most intense (Gao et al., 2012). For example, mixed layer depths in much of the North Pacific Gyre are expected to shoal up to 20 m under future climate conditions (Luo and Rothstein, 2011). Since light driven eO_2^- production is widespread among phytoplankton (Figure 2.2 – 2.3), predicted increases in irradiance may increase eO_2^- production rates in future oceanic regimes. To determine how future shoaling of mixed layer depths may influence eO_2^- production rates in phytoplankton, we first estimated irradiance levels of current and future mixed layer depths (I_z; µmol m^{-2} s^{-1}) in the North Pacific Gyre using an equation that describes how light intensity decreases exponentially with depth:

$$I_z = I_0 e^{-kz} \quad (1)$$

Where $I_0$is the irradiance level at the surface obtained from seasonal PAR ranges (µmol m^{-2} s^{-1}), k is the average light attenuation coefficient (m^{-1}), and z is the mixed layer depth (m) under current and future conditions. The annual mixed layer depth at station Aloha ranges from ~ 20 m – ~120 m, with an annual mean of 60 m (Table 2.4). Assuming a shoaling of 20 m in this region, future mixed layer depths would range from ~ 0 m – ~100 m, with an annual mean of 40 m. Annual surface PAR at station Aloha ranges from 324 µmol m^{-2} s^{-1} – 637 µmol m^{-2} s^{-1} (Table 2.4). Based on our calculations, current I_z ranges from 2.7 – 286.2 µmol m^{-2} s^{-1} and future I_z

ranges from 5.9 – 637 μmol m^{-2} s^{-1} in this region (Table 2.5). Therefore, a shoaling of 20 m at each depth will increase I_z by 123% in the North Pacific Gyre.

Table 2.4: Parameters for estimating eO_2^- production rates from representative phytoplankton groups at current and future mixed layer depth in the North Pacific Gyre. * = data obtained from the Hawaii Ocean Time-series HOT-DOGS application; University of Hawai'i at Mānoa. National Science Foundation Award # 1756517

Parameter (units)	Value	Notes	Source
Surface Par Range (µmol m^{-2} s^{-1})	324 – 637		Estimated from Figure 2 (Letelier et al., 2004)
Surface PAR Median (µmol m^{-2} s^{-1})	480		
Light attenuation coefficient (m^{-1})	0.04		(Letelier et al., 2004)
Mixed Layer Depth Range (m)	20 – 120		HOT-DOGS*
Average Mixed Layer Depth (m)	60		
Prochlorococcus Abundance (cells L^{-1})	5.7×10^7	Divided 10×10^{12} m^{-2} by listed depth integration (175 m)	Table 2 (Bjorkman et al., 2015)
Synechococcus Abundance Range (cells L^{-1})	4.17×10^5 – 2.5×10^6	Divided 0.5×10^{11} m^{-2} by shallowest (20 m) and deepest mixed layer depth (120 m)	HOT-DOGS*
Diatoms Abundance (cells L^{-1})	8.33×10^2 – 5×10^3	Divided 1×10^8 m^{-2} by shallowest (20 m) and deepest mixed layer depth (120 m)	Estimated from Figure 1 (Scharek et al., 1999)
Ostreococcus Abundance (cells L^{-1})	10^3		Figure 9 (Not et al., 2008)
Micromonas Abundance (cells L^{-1})	7×10^3 – 21 $\times 10^3$		Table VI (Furuya and Marumo, 1983)
Coccolithophores Abundance (cells L^{-1})	10^3		Figure 3 (Cortés et al., 2001)

Table 2.5: Current and future ocean conditions of the North Pacific Gyre. MLD = mixed layer depth, I_z = irradiance at depth z, $P_{MLD}^{O_2^-}$ = production of eO_2^- at the mixed layer depth by *Prochlorococcus* which constitute 93% – 99% of $P_{MLD}^{O_2^-}$

		Surface PAR = 324 µmol m^{-2} s^{-1}		**Surface PAR = 637 µmol m^{-2} s^{-1}**	
Ocean Conditions	**MLD (m)**	I_z **(µmol m^{-2} s^{-1})**	$P_{MLD}^{O_2^-}$ **(nM d^{-1})**	I_z **(µmol m^{-2} s^{-1})**	$P_{MLD}^{O_2^-}$ **(nM d^{-1})**
Future	0	324.0	83	637.0	88
Current	20	145.6	66	286.2	81
Future	40	65.4	48	128.6	63
Current	60	29.4	37	57.8	46
Future	100	5.9	27	11.7	30
Current	120	2.7	26	5.2	27

Next, we determined the eO_2^- production rates at each mixed layer irradiance level ($P_{MLD}^{O_2^-}$; amol cell^{-1} h^{-1}) in current and future ocean conditions using the PI model by Platt et al. (1980) which was adapted for eO_2^- production by Diaz et al. (2019) for each representative phytoplankton:

$$P_{MLD}^{O_2^-} = P_D^{O_2^-} + P_S^{O_2^-}\left[1 - e^{\frac{-\alpha}{P_S^{O_2^-}}I_z}\right]e^{\frac{-\beta}{P_S^{O_2^-}}I_z} \quad (2)$$

where, α is the initial linear slope of the best fit curve $\left(\frac{amol\ cell^{-1}h^{-1}}{\mu mol\ m^{-2}s^{-1}}\right)$, β describes the decrease of eO_2^- at high irradiances $\left(\frac{amol\ cell^{-1}h^{-1}}{\mu mol\ m^{-2}s^{-1}}\right)$, $P_D^{O_2^-}$ is the eO_2^- production rate in the dark (amol cell^{-1} h^{-1}), $P_S^{O_2^-}$ is the estimated light-saturated rate of eO_2^- production if β = 0 (amol cell^{-1} h^{-1}), and I_z is the irradiance at the mixed layer depth (µmol m^{-2} s^{-1}) determined from equation 1. Values for variables for equation 2 are listed in Table 2.3. $P_{MLD}^{O_2^-}$ was then multiplied by the mixing layer depth cell concentration (cells L^{-1}) of representative phytoplankton groups using data obtained from oligotrophic gyres (Table 2.4). Here, we assumed that cell abundances in the future would not change. Based on our calculations, *Prochlorococcus* is the dominant eO_2^- producer in the North Pacific Gyre when accounting for cell abundance, producing 93% – 99% of phytoplankton-derived eO_2^-, followed by *Synechococcus* producing 0.5% – 6% of phytoplankton derived eO_2^-. Therefore, we present how eO_2^- production rates by the dominant producer, *Prochlorococcus*, would change under predicted future light levels and mixed layer depths in the North Pacific Gyre.

To calculate *Prochlorococcus* eO_2^- production rates of current and future mixed layer depths ($P_{MLD}^{O_2^-}$), we used the average of parameters in equation 2 measured from *P. marinus* NATL2A and MIT9312. The rates of $P_{MLD}^{O_2^-}$ were then multiplied by 5.71×10^7 cells L^{-1} to extrapolate for cell abundance at mixed layer depths (Table 2.4) and converted to units of nmol L^{-1} d^{-1}. Our estimates of $P_{MLD}^{O_2^-}$ by *Prochlorococcus*, which constitute the majority of $P_{MLD}^{O_2^-}$, ranged from 26 to 81 nM d^{-1} (Table 2.5). These rates are in the same order of magnitude of the upper range of previously measured eO_2^- production rates at station Aloha (Roe et al., 2016). Our estimates may be higher than previous measurements by Roe et al. (2016) due to differences in light levels during analysis or because our estimates are based on models of eO_2^- production measurements from laboratory cultures, which would lack some sources of eO_2^- decay present in natural waters (e.g., bacteria, metals). Based on these calculations, we estimate that *Prochlorococcus* eO_2^- production rates will increase between 6% (for deepest mixing layer depths of 100 m and 120 m when $I_{0\,m} = 324$ µmol m^{-2} s^{-1}) and 37% (for average mixing layer depths of 40 m and 60 m when $I_{0\,m} = 637$ µmol m^{-2} s^{-1}) from current to future conditions in the North Pacific Gyre depending on the season. At the shallowest mixing layer depths (0 m and 20 m) when $I_{0\,m} = 637$ µmol m^{-2} s^{-1}, eO_2^- production rates will increase only by 9% from current to future conditions due to photoinhibition of eO_2^- production. Because *Prochlorococcus* abundances are predicted to increase in this region in the future (at least at the surface) (Flombaum et al., 2013), the estimated future eO_2^- production rates and therefore estimated changes from current to future conditions are likely conservative. Potential increases in eO_2^- production by phytoplankton in brighter mixed layers may have consequences on ROS-driven biogeochemical cycling. For example, dark biological production of eO_2^- was recently estimated to be a sink between 5% and 19% of the global O_2 budget (Sutherland et al., 2020). Given that

light stimulates eO_2^- production in diverse phytoplankton (Figure 2.2 – 2.3), and that light dependent eO_2^- production rates will likely increase in oceanic regions such as the North Pacific Gyre, this sink is likely larger and could increase in the future. ROS also influence biogeochemical cycling of metals and carbon, thereby influencing nutrients and carbon flow, which may be impacted by future changes in eROS production. Overall, we demonstrate that uncovering physiological drivers of microbial eROS production helps our understanding of biogeochemical cycling, microbial functioning, and health of current and future oceans.

Acknowledgements

Chapter 2 is currently being prepared for submission for publication of the material, Plummer, Sydney; Diaz, Julia M. The dissertation author was the primary researcher and author of this material.

The authors thank the Palenik lab, the Bowman lab, the Allen lab, and the Chisholm lab for supplying phytoplankton cultures. Allison Coe from the Chisholm lab is thanked for guidance in culturing *Prochlorococcus*. Susan Garcia is thanked for conducting initial growth and physiology experiments on *Prochlorococcus*. Finally, Whitney King is thanked for assisting in troubleshooting equipment.

CHAPTER 3: BIOLOGICAL REACTIVE OXYGEN SPECIES MAY ACT AS SIGNALS IN MICROZOOPLANKTON GRAZING AND PHYTOPLANKTON GROWTH

Abstract

Reactive oxygen species (ROS), including hydrogen peroxide (H_2O_2) and superoxide (O_2^-), are ever-present in aquatic systems where they play important biogeochemical roles. Phytoplankton are a major source of ROS in marine waters; however, the ecological and physiological relevance of this extracellular ROS (eROS) production is mysterious because natural ROS concentrations are usually too low to be directly harmful. To clarify the ecophysiological function of eROS, we interrogated whether extracellular H_2O_2 (eH_2O_2) influences microzooplankton grazing and phytoplankton growth rates as a signaling molecule in natural plankton communities of the South Atlantic Bight (southeastern USA). Biological eH_2O_2 production rates were inversely correlated with microzooplankton grazing and phytoplankton intrinsic growth rates. Consistent with these in situ observations, community phytoplankton intrinsic growth and microzooplankton grazing rates decreased in field incubations where eH_2O_2 production was stimulated by additions of the enzyme superoxide dismutase (SOD). Additionally, biological eH_2O_2 production rates were inversely related to phytoplankton abundance, indicating population density-dependent controls over H_2O_2 production consistent with a signaling function. Biological eH_2O_2 production rates measured under dark conditions were also inversely related to in situ levels of photosynthetically active radiation (PAR), consistent with cells maintaining internal clock regulation of eH_2O_2 production. We propose that plankton-derived eH_2O_2 acts as a dynamic signaling molecule that may shape microbial community dynamics by mediating phytoplankton growth and microzooplankton grazing interactions.

Introduction

Reactive oxygen species (ROS) are prevalent throughout aquatic systems. ROS include intermediates that form during the reduction of molecular oxygen (O_2) to water: superoxide (O_2^-), hydrogen peroxide (H_2O_2), and the hydroxyl radical (OH•). In marine and freshwater environments, ROS drive biogeochemical reactions that can shape the fate and availability of metal nutrients (e.g., iron) (Rose, 2012, Wuttig et al., 2013), toxic metals (e.g., mercury) (Siciliano et al., 2002), carbon (Heller and Croot, 2010b), and oxygen (Sutherland et al., 2020).

Aquatic ROS can form through abiotic and biotic mechanisms. Photochemical degradation of chromophoric dissolved organic matter (CDOM) is the ultimate abiotic source of ROS (Garg et al., 2011, Zinser, 2018). In addition to abiotic sources, microbes influence aquatic ROS pools through both decay (Hopwood et al., 2018, Morris et al., 2022) and production pathways (Diaz and Plummer, 2018) across diverse aquatic environments (Marsico et al., 2015, Rose et al., 2008, Zhang et al., 2016b). Extracellular ROS (eROS) production by marine microbes is taxonomically widespread (Sutherland et al., 2019, Diaz et al., 2013, Diaz and Plummer, 2018) , and at times, microbial eROS production can even exceed abiotic sources in aquatic systems (Marsico et al., 2015, Rose et al., 2008, Vermilyea et al., 2010b).

Unlike photochemically-derived ROS, phytoplankton and bacteria produce eROS (Hansel et al., 2016, Marshall et al., 2002, Saragosti et al., 2010) through a number of pathways that do not necessarily depend on light (Hansel and Diaz, 2021). Indeed, microbial eROS production occurs over entire diel cycles (Morris et al., 2016, Rose et al., 2008, Zhang et al., 2016b), and during the night or in aphotic waters, microbes are the dominant contributors to extracellular H_2O_2 (eH_2O_2) (Zhang et al., 2016b, Vermilyea et al., 2010b) and O_2^- (eO_2^-) production (Diaz et al., 2013, Rose et al., 2008, Zhang et al., 2016b). In fact, most biologically-

derived aquatic eROS originates from active enzymatic production at the cell surface, rather than diffusion or passive bursts of ROS via cell lysis (Rose, 2012).

Although microbial communities clearly play an important role in aquatic eROS cycling, the impact of eROS on aquatic life is not completely understood. Overproduction and accumulation of ROS can lead to oxidative stress and damage to biomolecules. However, aquatic eROS concentrations are typically below levels that could cause any harm to most microorganisms (Morris et al., 2022). Instead, eROS production serves beneficial signaling functions across diverse life forms (Aguirre and Lambeth, 2010, Babior, 1999, Hansel et al., 2019, Oda et al., 1995, Saran, 2003, Weinberger, 2007). From microbes to mammals, one of the beneficial signaling roles of ROS is growth regulation (Hansel et al., 2019, Aguirre and Lambeth, 2010, Bauer, 2014, Rossi et al., 2017, Aguirre et al., 2005). Indeed, laboratory evidence from monocultures suggests that eROS serve as autocrine growth promoters and population density-dependent cell signaling molecules in phytoplankton (Diaz et al., 2018, Marshall et al., 2005b, Oda et al., 1995, Sutherland et al., 2019). However, the potential role of eROS as growth promoters in natural marine microbial communities remains largely unexplored.

Additionally, some evidence suggests eROS signaling could shape microbial predator-prey interactions. For example, degrading eROS increased survival of protistan predators in the presence of the toxic phytoplankton prey species *Alexandrium* (Flores et al., 2012). Also, some phytoplankton species increase eO_2^- production in response to lectins (Oda et al., 1998), which are carbohydrate binding proteins involved in prey sensing and capture by microzooplankton (Wootton et al., 2007). Based on these findings, Martel (2009) proposed that the binding of grazer-derived lectins to prey cell membranes stimulates an oxidative burst to deter predators, however this hypothesis was not tested (Martel, 2009). Similar dynamics may be conserved in

higher taxa, such as macroalgae like the kelp *Ascoseira mirabilis*, which produces an oxidative burst of eH_2O_2 that inhibits amphipod grazing (McDowell et al., 2016, McDowell et al., 2014). However, to our knowledge the effect of eROS on microzooplankton grazing rates has not been tested.

The goal of the present study was to determine whether eH_2O_2 influences microzooplankton grazing and phytoplankton growth in the field. Consistent with this hypothesis, we found that eH_2O_2 production varied inversely with microzooplankton grazing and phytoplankton intrinsic growth, as well as photosynthetically active radiation (PAR) and phytoplankton abundance, indicating dynamic regulation consistent with a signaling role. In further agreement, we accelerated natural rates of eH_2O_2 production via enzyme additions in field experiments and found that bulk community phytoplankton intrinsic growth and microzooplankton grazing rates declined in response. Overall, these results help illuminate the community-level ecophysiology of biological eROS production and its impacts on microbial communities and phytoplankton population dynamics.

Methods

Field stations and sampling

Phytoplankton intrinsic growth, microzooplankton grazing rates, phytoplankton cell abundance and biomass (i.e., chlorophyll concentrations), physicochemical conditions (Table 3.1), and eH_2O_2 production were measured in October 2017 at the continental shelf station Grazer (31°28'39.00"N, 80°28'14.16"W; Figure 3.1). At station Grazer, water samples were collected from the *R/V Savannah* at 5 m depth using a Niskin rosette equipped with a Conductivity Temperature Depth (CTD) instrument. Water samples were collected every 3-4 hours over one day while the ship maintained its position. Physicochemical data were collected

via the ship's automated in situ sensors. Phytoplankton intrinsic growth, microzooplankton grazing rates, and physicochemical conditions (Table 3.1) were also assessed in the Skidaway River estuary from the Skidaway Institute of Oceanography dock in July 2017 (station Skidaway; 31°59'21.48"N, 81° 1'25.82"W; Figure 3.1). At station Skidaway, water samples and physicochemical data were collected at one timepoint (i.e., noon) at 1 m depth during high tide using a single Niskin bottle and a Yellow Springs Instruments (YSI) field probe (YSI 600 QS), respectively.

Table 3.1: Physicochemical data and biological eH_2O_2 production rates volume-normalized (nM h^{-1}) and normalized to biomass (nmol µg chl^{-1} h^{-1}, nmol µg C h^{-1}) and cell abundance (fmol $cell^{-1}$ h^{-1}) collected over the one-day sampling period at station Grazer in the South Atlantic Bight and at station Skidaway in the Skidaway River estuary. The average ± standard deviation of replicate measurements of H_2O_2 production rates is shown (n = 3 except for the eH_2O_2 production rates at 12:00 where n = 2). PAR = photosynthetically active radiation

Station	Time	Temperature (°C)	Salinity (PSU)	PAR (µmol photons m^{-2} s^{-1})	eH_2O_2 (nM h^{-1})	eH_2O_2 (nmol µg chl^{-1} h^{-1})	eH_2O_2 (fmol $cell^{-1}$ h^{-1})	H_2O_2 (nmol µg C^{-1} h^{-1})
Grazer	12:00	23.5	35	160.7	15 ± 5	17 ± 5	115 ± 36	387 ± 120
	16:00	23.6	35	28.02	38 ± 11	35 ± 10	346 ± 101	1270 ± 337
	20:00	23.4	35	4.14	48 ± 10	46 ± 9	424 ± 87	1502 ± 170
	0:00	23.5	35	0	33 ± 5	43 ± 6	267 ± 40	992 ± 342
	4:00	23.2	35	4.22	29 ± 7	42 ± 10	220 ± 50	791 ± 128
	8:00	23	35	23.5	28 ± 9	35 ± 12	221 ± 75	799 ± 406
	11:00	23	35	44.94	27 ± 3	32 ± 4	236 ± 29	855 ± 65
Skidaway	12:00	29.8	32	-	-	-	-	-

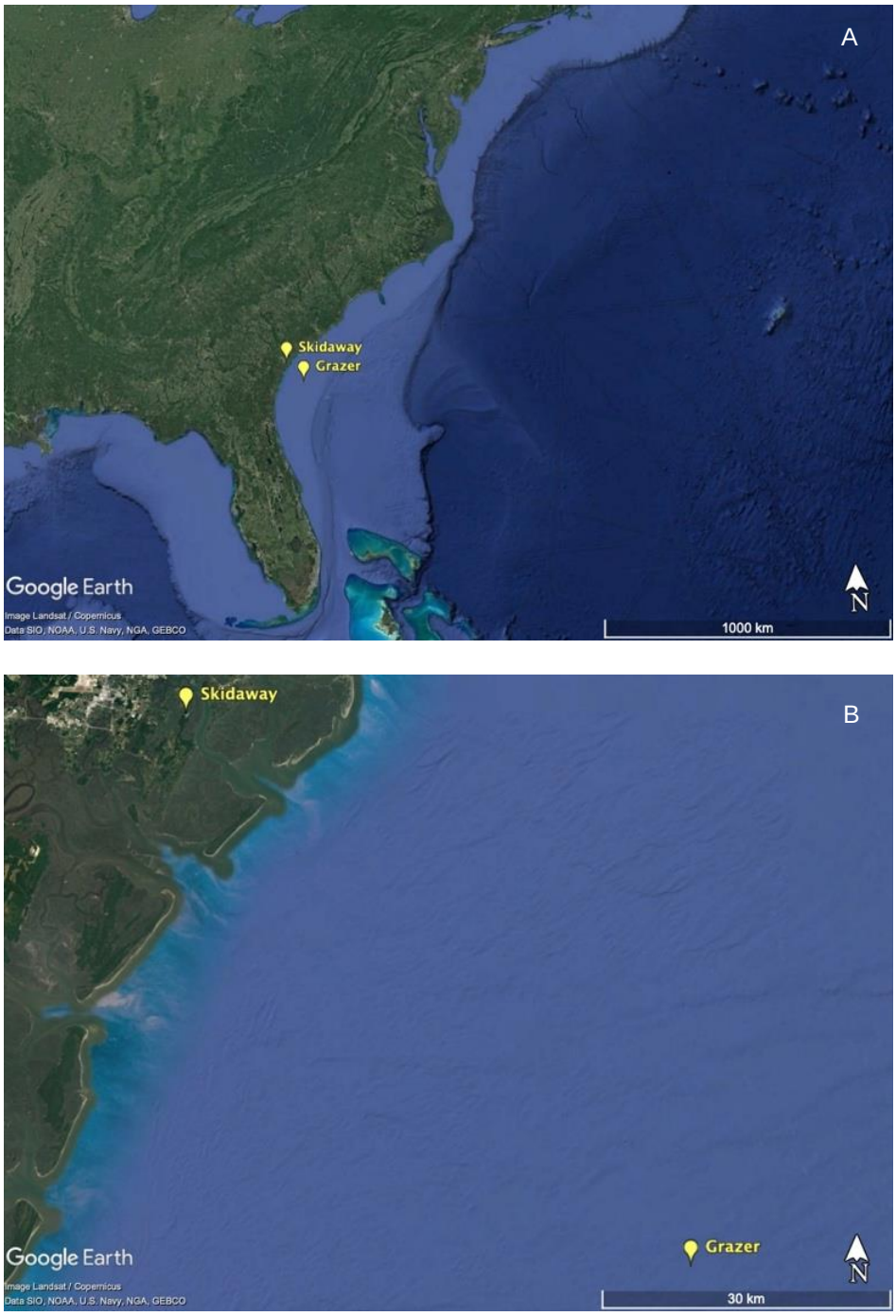

Figure 3.1: Dilution incubations and sampling were conducted at station Skidaway in the Skidaway River estuary (31°59'21.48"N, 81° 1'25.82"W) and on the continental shelf at station Grazer in the South Atlantic Bight (31°28'39.00"N, 80°28'14.16"W) off the coast of Georgia, USA. Zoomed out view of stations off the eastern USA coastline (A) and detail of the Georgia coastline (B) are provided.

Flow cytometry

Flow cytometry samples were filtered (40 µm) to remove larger particles, preserved using 0.5% glutaraldehyde (final concentration), and stored at -80°C prior to analysis. Phytoplankton abundances (cells mL^{-1}) were obtained by analyzing samples at a low flow rate (0.24 µL s^{-1}) for 3 min on a Guava® easyCyte flow cytometer. Three phytoplankton groups (< 15 µm) were distinguishable based on plots of red fluorescence and forward scatter (picoeukaryotes, nanoeukaryotes) and orange fluorescence and forward scatter (phycoerythrin-containing *Synechococcus* spp.). Cell concentrations of each phytoplankton group were converted to phytoplankton carbon biomass (µg C^{-1} L^{-1}), as described by (Anderson et al., 2018).

Chlorophyll

Samples were collected for chlorophyll analysis by filtering seawater (150-200 mL) onto 25 mm GF/F filters (0.7 µm nominal pore size) in the dark. Samples were extracted in the dark for 8-15 hours and according to standard procedures (Jespersen and Christoffersen, 1987, Strickland, 1972). Then, chlorophyll content was measured using a 10-AU™ fluorometer with and without additions of hydrochloric acid to distinguish the phaeopigment content of each sample. The chlorophyll concentrations presented are corrected for phaeopigment concentrations.

Biological eH_2O_2 production

Extracellular H_2O_2 was quantified using a colorimetric technique, in which horseradish peroxidase (HRP) catalyzes the reaction between eH_2O_2 and the colorimetric probe Ampiflu™ Red, as previously described (Diaz et al., 2018, Zhang et al., 2016b). HRP is too large (40 kDa) to move across cellular membranes and can only interact with eH_2O_2. Therefore, this technique only measures eH_2O_2. Seawater was collected and filtered (200 µm) directly from Niskin bottles

into opaque, amber bottles and immediately analyzed in microplates using a SpectraMax M series multimode plate reader using absorbance mode (530 nm and 700 nm). Each well received 50 µM Ampiflu^{TM} Red and 1 kU L^{-1} HRP (final concentrations). The H_2O_2-degrading enzyme catalase (20 mg L^{-1}) was added to seawater blanks to account for autooxidation of Ampiflu^{TM} Red. Three-point standard calibration curves were created in 0.22 µm filtered seawater using H_2O_2 stocks with known concentrations (Figure 3.2). The R^2 of calibration curves was 0.96 ±0.04 (avg. ±SD) (Table 3.2).

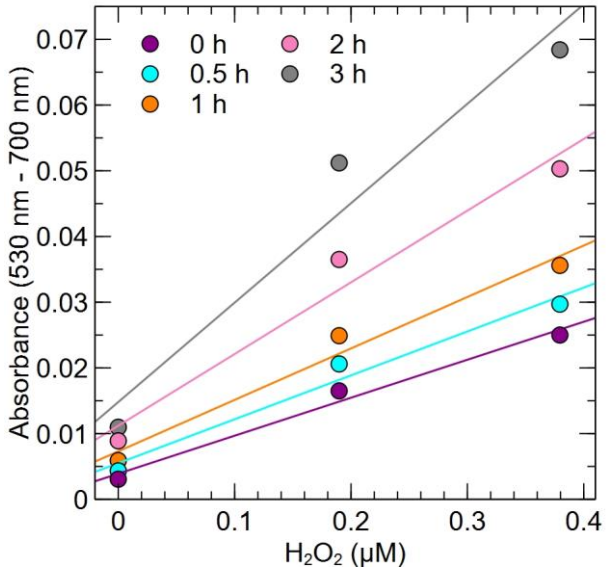

Figure 3.2: Representative standard calibration curve for eH_2O_2 production analyses conducted at each timepoint (see legend, e.g., 0 h) at the 12:00 sampling time over the one-day sampling period. To create a calibration curve, a primary stock solution of H_2O_2 was quantified by measuring absorbance at 240 nm and applying the molar extinction coefficient of H_2O_2 at this wavelength (38.1 L mol^{-1} cm^{-1}) (Miller and Kester, 1988). Three-point standard calibration curves with known H_2O_2 concentrations were created in 0.22 µm filtered seawater (0 µM H_2O_2, 0.190 µM H_2O_2, 0.380 µM H_2O_2). Simple linear regression analyses were used to find the slope and y-intercept of standard curves at each timepoint (e.g., 0 h). Slopes, y-intercepts, and correlation coefficients (R^2) of standard calibrations curves from each sampling time (e.g., 12:00) are listed in Table 3:2.

Table 3.2: Slope, y-intercept, and R^2 of H_2O_2 standard calibration curves at each timepoint throughout the one-day sampling period.

Sampling time (h)	Timepoint (h)	Slope	y-intercept	R^2
12:00	0	0.0578	0.0039	0.98
	0.5	0.0668	0.0055	0.97
	1	0.0783	0.0073	0.97
	2	0.1091	0.0112	0.96
	3	0.1513	0.0148	0.95
16:00	0	-	-	-
	0.5	0.0566	0.0052	0.99
	1	0.0662	0.0072	0.99
	2	0.0942	0.0105	0.97
	3	0.1295	0.0138	0.94
20:00	0	0.0569	0.0049	0.96
	0.5	0.0626	0.0062	0.95
	1	0.0725	0.0082	0.93
	2	0.0996	0.0126	0.88
	3	0.1356	0.0179	0.84
24:00	0	0.0524	0.0049	0.98
	0.5	0.0592	0.0067	0.96
	1	0.0717	0.0085	0.95
	2	0.1268	0.0116	0.98
	3	0.1301	0.0183	0.85
4:00	0	0.0578	0.0056	0.99
	0.5	0.0641	0.0065	0.98
	1	0.0753	0.0085	0.97
	2	0.1149	0.0115	0.97
	3	0.1445	0.0156	0.96
8:00	0	0.0532	0.0051	1.00
	0.5	0.0610	0.0067	0.99
	1	0.0704	0.0080	0.99
	2	0.1064	0.0113	0.97
	3	0.1419	0.0136	0.97
11:00	0	0.0585	0.0033	1.00
	0.5	0.0643	0.0047	1.00
	1	0.0704	0.0063	1.00
	2	0.0806	0.0125	0.84
	3	0.1240	0.0136	0.98
Average ± SD		-	-	**0.96 ± 0.04**

Microplates were analyzed every 0.5-1 h for 3 h to determine eH_2O_2 production rates. First, the absorbance value at 700 nm was subtracted from the absorbance value at 530 nm at each time point. Then, the corrected absorbance values were converted to H_2O_2 concentrations using the slope and y-intercept of the standard calibration curve (Table 3.2). Next, eH_2O_2 concentrations in catalase-amended seawater blanks were subtracted from eH_2O_2 concentrations at each time point. Production rates of eH_2O_2 were determined as the increase in eH_2O_2 concentration over time using simple linear regression ($R^2 \geq 0.91$) (Figure 3.3).

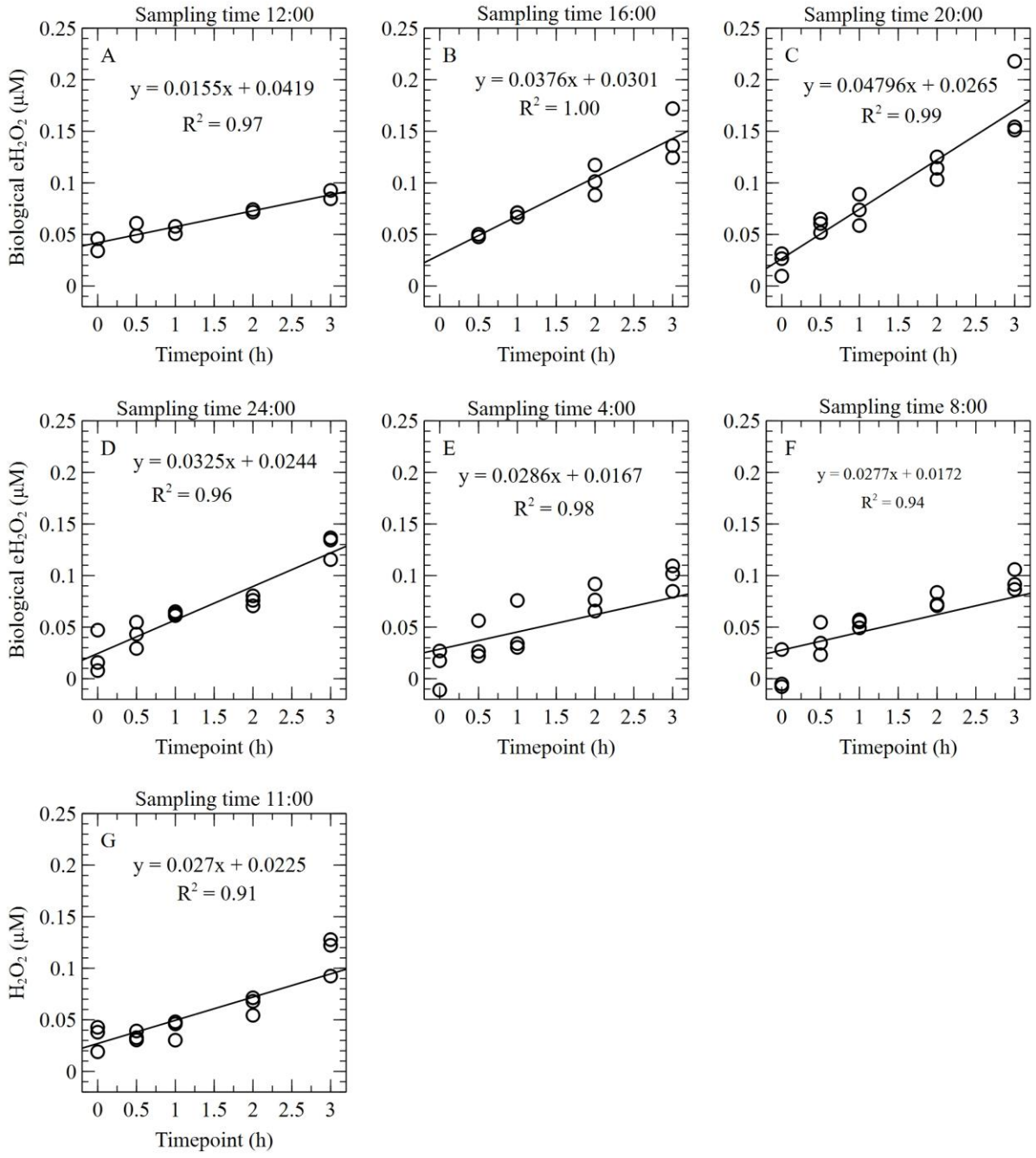

Figure 3.3: Concentrations of eH_2O_2 measured at each timepoint (e.g., 0 h) at each sampling time (e.g., 12:00) over the one-day sampling period. Simple linear regression analyses were used to find the slope of concentrations over time, thereby giving the production rate. Correlation coefficients (R^2) are provided.

Samples were incubated in the dark by leaving the microplate inside the plate reader between timepoints. Therefore, eH_2O_2 production rates exclude the dominant abiotic source of H_2O_2, which is photochemistry, and instead represent eH_2O_2 production by microbial processes only. These rates account for simultaneous production and decay of H_2O_2 by microbes and therefore reflect net production, as previously described (Audi et al., 2018, Roach et al., 2015). We normalized eH_2O_2 production rates to bulk biological parameters (i.e., chlorophyll, phytoplankton cell abundance, or phytoplankton carbon biomass) to account for any variability due to biomass fluctuations.

Dilution incubations

Rates of phytoplankton intrinsic growth and microzooplankton grazing were quantified using a modified version of the Landry and Hassett dilution method, which creates a gradient of predator-prey encounter rates via seawater dilution (Landry and Hassett, 1982). Intrinsic growth rate refers to the growth rate of phytoplankton in the absence of grazing. Here, a two-point dilution method was employed, which is comparably accurate to the original multilevel dilution technique (Morison and Menden-Deuer, 2017).

To conduct the two-point dilution incubations, seawater was gravity-filtered through 200 µm Nitex mesh to remove mesozooplankton. A portion of this seawater was left undiluted, while the rest was diluted 5-fold with 0.45 µm gravity filtered seawater collected on site (PALL Acropak™ Supor® membrane capsule), similar to previous studies (Anderson et al., 2018, Anderson and Harvey, 2019). Aliquots of the undiluted and 5-fold diluted seawater were carefully siphoned into triplicate polycarbonate bottles. Bottles were incubated for 24 hours in tanks with seawater flow-through from the sampling site. Tanks were covered with mesh screening to mimic in situ light conditions.

Rates of community-level and group-specific microzooplankton grazing (g; d^{-1}) and phytoplankton intrinsic growth (μ; d^{-1}) were estimated from chlorophyll content and group-specific cell concentration measurements, respectively. Apparent growth rates (k; d^{-1}) were found using the equation:

$$k = \frac{ln\frac{A_1}{A_0}}{t}$$

where A_0 and A_1 refer to the average chlorophyll concentration or cell concentration before (0 h) and after (24 h) incubation, respectively, and t is the incubation time of one day. The presence of nutrient limitation was assessed to control for effects on k (Morison and Menden-Deuer, 2017). Potential nutrient limitation was assessed by performing an independent Student's t-test on the apparent growth rates (k) in unamended vs. nutrient amended treatments (10 µM nitrate + 1.1 µM phosphate at station Skidaway, 40 µM nitrate + 4 µM phosphate at station Grazer). At station Grazer, half of the undiluted bottles were amended with nutrients since a lack of nutrient limitation was predicted. Since nutrient limitation had been confirmed previously at station Skidaway (Anderson and Harvey, 2019), half of the undiluted and all of the diluted bottles at station Skidaway were amended with nutrients. If a significant difference in k was found between unamended and nutrient amended treatments, nutrient limitation was inferred, and k from the unamended treatment was used to calculate μ and k from the nutrient-amended treatment was used to calculate g. If no significant difference was found, a lack of nutrient limitation was inferred, and k from both the nutrient-amended and unamended treatments were used to calculate μ and g.

To determine g (d^{-1}), first an independent Student's t-test was used to determine if k was significantly different ($p < 0.05$) in the undiluted and diluted treatments. If a significant

difference was not found, g was set to 0 and used in all further equations described. If a significant difference was found, g was calculated using the equation:

$$g = \left(\frac{k_D - k_U}{1 - x}\right)$$

where, k_D and k_U refer to the apparent growth rates from the diluted and undiluted bottles and x refers to the true dilution factor used in the incubations. True dilution factors were calculated as the ratio of chlorophyll or cell concentration in the diluted treatment (i.e., 20%) to the undiluted (i.e., 100%) at time zero. Grazing (g) was also set to 0 if grazing rates were negative (i.e., positive slope). Intrinsic growth rates (μ; d^{-1}), which reflect the change in phytoplankton abundance without losses from grazing, were determined using the equation:

$$\mu = g + k_U$$

In two dilution incubation experiments (one each at stations Skidaway and Grazer, both conducted at noon), duplicate incubation bottles were amended with superoxide dismutase, or SOD (final concentration 50 U mL^{-1}; Millipore Sigma S5395) in order to manipulate natural levels of eROS. SOD catalyzes the dismutation of O_2^- to H_2O_2, thereby removing eO_2^- and increasing eH_2O_2 production. The SOD applied in these experiments targeted O_2^- in the extracellular milieu since the enzyme cannot cross biological membranes due to its large size (>31 kDa) (Cass, 1985). Rather than adding a pulse of H_2O_2 at a discrete timepoint, SOD was used because it provides a sustained source of increased eH_2O_2 production. In our experiments, the increase in eH_2O_2 production induced by SOD additions can be estimated based on the photoproduction ratio of ~$4O_2^-$:$1H_2O_2$ reported by Powers et al. (2015) and the ideal stoichiometric ratio of $2O_2^-$:$1H_2O_2$ for the SOD-catalyzed dismutation of O_2^- to H_2O_2 (Powers et al., 2015). First, we multiply our highest and lowest observed eH_2O_2 production rates by 4 to estimate the ambient O_2^- production rate based on photoproduction. Then, we divide by 2 to

estimate an eH_2O_2 production rate by SOD. Following this approach, the additional H_2O_2 production due to SOD was between 31 ± 10 nM h^{-1} and 96 ± 20 nM h^{-1}. These rates represent a ~3-fold increase in natural levels of eH_2O_2 production observed at our field site. The concentration of SOD used in these incubations (50 U mL^{-1}) should be sufficient to convert all O_2^- to H_2O_2, given that Powers and Miller (2016) found that 3 U mL^{-1} SOD was enough to do the same in photochemical experiments (Powers and Miller, 2016).

Statistical analyses

Potential correlations between biological eH_2O_2 production rates and other in situ observations were determined with simple linear regression and Spearman's rank order correlation, which can reveal potential non-linear or monotonic correlations. Correlation coefficients for linear regression and Spearman's rank order correlation are indicated by R and ρ, respectively. To determine the effect of SOD on phytoplankton intrinsic growth and microzooplankton grazing rates, a nonparametric Wilcoxon test was used. Statistical analyses were performed in JMP® Pro 15.0.0. Alpha was set to 0.05.

Results

Biological eH_2O_2 production

Biological eH_2O_2 production was measured in discrete seawater samples taken every ~4 hours over one day at a continental shelf site in the South Atlantic Bight (station Grazer, Figure 3.1). Rates of biological eH_2O_2 production ranged from 15 – 48 nM h^{-1} (Table 3.1). The lowest eH_2O_2 production rates occurred at 12:00 noon and maximal rates occurred during the night at 20:00 (Figure 3.4A, Table 3.1).

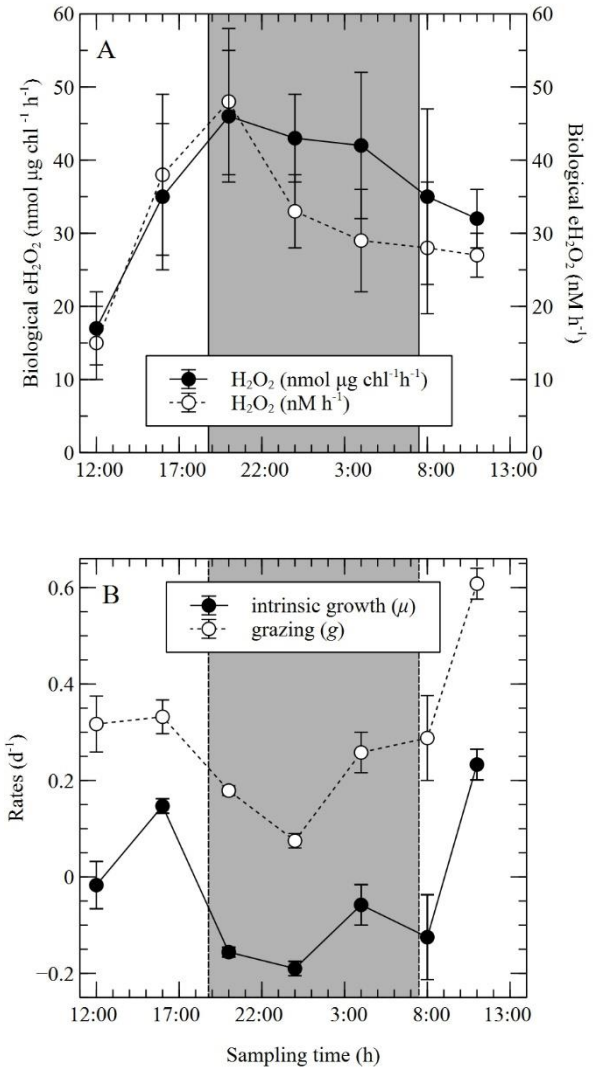

Figure 3.4: Biological eH_2O_2 production rates normalized to seawater volume (white circles) and normalized to chlorophyll (black circles) (A), and rates of daily phytoplankton intrinsic growth (μ, black circles) and microzooplankton grazing (g, white circles) (B) estimated with bulk chlorophyll concentrations measured over a one-day period. Plotted timepoints indicate the time at which samples were collected. Dashed vertical lines indicate sunset and sunrise with the shaded grey area indicating nighttime. Error bars show one standard deviation of the mean of three biological replicates (except for the 17 ± 5 nmol µg chl^{-1} h^{-1} eH_2O_2 production rate and the 15 ± 5 nM h^{-1} eH_2O_2 production rate, where n = 2).

Photosynthetically Active Radiation (PAR)

Over the diel sampling period at station Grazer, daytime PAR levels were typically less than 50 μmol m^{-2} s^{-1} but increased to 160.7 μmol m^{-2} s^{-1} at noontime. PAR was inversely correlated with eH_2O_2 production rates (Table 3.3). This negative trend was driven by the high PAR and low eH_2O_2 production rates observed at noon, except when eH_2O_2 production rates were normalized to chlorophyll. Indeed, the inverse correlation between chlorophyll-normalized eH_2O_2 production and PAR is still significant with the lowest (noontime) production rate omitted (Figure 3.5A). This inverse trend was not driven by changes in chlorophyll, which lacked a statistically significant correlation with PAR (Figure 3.5B).

Table 3.3: Statistical summaries of biological eH_2O_2 production as a function of biological and physicochemical parameters collected over a one-day period in the South Atlantic Bight. Correlation coefficients for Spearman's rank order correlation and simple linear regression (ρ and R, respectively) are provided. Significant differences are indicated by asterisks, where a p-value of < 0.05, < 0.01, < 0.001 is represented by *, **, and ***, respectively. Bold font indicates a statistically significant result. Phytoplankton intrinsic growth (d^{-1}) and microzooplankton grazing (d^{-1}) rates were estimated with bulk chlorophyll concentrations. Phytoplankton (cells mL^{-1}) and phytoplankton carbon (µg C L^{-1}) are calculated as the sum of *Synechococcus* spp., picoeukaryote, and nanoeukaryote cell concentrations and carbon biomass concentrations, respectively. PAR = photosynthetically active radiation

	eH_2O_2 Production (nM h^{-1})		eH_2O_2 Production (fmol $cell^{-1}$ h^{-1})		eH_2O_2 Production (nmol µg chl^{-1} h^{-1})		eH_2O_2 Production (nmol µg C^{-1} h^{-1})	
	Spearman's (ρ)	Linear regression (R)	Spearman's (ρ)	Linear regression (R)	Spearman's (ρ)	Linear regression (R)	Spearman's (ρ)	Linear regression (R)
Temperature (°C)	0.25	0.26	0.27	0.29	0.05	0.04	0.28	0.30
Salinity (PSU)	-0.29	-0.38	-0.31	-0.40	0.00	0.02	-0.29	-0.36
PAR (µmol photons m^{-2} s^{-1})	**-0.52***	**-0.56***	-0.42	**-0.53***	**-0.70*****	**-0.72*****	**-0.46***	**-0.55***
Grazing (d^{-1})	-0.37	-0.30	-0.25	-0.23	**-0.58****	-0.40	-0.27	-0.24
Intrinsic growth (d^{-1})	-0.37	-0.19	-0.26	-0.09	**-0.55***	-0.35	-0.29	-0.08
Synechococcus spp. (cells mL^{-1})	**-0.60****	**-0.56****	**-0.70*****	**-0.67****	-0.23	-0.21	**-0.73*****	**-0.68****
Picoeukaryotes (cells mL^{-1})	-0.14	-0.44	-0.18	**-0.46***	-0.16	**-0.56***	-0.22	**-0.50***
Nanoeukaryotes (cells mL^{-1})	0.43	0.33	0.32	0.26	**0.54***	0.44	0.31	0.24
Phytoplankton (cells mL^{-1})	**-0.60****	**-0.58****	**-0.70*****	**-0.68*****	-0.23	-0.27	**-0.73*****	**-0.69*****
Phytoplankton carbon (µg C L^{-1})	-0.44	**-0.58****	**-0.57****	**-0.66****	-0.10	-0.38	**-0.59****	**-0.68****

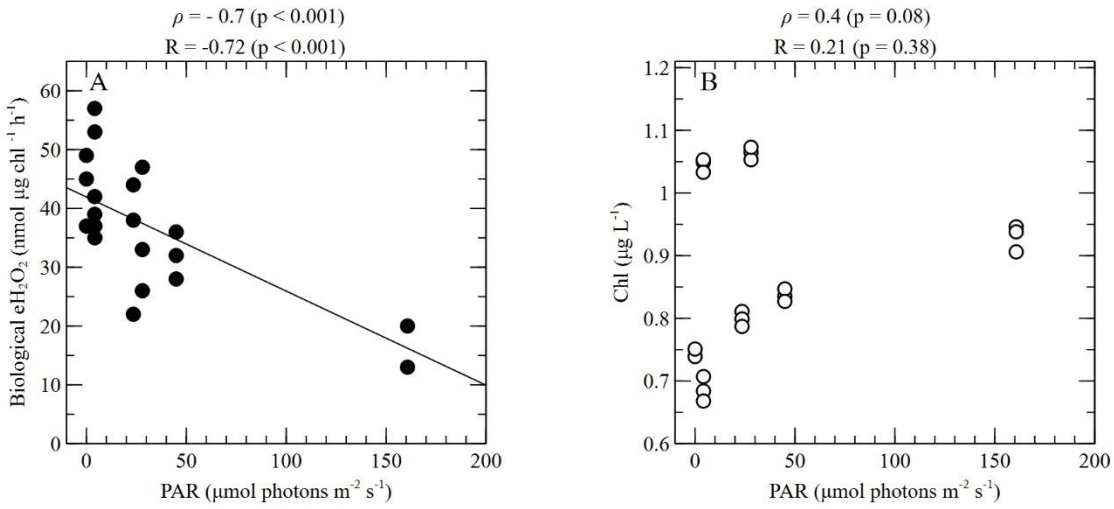

Figure 3.5: Biological eH_2O_2 production rates normalized to chlorophyll (A) and chlorophyll concentrations (B) as a function of photosynthetically active radiation (PAR) measured over a one-day period. Correlation coefficients for Spearman's rank order correlation and simple linear regression (ρ and R, respectively) and their level of significance (p) are provided. In panel A, the inverse correlation between chlorophyll-normalized eH_2O_2 production and PAR is still significant with the lowest (noontime) production rate omitted (R = -0.54, p = 0.02; Spearman's ρ = -0.59, p = 0.01).

Phytoplankton abundance

Picoeukaryotes, nanoeukaryotes, and *Synechococcus* spp. were present at station Grazer at all times during the sampling period. *Synechococcus* spp. dominated the phytoplankton community in both abundance and carbon biomass (Figure 3.6, Table 3.4). Several significant negative correlations between microbial eH_2O_2 production and phytoplankton abundances were found. For example, the rate of eH_2O_2 production normalized to total phytoplankton cell counts was inversely related to total phytoplankton abundance (Figure 3.7, Table 3.3) and carbon biomass (Table 3.3). In contrast, eH_2O_2 production normalized to chlorophyll did not show a significant trend with phytoplankton abundance (Figure 3.8, Table 3.3) or carbon biomass (Table 3.3). *Synechococcus* spp. dominated the phytoplankton community in both abundance and carbon biomass at the field site (Figure 3.6, Table 3.4) but is typically chlorophyll-poor, which likely drove these results. Indeed, *Synechococcus* spp. abundance was inversely related to cell-normalized eH_2O_2 production (Fig 3.9A, Table 3.3) but not chlorophyll-normalized eH_2O_2 production (Figure 3.9D, Table 3.3).

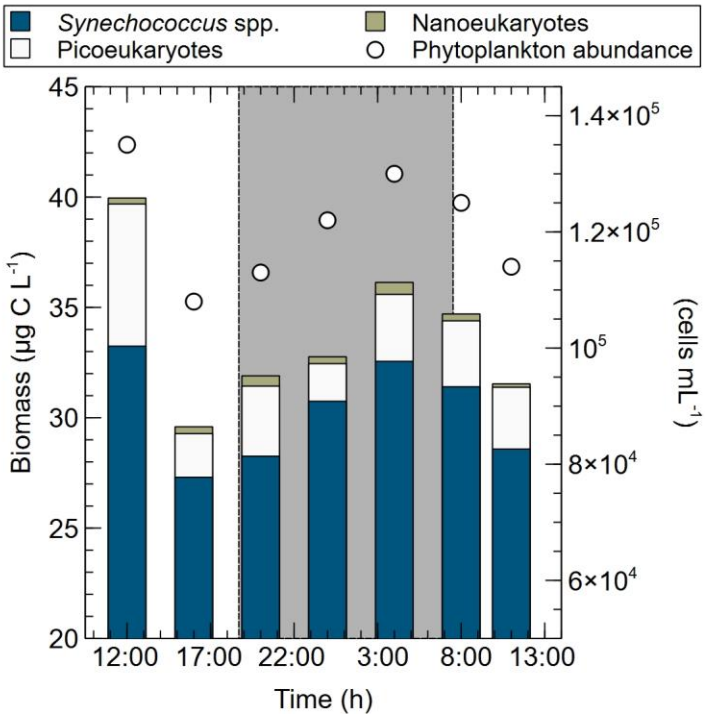

Figure 3.6: Phytoplankton abundance (sum of *Synechococcus* spp., picoeukaryotes and nanoeukaryotes; cells mL^{-1}, circles) and group-specific phytoplankton carbon biomass (µg C L^{-1}, bars) measured over the one-day sampling period. Dashed vertical lines indicate sunset and sunrise with the shaded grey area indicating nighttime.

Table 3.4: Biological data collected over the one-day sampling period at station Grazer in the South Atlantic Bight. The average ± standard deviation of replicate samples is shown (n = 3). Grazing and intrinsic growth rates are estimated with bulk chlorophyll concentrations. Chl = chlorophyll

Station	Time	Chl ($\mu g\ L^{-1}$)	*Synechococcus* spp. abundance ($cells\ mL^{-1}$)	Picoeukaryote abundance ($cells\ mL^{-1}$)	Nanoeukaryote abundance ($cells\ mL^{-1}$)	*Synechococcus* spp. biomass ($\mu g\ C\ L^{-1}$)	Picoeukaryote Biomass ($\mu g\ C\ L^{-1}$)	Nanoeukaryote biomass ($\mu g\ C\ L^{-1}$)	Grazing (d^{-1})	Intrinsic growth (d^{-1})
Grazer	12:00	0.930 ± 0.021	1.30E+05	4.29E+03	9.82E+01	33.24	6.44	0.27	0.317 ± 0.058	-0.017 ± 0.049
	16:00	1.064 ± 0.010	1.07E+05	1.32E+03	1.12E+02	27.30	1.98	0.31	0.332 ± 0.035	0.147 ± 0.015
	20:00	1.045 ± 0.011	1.11E+05	2.12E+03	1.68E+02	28.26	3.18	0.46	0.179 ± 0.010	-0.156 ± 0.010
	0:00	0.747 ± 0.007	1.21E+05	1.14E+03	1.12E+02	30.75	1.70	0.31	0.075 ± 0.015	-0.190 ± 0.015
	4:00	0.686 ± 0.020	1.28E+05	2.02E+03	1.97E+02	32.56	3.03	0.54	0.258 ± 0.042	-0.058 ± 0.042
	8:00	0.799 ± 0.012	1.23E+05	1.99E+03	1.12E+02	31.40	2.99	0.31	0.288 ± 0.088	-0.125 ± 0.088
	11:00	0.836 ± 0.010	1.12E+05	1.87E+03	5.61E+01	28.58	2.80	0.16	0.608 ± 0.032	0.233 ± 0.032

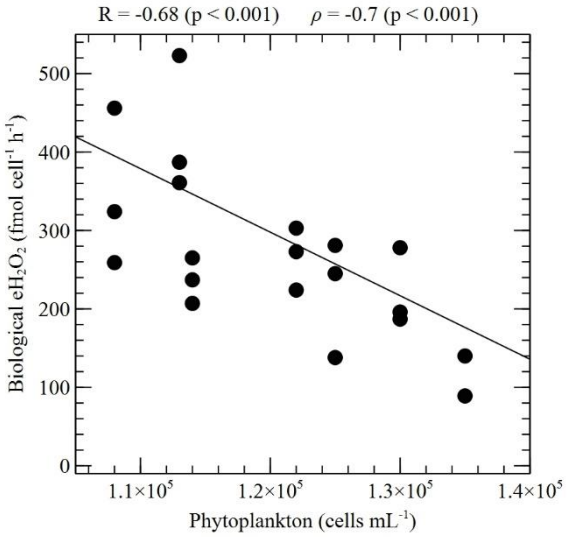

Figure 3.7: Biological eH_2O_2 production rates normalized to phytoplankton cell abundance as a function of phytoplankton cell counts measured over a one-day period. Phytoplankton counts (cells mL^{-1}) reflect the sum of *Synechococcus* spp., picoeukaryotes, and nanoeukaryotes. Correlation coefficients for Spearman's rank order correlation and simple linear regression (ρ and R, respectively) and their level of significance (p) are provided.

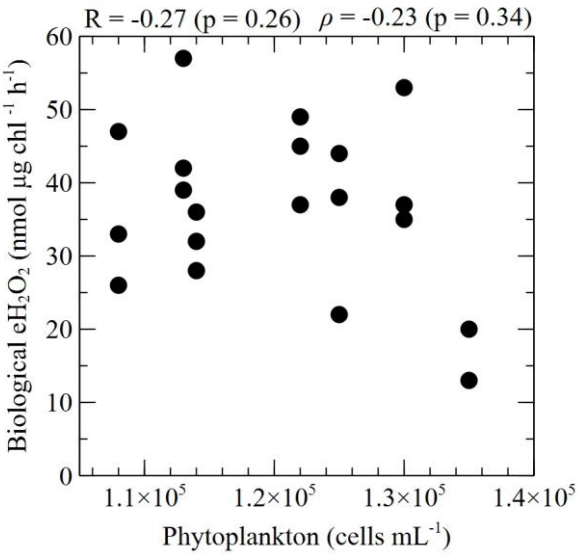

Figure 3.8: Biological eH_2O_2 production rates normalized to chlorophyll as a function of phytoplankton abundance measured over the one-day sampling period. Regression analyses were performed using simple linear regression and Spearman's rank order correlation. Correlation coefficients (R and ρ, respectively) and their level of significance (p) are provided. Error bars represent the standard deviation of the mean of replicate samples (n = 3 except for the 17 ± 5 nmol µg chl^{-1} h^{-1} H_2O_2 production measurement, where n = 2).

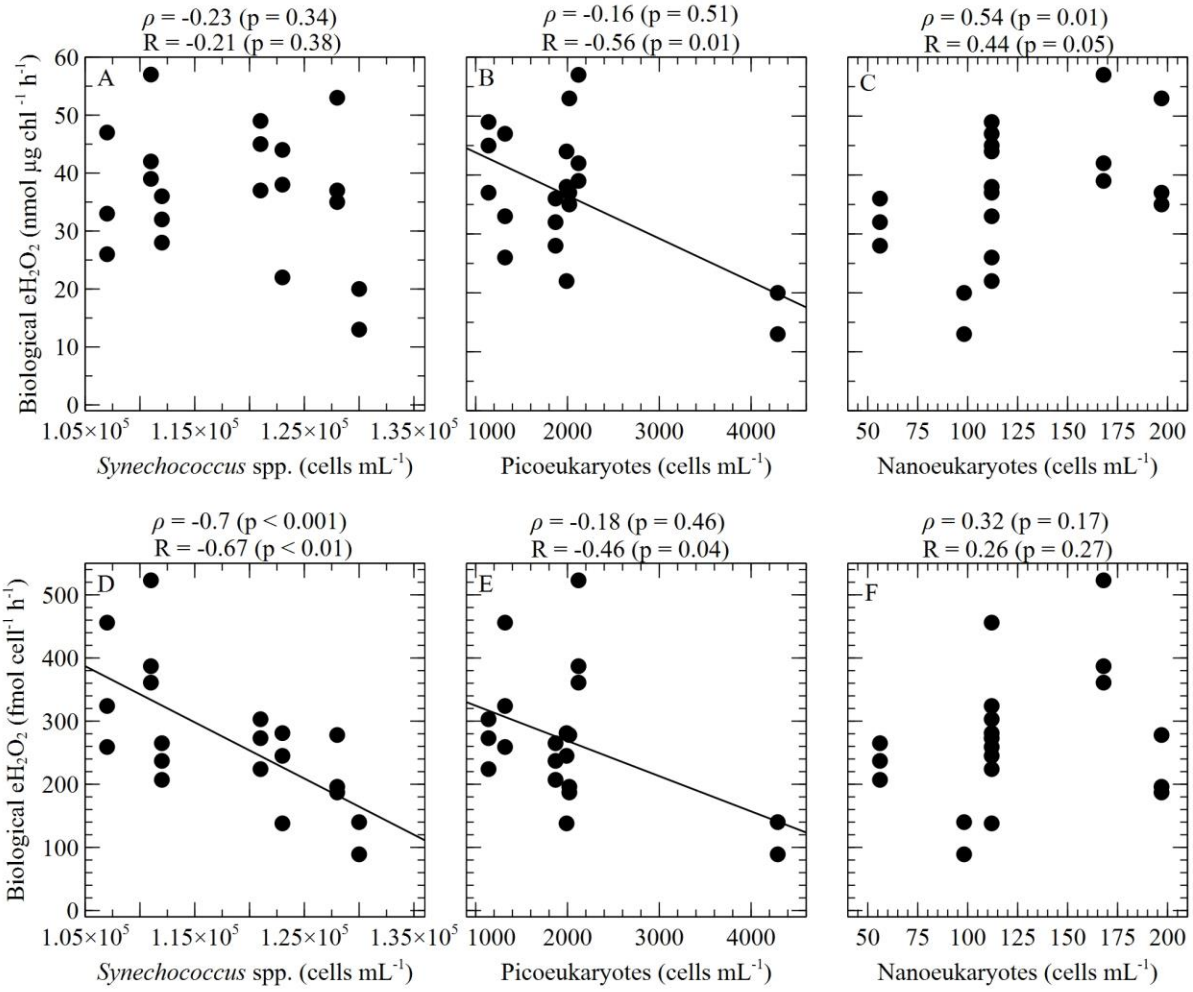

Figure 3.9: Biological eH_2O_2 production rates normalized to chlorophyll (A-C) or total phytoplankton cell counts (D-F) as a function of *Synechococcus* spp. (A, D), picoeukaryotes (B, E), and nanoeukaryotes (C, F) measured over the one-day sampling period. Regression analyses were performed using simple linear regression and Spearman's rank order correlation. Correlation coefficients (R and ρ, respectively) and their level of significance (p) are provided. Error bars show one standard deviation of the mean of replicate samples (n = 3 except for the 17 ± 5 nmol µg chl^{-1} h^{-1} and 115 ± 36 fmol cell^{-1} h^{-1} H_2O_2 production rate measurements, where n = 2). The negative linear trend in panels B and E are driven by a single outlier (4290 picoeukaryotes cells mL^{-1}). Once the outlier is removed, the significant negative linear trend is no longer observed (panel b, y = 38.0565 + 0.001x, R = 0.00, p = 0.98; panel e, y = 290.834 - 0.003x, R = 0.00, p = 0.96).

Phytoplankton growth and microzooplankton grazing rates

Dilution incubations were conducted at station Grazer alongside eH_2O_2 measurements over the same day to determine phytoplankton intrinsic growth and microzooplankton grazing rates. Plankton communities sampled at night exhibited the lowest microzooplankton grazing rates (nighttime [avg. ± SD] 0.171 ± 0.092 d^{-1} versus daytime 0.387 ± 0.149 d^{-1}), with minimum grazing observed in the community sampled at midnight (Figure 3.4B, Table 3.4). Phytoplankton intrinsic growth, which is defined as phytoplankton growth rate in the absence of grazing, was also generally lower among phytoplankton sampled at night (-0.135 ± 0.069 d^{-1} [avg. ± SD]) compared to daytime (0.060 ± 0.161 d^{-1}) (Figure 3.4B, Table 3.4).

Overall, grazing and growth tended to be lower in plankton assemblages sampled at night, whenever biological eH_2O_2 production was highest (Figure 3.4). Consistent with these trends, eH_2O_2 production normalized to chlorophyll showed a significant negative monotonic relationship with intrinsic growth rate (Spearman's ρ = -0.55, p = 0.01) and microzooplankton grazing rate (Spearman's ρ = -0.58, p < 0.01) (Figure 3.10, Table 3.3). These results were not driven by changes in chlorophyll, which correlated positively, but insignificantly, with intrinsic growth (linear regression R = 0.26, p = 0.27; Spearman's ρ = 0.35, p = 0.13) and grazing (R = 0.08, p = 0.74; ρ = 0.43, p = 0.06).

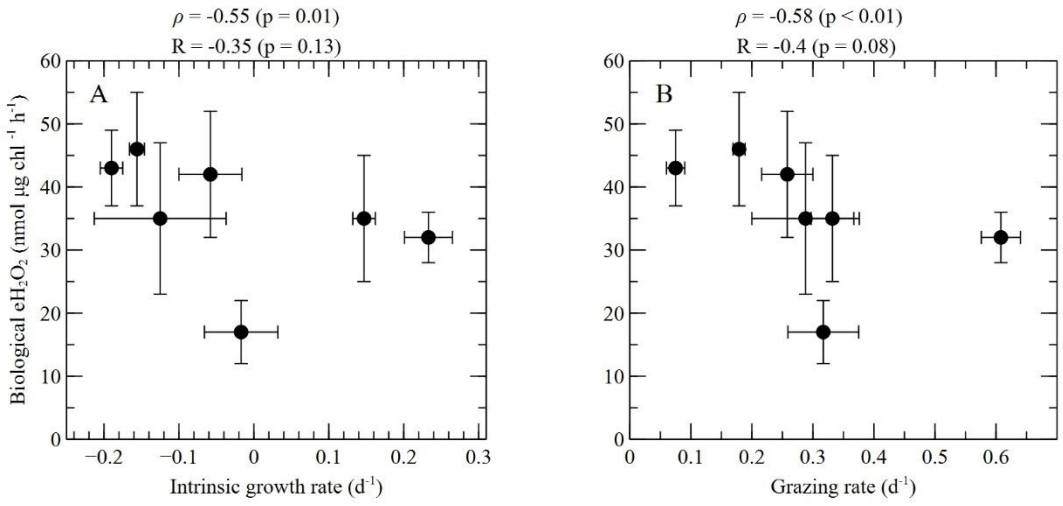

Figure 3.10: Biological eH_2O_2 production rates normalized to chlorophyll as a function of daily rates of phytoplankton intrinsic growth (μ) (A) and microzooplankton grazing (g) (B) estimated with bulk chlorophyll concentrations measured over a one-day period in the South Atlantic Bight. Correlation coefficients for Spearman's rank order correlation and simple linear regression (ρ and R, respectively) and their level of significance (p) are provided. Error bars show one standard deviation of the mean of three biological replicates (except for the 17 ± 5 nmol µg chl^{-1} h^{-1} eH_2O_2 production measurement, where n = 2).

ROS manipulation incubations

SOD is the enzyme that converts O_2^- to H_2O_2. We added SOD to a subset of dilution incubations to manipulate natural levels of these ROS. SOD increased natural rates of eH_2O_2 production in our ROS-manipulated dilution incubations by ~three-fold (see methods). In response, bulk microzooplankton grazing rates decreased (Figure 3.11A) at station Grazer (0.738 ± 0.255 d^{-1} without SOD versus 0.00 d^{-1} with SOD; Wilcoxon test, n = 4, $p < 0.05$). The same trend was observed at station Skidaway, a nearby estuarine site (Figure 3.1 [0.852 ± 0.307 d^{-1} without SOD versus 0.116 d^{-1} with SOD; Wilcoxon test, n = 2, p = 0.245]). These findings are consistent with the negative relationships revealed from in situ data collected at station Grazer, where grazing rates were inversely correlated with eH_2O_2 production (Figure 3.10). At station Skidaway, substantial biomass of phytoplankton subgroups allowed examination of group-specific grazing and growth rates. This analysis revealed that SOD additions eliminated grazing of nanoeukaryotes and picoeukaryotes but had no effect on grazing of *Synechococcus* spp. (Figure 3.11B).

Similar to grazing rates, the intrinsic growth rates of the bulk phytoplankton community decreased in the presence of SOD at station Grazer. This effect rendered the intrinsic growth rate negative (0.347 ± 0.080 d^{-1} without SOD versus -0.274 ± 0.263 d^{-1} with SOD; Wilcoxon test n = 4, $p < 0.05$). Thus, SOD additions were lethal to the phytoplankton community at station Grazer. A non-lethal decline in growth by the phytoplankton community was observed due to SOD additions at station Skidaway (Figure 3.11A). These findings are consistent with the negative correlation between phytoplankton intrinsic growth rates and eH_2O_2 production rates observed at station Grazer (Figure 3.10A). Within the phytoplankton community at station Skidaway, growth of *Synechococcus* spp. was stimulated (1.542 ± 0.079 d^{-1} n = 6 without SOD versus 1.631 ±

0.067 d^{-1} with SOD; Wilcoxon test, $n = 3$, $p < 0.05$), but this response was not observed in the other phytoplankton groups (Figure 3.11B).

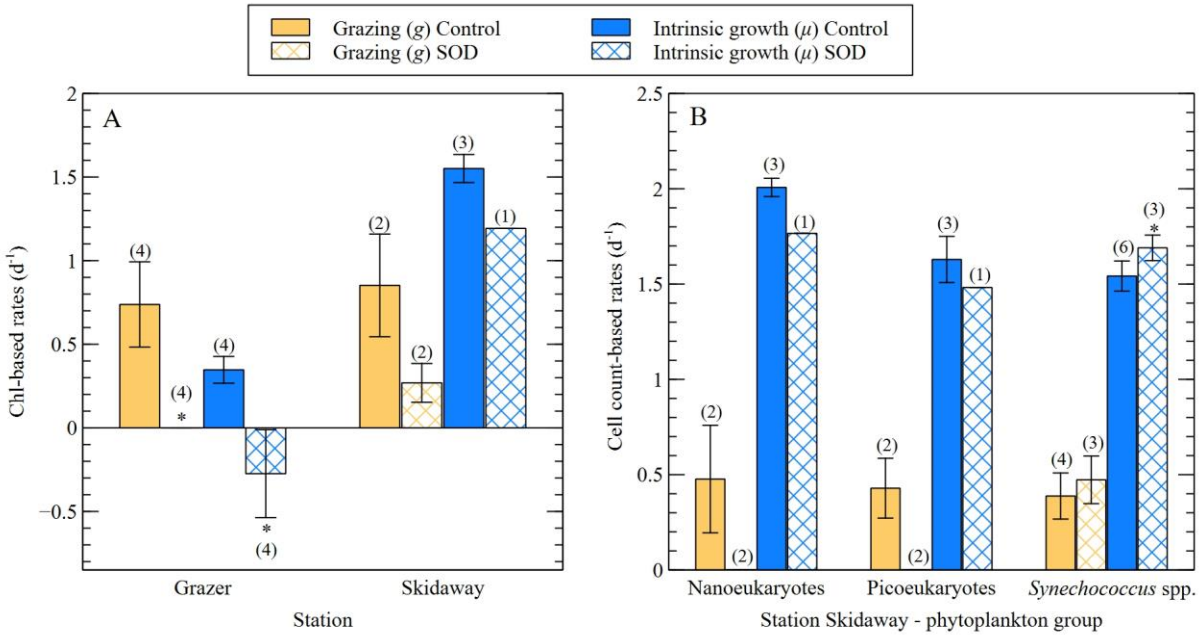

Figure 3.11: Rates of phytoplankton community (A) and group-specific (B) microzooplankton grazing (g) and intrinsic growth (μ) with and without (control) the addition of superoxide dismutase (SOD). SOD removes eO_2^- and accelerates eH_2O_2 production (see methods). Significant differences compared to the control (Wilcoxon test) are indicated by asterisks, where a p-value of < 0.05 is represented by *. Error bars show one standard deviation of the mean of replicate samples (n is shown in parentheses above each measurement).

Discussion

In this study, we undertook a field campaign in the South Atlantic Bight to clarify the ecophysiological function of biological eH_2O_2 production. First, we measured biological eH_2O_2 production over one day at station Grazer (Figure 3.4A). The rates were within the range of previous measurements in aquatic systems ($<10^{-1} – 10^{2}$ nM h^{-1}) (Marsico et al., 2015, Vermilyea et al., 2010a, Vermilyea et al., 2010b, Zhang et al., 2016b). Moreover, biological eH_2O_2 production rates were generally lower during the day than at night (Figure 3.4A, Table 3.1).

In addition to measuring biological eH_2O_2 production, we simultaneously measured microzooplankton grazing and phytoplankton growth rates at station Grazer. In contrast to eH_2O_2 production, grazing and growth rates were generally lower at night than during the day (Figure 3.4B). Similar diel patterns of high daytime and low nighttime grazing have been have been observed previously, which have been attributed to multiple factors (Jakobsen and Strom, 2004, Ng and Liu, 2016, Ng et al., 2017) but remain unresolved (Bulbena, 2020). In our study, biological eH_2O_2 production was also negatively correlated with grazing and growth rates (Figure 3.10). These observations could be interpreted as correlational and not causational and possibly due to diel patterns independently influencing eH_2O_2 production, grazing and growth rates. Therefore, we also directly tested the effect of eROS on grazing and growth rates by manipulating eROS in field incubations. Our field incubation results and other observations (see below) suggest these correlations are not coincidental and may be causational. Indeed, by removing eO_2^- and accelerating eH_2O_2 production with additions of the enzyme SOD, we observed a decrease in community-level phytoplankton growth and microzooplankton grazing. These findings and previous evidence from model organisms (Martel, 2009, Flores et al., 2012, Oda et al., 1995, Wootton et al., 2007, Oda et al., 1998, Plummer et al., 2019, Hansel et al.,

2019) support the hypothesis that biological eH_2O_2 production mediates phytoplankton growth and microzooplankton grazing.

We present several lines of evidence to show that eH_2O_2 production is dynamically regulated as part of a potential signaling process consistent with a role in growth and grazing. First, the inverse correlations between eH_2O_2 production and phytoplankton growth and microzooplankton grazing rates (Figure 3.10) indicate that cell division and lysis, which can release ROS into seawater during growth and grazing, were not major sources of eH_2O_2. Instead, active production by intact microbial cells was likely the dominant origin of biological eH_2O_2.

Second, as natural PAR levels increased, biological eH_2O_2 production decreased (Figure 3.5A, Table 3.3), yet production rates were measured under dark conditions. This result shows that irradiance did not control eH_2O_2 production directly and instead suggests regulation by an internal clock. Prior evidence also suggests that diel patterns in biological eH_2O_2 cycling may be controlled by circadian processes (Morris et al., 2016). Additionally, diel patterns in eH_2O_2 cycling may be driven by microbial degradation of eH_2O_2 to protect against photochemically generated ROS (Morris et al., 2016).

Third, eH_2O_2 production was inversely correlated with total phytoplankton abundance (Figure 3.7, Table 3.3). Similar cell density dependent eROS production has been observed in several prokaryotic and eukaryotic phytoplankton species in both laboratory experiments (Diaz et al., 2018, Sutherland et al., 2019, Plummer et al., 2019, Marshall et al., 2005b) and field studies (Morris et al., 2016, Hansel et al., 2016), which has been attributed to a signaling role for eROS (Marshall et al., 2005b, Hansel et al., 2016, Plummer et al., 2019, Diaz et al., 2018, Sutherland et al., 2019). ROS may serve signaling roles between different cells or within the same cell, depending, in part, on which ROS is involved (Diaz and Plummer, 2018).

Extracellular ROS play signaling roles in the growth and development of diverse organisms including phytoplankton (Hansel and Diaz, 2021, Aguirre and Lambeth, 2010, Bauer, 2014, Rossi et al., 2017). For instance, in laboratory studies, additions of SOD and the H_2O_2-degrading enzyme catalase (either separately or together) inhibited proliferation and development of the prolific eROS-producing alga *Chattonella marina* (Oda et al., 1995). These results suggest that both eO_2^-, as observed in bacteria (Hansel et al. 2019 and references therein), and eH_2O_2, as observed in pathogenic yeast (Rossi et al., 2017) and human cancer cells (Bauer, 2014), both act as autocrine growth promoters in *C. marina*. Similarly, in our field incubations, additions of SOD decreased intrinsic growth rates of the bulk phytoplankton community (Figure 3.11A), which may suggest that eO_2^- acts as a growth promoter. In some phytoplankton, however, eH_2O_2 may be the growth promoter instead of eO_2^-. For example, SOD additions stimulate growth of the widespread coccolithophore *Emiliania huxleyi* (Plummer et al., 2019) and the diatom *Thalassiosira oceanica* (Diaz et al., 2019). Therefore, eROS exert variable effects on the growth of different phytoplankton. Indeed, we observed group-specific responses in our field incubations as well, with growth rates of *Synechococcus* spp. increasing due to SOD, while growth rates of picoeukaryotes and nanoeukaryotes did not increase (Figure 3.11B).

In addition to growth regulation, our results suggest that eROS may play a signaling role in grazing interactions, consistent with prior work on model organisms (Flores et al., 2012, Wootton et al., 2007, Oda et al., 1998, Martel, 2009). The decline in microzooplankton grazing rates that we observed due to SOD (Figure 3.11A), is not likely due to a direct cytotoxic effect of SOD on microzooplankton, since SOD promotes the viability of protozoa (Flores et al., 2012). The production of eH_2O_2 may not be directly toxic to phytoplankton or microzooplankton either since high concentrations relative to natural seawater are required to induce negative impacts on

most of these microorganisms (Morris et al., 2022). Perhaps more likely, and consistent with the documented signaling role of H_2O_2 (Gough and Cotter, 2011), eH_2O_2 may be an intermediate messenger or infochemical involved in grazing deterrence that may regulate production of another compound or secondary metabolite involved in predator defense. For example, eH_2O_2 production by some macroalgae is involved in biological defense by stimulating production of organohalogens, which have noxious properties like inhibiting microbial quorum sensing (Hansel and Diaz, 2021). Our results also demonstrated phytoplankton group-specific responses. For instance, grazing was inhibited at the community level by manipulating ROS levels with SOD yet grazing on *Synechococcus* spp. was not (Figure 3.11B).

Conclusion

Numerous studies on model cultures and natural microbial communities indicate that phytoplankton-derived eROS act as signaling molecules, yet the ecophysiological role of eROS signaling in phytoplankton has remained mysterious. Here, we corroborate the view of eROS as signaling molecules by showing evidence that biological eH_2O_2 production is internally regulated and as a function of cell density. Furthermore, we find evidence that eH_2O_2 production may play a signaling role in the mediation of phytoplankton growth and microzooplankton grazing. The potential for biological eH_2O_2 production to influence plankton community and group-specific dynamics by playing roles in bottom-up (i.e., growth) and top-down processes (i.e., grazing) has implications for shaping microbial community composition, marine ecosystem functioning, and carbon flow. Further studies, including laboratory and field experiments in other systems, should be conducted to continue exploring the proposed role of eROS signaling in phytoplankton growth and microzooplankton grazing deterrence including species specific differences.

Acknowledgements

Chapter 3 has been submitted for publication of the material as it may appear in Journal of Plankton Research, 2022, Plummer, Sydney; Holland, Alisia R.; Anderson, Sean R.; Duffy, Patrick I.; Diou-Cass Quintin P.; Bulski, Karrie; Bittar, Thais B.; Talmy David; Harvey Elizabeth L.; Diaz, Julia M., Oxford University Press, 2022. The dissertation author was the primary researcher and author of this paper.

The authors thank the captain and crew of the *R/V Savannah* for facilitating research cruise sampling, thereby making the study possible.

CONCLUSION

Since the discovery of eROS production among marine phytoplankton over 30 years ago, scientists have attempted to identify its purpose and cellular source to better understand its impacts on marine ecology and geochemical cycling. ROS are commonly associated with stress in organisms; however, my research advances a growing paradigm shift among scientific communities that ROS are also essential for normal physiological functioning. Indeed, here we reveal that eO_2^- production promotes health potentially by serving as an alternative electron pathway in several diverse phytoplankton species. Further, we provide evidence that eROS act as signaling molecules that are dynamically regulated by phytoplankton cells. These eROS signals seem to elicit changes in growth and be involved in defense against grazing. Thus, eROS appear to regulate bottom-up (i.e., growth) and top-down (i.e., grazing) control of phytoplankton standing stocks. Given that growth and grazing are major controls over phytoplankton bloom initiation and termination, ROS production and decay dynamics should be tracked in mesocosm or bloom formation studies to better understand their role(s) in bloom phenology.

Biotic studies of eROS dynamics (e.g., eROS and bloom phenology), should be put into the context of abiotic studies to help untangle the influence of eROS from different sources on marine microbes. To begin this untangling, the spatiotemporal qualities of eROS in marine environments should be interrogated similar to the work of Omar et al. (2022), which used reactivity and diffusion rate modeling to confirm that phytoplankton derived eH_2O_2 can interact with other cells (2022). In the case of eO_2^-, this molecule may be limited to serving as an autocrine signal due to its physiochemical properties (Lesser 2006; Brown and Griendling, 2009). Another question to address is the specificity of ROS as signals for a particular response

in marine microorganisms. For example, Mittler describes how ROS signals in plants may act as general signals that stimulate signaling networks in which molecules react with ROS in a concerted effort to become specific signals (2011). Similar explanations should be interrogated in phytoplankton through molecular biology studies such as manipulating eROS and sampling RNA in monocultures and cocultures (e.g., predator-prey cocultures).

Biochemically characterizing enzymes that regulate eROS dynamics is an important step in the field of biological marine eROS. My work implicates flavoenzymes in eROS production in many phytoplankton species, thereby narrowing down enzymatic targets for purification and biochemical assays as well as genetic manipulation in model organisms. This approach would definitively test the source of biological eROS and their role(s) as signals in phytoplankton growth and anti-grazing defense. However, to gain a more complete understanding of how ROS affects phytoplankton ecophysiology and biogeochemical cycling, efforts to identify enzymes involved in eROS decay should be pursued, as well.

By understanding the biological role and physiological drivers of eROS, we can better understand biogeochemical cycling, microbial functioning, and health of current and future oceans. For example, since eO_2^- production is light dependent in phytoplankton and because oceanic light regimes are predicted to shift due to climate change, phytoplankton may adjust eO_2^- production in future oceans. These shifts in eO_2^- production could have dramatic impacts on biogeochemical cycling of carbon, metals, and oxygen in already sensitive oceanic regions. My work provides the basis for modeling these changes by providing light-dependent eO_2^- production rates in globally representative phytoplankton, and by estimating the increase in eO_2^- production rates in *Prochlorococcus* in the North Pacific Gyre as proof of concept. Overall, my

dissertation helps uncover how and why diverse phytoplankton produce eROS, thereby advancing our understanding of geochemical cycling and ecosystem health.

REFERENCES

AGUIRRE, J. & LAMBETH, J. D. 2010. Nox enzymes from fungus to fly to fish and what they tell us about Nox function in mammals. *Free Radic Biol Med,* 49**,** 1342-53.

AGUIRRE, J., RIOS-MOMBERG, M., HEWITT, D. & HANSBERG, W. 2005. Reactive oxygen species and development in microbial eukaryotes. *Trends Microbiol,* 13**,** 111-8.

ANDERSON, A., LAOHAVISIT, A., BLABY, I. K., BOMBELLI, P., HOWE, C. J., MERCHANT, S. S., DAVIES, J. M. & SMITH, A. G. 2016. Exploiting algal NADPH oxidase for biophotovoltaic energy. *Plant Biotechnol J,* 14**,** 22-8.

ANDERSON, S. R., DIOU-CASS, Q. P. & HARVEY, E. L. 2018. Short-term estimates of phytoplankton growth and mortality in a tidal estuary. *Limnol Oceanogr,* 63**,** 2411-2422.

ANDERSON, S. R. & HARVEY, E. L. 2019. Seasonal variability and drivers of microzooplankton grazing and phytoplankton growth in a subtropical estuary. *Front Mar Sci,* 6.

AUDI, S. H., FRIEDLY, N., DASH, R. K., BEYER, A. M., CLOUGH, A. V. & JACOBS, E. R. 2018. Detection of hydrogen peroxide production in the isolated rat lung using Amplex red. *Free Radic Res,* 52**,** 1052-1062.

BABIOR, B. M. 1999. NADPH oxidase: an update. *Blood,* 93**,** 1464-76.

BAKER, N. R. 2008. Chlorophyll fluorescence: a probe of photosynthesis in vivo. *Annu Rev Plant Biol,* 59**,** 89-113.

BAUER, G. 2014. Targeting extracellular ROS signaling of tumor cells. *Anticancer Res,* 34**,** 1467-82.

BEDARD, K., LARDY, B. & KRAUSE, K.-H. 2007. NOX family NADPH oxidases: Not just in mammals. *Biochimie,* 89**,** 1107-1112.

BEHRENFELD, M. J., HALSEY, K. H. & MILLIGAN, A. J. 2008. Evolved physiological responses of phytoplankton to their integrated growth environment. *Philos Trans R Soc Lond B Biol Sci,* 363**,** 2687-703.

BHATTACHARJEE, S. 2012. The Language of Reactive Oxygen Species Signaling in Plants. *J Bot,* 2012**,** 1-22.

BIELSKI, B. H. J., CABELLI, D. E., ARUDI, R. L. & ROSS, A. B. 1985. Reactivity of Ho2/O-2 Radicals in Aqueous-Solution. *J Phys Chem Ref Data,* 14**,** 1041-1100.

BJORKMAN, K. M., CHURCH, M. J., DOGGETT, J. K. & KARL, D. M. 2015. Differential Assimilation of Inorganic Carbon and Leucine by Prochlorococcus in the Oligotrophic North Pacific Subtropical Gyre. *Front Microbiol,* 6**,** 1401.

BOETIUS, A. & JOYE, S. 2009. Ecology. Thriving in salt. *Science,* 324**,** 1523-5.

BROWN, C. W. & YODER, J. A. 1994. Coccolithophorid blooms in the global ocean. *J Geophys Res Oceans,* 99**,** 7467-7482.

BROWN, D. I. & GRIENDLING, K. K. 2009. Nox proteins in signal transduction. *Free Radic Biol Med,* 47**,** 1239-53.

BULBENA, A. A. 2020. *Diel feeding rythms in marine protistan grazers.* PhD, University of Barcelona.

CARDOL, P., FORTI, G. & FINAZZI, G. 2011. Regulation of electron transport in microalgae. *Biochim Biophys Acta,* 1807**,** 912-8.

CASS, A. E. G. 1985. Superoxide Dismutases. *In:* HARRISON, P. M. (ed.) *Metalloproteins.* London: Palgrave Macmillan UK.

CORTÉS, M. Y., BOLLMANN, J. & THIERSTEIN, H. R. 2001. Coccolithophore ecology at the HOT station ALOHA, Hawaii. *Deep Sea Res Part II: Top Stud Oceanogr,* 48**,** 1957-1981.

CORY, R. M., DAVIS, T. W., DICK, G. J., JOHENGEN, T., DENEF, V. J., BERRY, M. A., PAGE, S. E., WATSON, S. B., YUHAS, K. & KLING, G. W. 2016. Seasonal dynamics in dissolved organic matter, hydrogen peroxide, and cyanobacterial blooms in Lake Erie. *Front Mar Sci,* 3.

CURIEN, G., FLORI, S., VILLANOVA, V., MAGNESCHI, L., GIUSTINI, C., FORTI, G., MATRINGE, M., PETROUTSOS, D., KUNTZ, M. & FINAZZI, G. 2016. The Water to Water Cycles in Microalgae. *Plant Cell Physiol,* 57**,** 1354-1363.

DIAZ, J. M., HANSEL, C. M., APPRILL, A., BRIGHI, C., ZHANG, T., WEBER, L., MCNALLY, S. & XUN, L. 2016. Species-specific control of external superoxide levels by the coral holobiont during a natural bleaching event. *Nat Commun,* 7**,** 13801.

DIAZ, J. M., HANSEL, C. M., VOELKER, B. M., MENDES, C. M., ANDEER, P. F. & ZHANG, T. 2013. Widespread production of extracellular superoxide by heterotrophic bacteria. *Science,* 340**,** 1223-1226.

DIAZ, J. M. & PLUMMER, S. 2018. Production of extracellular reactive oxygen species by phytoplankton: past and future directions. *J Plankton Res,* 40**,** 655-666.

DIAZ, J. M., PLUMMER, S., HANSEL, C. M., ANDEER, P. F., SAITO, M. A. & MCILVIN, M. R. 2019. NADPH-dependent extracellular superoxide production is vital to photophysiology in the marine diatom *Thalassiosira oceanica*. *Proc Natl Acad Sci USA,* 116**,** 16448-16453.

DIAZ, J. M., PLUMMER, S., TOMAS, C. & ALVES-DE-SOUZA, C. 2018. Production of extracellular superoxide and hydrogen peroxide by five marine species of harmful bloom-forming algae. *J Plankton Res,* 40**,** 667-677.

DIAZ, J. M. & SHI, X. Submitted.

DIXON, T. C., VERMILYEA, A. W., SCOTT, D. T. & VOELKER, B. M. 2013. Hydrogen peroxide dynamics in an agricultural headwater stream: Evidence for significant nonphotochemical production. *Limnol Oceanogr,* 58**,** 2133-2144.

DORANTES-ARANDA, J. J., NICHOLS, P. D., WAITE, T. D. & HALLEGRAEFF, G. M. 2013. Strain variability in fatty acid composition of *Chattonella marina*

(Raphidophyceae) and its relation to differing ichthyotoxicity toward rainbow trout gill cells. *J Phycol,* 49**,** 427-38.

DORANTES-ARANDA, J. J., SEGER, A., MARDONES, J. I., NICHOLS, P. D. & HALLEGRAEFF, G. M. 2015. Progress in understanding algal bloom-mediated fish kills: The role of superoxide radicals, phycotoxins and fatty acids. *PLoS One,* 10**,** e0133549.

DUPOUY, D., CONTER, A., CROUTE, F., MURAT, M. & PLANEL, H. 1985. Sensitivity of *Synechococcus lividus* to hydrogen peroxide. *Environ Exp Bot,* 25**,** 339-347.

EVANS, C., MALIN, G., MILLS, G. P. & WILSON, W. H. 2006. Viral infection of *Emiliania huxleyi* (Prymnesiophyceae) leads to elevated production of reactive oxygen species. *J Phycol,* 42**,** 1040-1047.

EXPOSITO-RODRIGUEZ, M., LAISSUE, P. P., YVON-DUROCHER, G., SMIRNOFF, N. & MULLINEAUX, P. M. 2017. Photosynthesis-dependent H2O2 transfer from chloroplasts to nuclei provides a high-light signalling mechanism. *Nat Commun,* 8**,** 49.

FLOMBAUM, P., GALLEGOS, J. L., GORDILLO, R. A., RINCON, J., ZABALA, L. L., JIAO, N., KARL, D. M., LI, W. K., LOMAS, M. W., VENEZIANO, D., VERA, C. S., VRUGT, J. A. & MARTINY, A. C. 2013. Present and future global distributions of the marine Cyanobacteria Prochlorococcus and Synechococcus. *Proc Natl Acad Sci U S A,* 110**,** 9824-9.

FLORES, H. S., WIKFORS, G. H. & DAM, H. G. 2012. Reactive oxygen species are linked to the toxicity of the dinoflagellate *Alexandrium* spp. to protists. *Aquat Microb Ecol,* 66**,** 199-209.

FRADA, M. J., BIDLE, K. D., PROBERT, I. & DE VARGAS, C. 2012. In situ survey of life cycle phases of the coccolithophore Emiliania huxleyi (Haptophyta). *Environ Microbiol,* 14**,** 1558-69.

FUJII, M., ROSE, A. L., OMURA, T. & WAITE, T. D. 2010. Effect of Fe(II) and Fe(III) Transformation Kinetics on Iron Acquisition by a Toxic Strain of Microcystis aeruginosa. *Environ Sci Technol,* 44**,** 1980-1986.

FUJII, M., ROSE, A. L., WAITE, T. D. & OMURA, T. 2006. Superoxide-mediated dissolution of amorphous ferric oxyhydroxide in seawater. *Environ Sci Technol,* 40**,** 880-7.

FUJIMORI, K., NAKAJIMA, H., AKUTSU, K., MITANI, M., SAWADA, H. & NAKAYAMA, M. 1993. Chemiluminescence of *Cypridina* luciferin analogues. Part 1. Effect of pH on rates of spontaneous autoxidation of CLA in aqueous buffer solutions. *J Chem Soc, Perkin Trans 2***,** 2405-2409.

FURUYA, K. & MARUMO, R. 1983. The structure of the phytoplankton community in the subsurface chlorophyll maxima in the western North Pacific Ocean. *J Plankton Res,* 5**,** 393-406.

GAO, K., HELBLING, E. W., HÄDER, D. P. & HUTCHINS, D. A. 2012. Responses of marine primary producers to interactions between ocean acidification, solar radiation, and warming. *Mar Ecol Prog Ser,* 470**,** 167-189.

GARG, S., ROSE, A. L., GODRANT, A. & WAITE, T. D. 2007. Iron uptake by the ichthyotoxic *Chattonella marina* (Raphidophyceae): impact of superoxide generation1. *J Phycol,* 43**,** 978-991.

GARG, S., ROSE, A. L. & WAITE, T. D. 2011. Photochemical production of superoxide and hydrogen peroxide from natural organic matter. *Geochim Cosmochim Acta,* 75**,** 4310-4320.

GODRANT, A., ROSE, A. L., SARTHOU, G. & WAITE, T. D. 2009. New method for the determination of extracellular production of superoxide by marine phytoplankton using the chemiluminescence probes MCLA and red-CLA. *Limnol Oceanogr: Methods,* 7**,** 682-692.

GOUGH, D. R. & COTTER, T. G. 2011. Hydrogen peroxide: a Jekyll and Hyde signalling molecule. *Cell Death Dis,* 2**,** e213.

GUILLARD, R. R. L. & HARGRAVES, P. E. 1993. Stichochrysis immobilis is a diatom, not a chrysophyte. *Phycologia,* 32**,** 234-236.

GUILLARD, R. R. L. & RYTHER, J. H. 1962. Studies of marine planktonic diatoms: i. *Cyclotella nana* hustedt, and *detonula confervacea* (cleve) gran. *Can J Microbiol,* 8**,** 229-239.

HANSARD, P. S., VERMILYEA, A. W. & VOELKER, B. M. 2010. Measurements of superoxide radical concentration and decay kinetics in the Gulf of Alaska. *Deep Sea Res Part I: Oceanogr Res Pap,* 57**,** 1111-1119.

HANSEL, C. M., BUCHWALD, C., DIAZ, J. M., OSSOLINSKI, J. E., DYHRMAN, S. T., VAN MOOY, B. A. S. & POLYVIOU, D. 2016. Dynamics of extracellular superoxide production by *Trichodesmium* colonies from the Sargasso Sea. *Limnol Oceanogr,* 61**,** 1188-1200.

HANSEL, C. M. & DIAZ, J. M. 2021. Production of extracellular reactive oxygen species by marine biota. *Ann Rev Mar Sci,* 13**,** 177-200.

HANSEL, C. M., DIAZ, J. M. & PLUMMER, S. 2019. Tight regulation of extracellular superoxide points to its vital role in the physiology of the globally relevant Roseobacter clade. *mBio,* 10**,** e02668-18.

HARVEY, E. L., BIDLE, K. D. & JOHNSON, M. D. 2015. Consequences of strain variability and calcification in Emiliania huxleyi on microzooplankton grazing. *J Plankton Res,* 37**,** 1137-1148.

HELLER, M. I. & CROOT, P. L. 2010a. Application of a superoxide (O2−) thermal source (SOTS-1) for the determination and calibration of O2− fluxes in seawater. *Analytica Chimica Acta,* 667**,** 1-13.

HELLER, M. I. & CROOT, P. L. 2010b. Kinetics of superoxide reactions with dissolved organic matter in tropical Atlantic surface waters near Cape Verde (TENATSO). *J Geophys Res,* 115**,** C12038.

HERVÉ, C., TONON, T., COLLÉN, J., CORRE, E. & BOYEN, C. 2006. NADPH oxidases in Eukaryotes: red algae provide new hints! *Curr Genet,* 49**,** 190-204.

HOPWOOD, M. J., RIEBESELL, U., ARÍSTEGUI, J., LUDWIG, A., ACHTERBERG, E. P. & HERNÁNDEZ, N. 2018. Photochemical vs. Bacterial Control of H2O2 Concentration

Across a pCO2 Gradient Mesocosm Experiment in the Subtropical North Atlantic. *Front Mar Sci*, 5.

JAKOBSEN, H. H. & STROM, S. L. 2004. Circadian cycles in growth and feeding rates of heterotrophic protist plankton. *Limnol Oceanogr,* 49**,** 1915-1922.

JESPERSEN, A. M. & CHRISTOFFERSEN, K. 1987. Measurements of chlorophyll a from phytoplankton using ethanol as extraction solvent. *Archiv fuer Hydrobiologie,* 109**,** 445-454.

JOOSTEN, V. & VAN BERKEL, W. J. 2007. Flavoenzymes. *Curr Opin Chem Biol,* 11**,** 195-202.

KIM, C. S., LEE, S. G., LEE, C. K., KIM, H. G. & JUNG, J. 1999. Reactive oxygen species as causative agents in the ichthyotoxicity of the red tide dinoflagellate *Cochlodinium polykrikoides*. *J Plankton Res,* 21**,** 2105-2115.

KIM, D., NAKAMURA, A., OKAMOTO, T., KOMATSU, N., ODA, T., IIDA, T., ISHIMATSU, A. & MURAMATSU, T. 2000. Mechanism of superoxide anion generation in the toxic red tide phytoplankton *Chattonella marina*: possible involvement of NAD(P)H oxidase. *Biochim Biophys Acta,* 1524**,** 220-7.

KIM, D., NAKASHIMA, T., MATSUYAMA, Y., NIWANO, Y., YAMAGUCHI, K. & ODA, T. 2007. Presence of the distinct systems responsible for superoxide anion and hydrogen peroxide generation in red tide phytoplankton *Chattonella marina* and *Chattonella ovata*. *J Plankton Res,* 29**,** 241-247.

KIM, D. & ODA, T. 2010. Possible Factors Responsible for the Fish-Killing Mechanisms of the Red Tide Phytoplankton, *Chattonella marina* and *Cochlodinium polykrikoides*. *Coastal Environmental and Ecosystem Issues of the East China Sea***,** 245-268.

KLEIN, R. S., SAYRE, R. M., DOWDY, J. C. & WERTH, V. P. 2009. The risk of ultraviolet radiation exposure from indoor lamps in lupus erythematosus. *Autoimmun Rev,* 8**,** 320-4.

KORSHUNOV, S. S. & IMLAY, J. A. 2002. A potential role for periplasmic superoxide dismutase in blocking the penetration of external superoxide into the cytosol of Gram-negative bacteria. *Mol Microbiol,* 43**,** 95-106.

KUSTKA, A. B., SHAKED, Y., MILLIGAN, A. J., KING, D. W. & MOREL, F. M. M. 2005. Extracellular production of superoxide by marine diatoms: Contrasting effects on iron redox chemistry and bioavailability. *Limnol Oceanogr,* 50**,** 1172-1180.

LANDRY, M. R. & HASSETT, R. P. 1982. Estimating the grazing impact of marine micro-zooplankton. *Mar Biol,* 67**,** 283-288.

LAOHAVISIT, A., ANDERSON, A., BOMBELLI, P., JACOBS, M., HOWE, C. J., DAVIES, J. M. & SMITH, A. G. 2015. Enhancing plasma membrane NADPH oxidase activity increases current output by diatoms in biophotovoltaic devices. *Algal Research-Biomass Biofuels and Bioproducts,* 12**,** 91-98.

LESSER, M. P. 2006. Oxidative stress in marine environments: biochemistry and physiological ecology. *Annu Rev Physiol,* 68**,** 253-78.

LETELIER, R. M., KARL, D. M., ABBOTT, M. R. & BIDIGARE, R. R. 2004. Light driven seasonal patterns of chlorophyll and nitrate in the lower euphotic zone of the North Pacific Subtropical Gyre. *Limnol Oceanogr,* 49**,** 508-519.

LIU, W., AU, D. W. T., ANDERSON, D. M., LAM, P. K. S. & WU, R. S. S. 2007. Effects of nutrients, salinity, pH and light:dark cycle on the production of reactive oxygen species in the alga *Chattonella marina*. *J Exp Mar Biol Ecol,* 346**,** 76-86.

LUO, Y. Y. & ROTHSTEIN, L. M. 2011. Response of the Pacific Ocean Circulation to Climate Change. *Atmos-Ocean,* 49**,** 235-244.

MACKEY, K. R. M., PAYTAN, A., GROSSMAN, A. R. & BAILEY, S. 2008. A photosynthetic strategy for coping in a high-light, low-nutrient environment. *Limnol Oceanogr,* 53**,** 900-913.

MARDONES, J. I., DORANTES-ARANDA, J. J., NICHOLS, P. D. & HALLEGRAEFF, G. M. 2015. Fish gill damage by the dinoflagellate *Alexandrium catenella* from Chilean fjords: Synergistic action of ROS and PUFA. *Harmful Algae,* 49**,** 40-49.

MARSHALL, J.-A., DE SALAS, M., ODA, T. & HALLEGRAEFF, G. 2005a. Superoxide production by marine microalgae : I. Survey of 37 species from 6 classes. *Mar Biol,* 147**,** 553-540.

MARSHALL, J.-A., DE SALAS, M., ODA, T. & HALLEGRAEFF, G. 2005b. Superoxide production by marine microalgae II. Towards understanding ecological consequences and possible functions. *Mar Biol,* 147**,** 533-540.

MARSHALL, J.-A., HOVENDEN, M., ODA, T. & HALLEGRAEFF, G. M. 2002. Photosynthesis does influence superoxide production in the ichthyotoxic alga *Chattonella marina* (Raphidophyceae). *J Plank Res,* 24**,** 1231-1236.

MARSHALL, J.-A., NICHOLS, P. D., HAMILTON, B., LEWIS, R. J. & HALLEGRAEFF, G. M. 2003. Ichthyotoxicity of *Chattonella marina* (Raphidophyceae) to damselfish (*Acanthochromis polycanthus*): the synergistic role of reactive oxygen species and free fatty acids. *Harmful Algae,* 2**,** 273-281.

MARSICO, R. M., SCHNEIDER, R. J., VOELKER, B. M., ZHANG, T., DIAZ, J. M., HANSEL, C. M. & USHIJIMA, S. 2015. Spatial and temporal variability of widespread dark production and decay of hydrogen peroxide in freshwater. *Aquat Sci,* 77**,** 523-533.

MARTEL, C. M. 2009. Conceptual bases for prey biorecognition and feeding selectivity in the microplanktonic marine phagotroph *Oxyrrhis marina*. *Microb Ecol,* 57**,** 589-97.

MCDOWELL, R. E., AMSLER, C. D., AMSLER, M. O., LI, Q. & LANCASTER, J. R. 2016. Control of grazing by light availability via light-dependent, wound-induced metabolites: The role of reactive oxygen species. *J Exp Mar Biol Ecol,* 477**,** 86-91.

MCDOWELL, R. E., AMSLER, C. D., MCCLINTOCK, J. B. & BAKER, B. J. 2014. Reactive oxygen species as a marine grazing defense: H_2O_2 and wounded *Ascoseira mirabilis* both inhibit feeding by an amphipod grazer. *J Exp Mar Biol Ecol,* 458**,** 34-38.

MIDDLEMISS, J. K., ANDERSON, A. M., STRATILO, C. W. & WEGER, H. G. 2001. Oxygen consumption associated with ferric reductase activity and iron uptake by iron-limited cells of chlorella kessleri (chlorophyceae). *J Phycol,* 37**,** 393-399.

MILLER, W. L. & KESTER, D. R. 1988. Hydrogen peroxide measurement in seawater by (p-hydroxyphenyl)acetic acid dimerization. *Anal Chem,* 60**,** 2711-2715.

MILNE, A., DAVEY, M. S., WORSFOLD, P. J., ACHTERBERG, E. P. & TAYLOR, A. R. 2009. Real-time detection of reactive oxygen species generation by marine phytoplankton using flow injection-chemiluminescence. *Limnol Oceanogr: Methods,* 7**,** 706-715.

MITTLER, R. 2017. ROS Are Good. *Trends Plant Sci,* 22**,** 11-19.

MITTLER, R., VANDERAUWERA, S., SUZUKI, N., MILLER, G., TOGNETTI, V. B., VANDEPOELE, K., GOLLERY, M., SHULAEV, V. & VAN BREUSEGEM, F. 2011. ROS signaling: the new wave? *Trends Plant Sci,* 16**,** 300-309.

MOORE, L. R., COE, A., ZINSER, E. R., SAITO, M. A., SULLIVAN, M. B., LINDELL, D., FROIS-MONIZ, K., WATERBURY, J. & CHISHOLM, S. W. 2007. Culturing the marine cyanobacterium Prochlorococcus. *Limnol Oceanogr: Methods,* 5**,** 353-362.

MORISON, F. & MENDEN-DEUER, S. 2017. Doing more with less? Balancing sampling resolution and effort in measurements of protistan growth and grazing-rates. *Limnol Oceanogr: Methods,* 15**,** 794-809.

MORRIS, J. J., JOHNSON, Z. I., SZUL, M. J., KELLER, M. & ZINSER, E. R. 2011. Dependence of the Cyanobacterium *Prochlorococcus* on Hydrogen Peroxide Scavenging Microbes for Growth at the Ocean's Surface. *PLOS ONE,* 6**,** e16805.

MORRIS, J. J., JOHNSON, Z. I., WILHELM, S. W. & ZINSER, E. R. 2016. Diel regulation of hydrogen peroxide defenses by open ocean microbial communities. *J Plankton Res,* 38**,** 1103-1114.

MORRIS, J. J., ROSE, A. L. & LU, Z. 2022. Reactive oxygen species in the world ocean and their impacts on marine ecosystems. *Redox Biol,* 52**,** 102285.

MURCHIE, E. H. & LAWSON, T. 2013. Chlorophyll fluorescence analysis: a guide to good practice and understanding some new applications. *J Exp Bot,* 64**,** 3983-98.

NG, W. H. A. & LIU, H. 2016. Diel periodicity of grazing by heterotrophic nanoflagellates influenced by prey cell properties and intrinsic grazing rhythm. *J Plankton Res,* 38**,** 636-651.

NG, W. H. A., LIU, H. & ZHANG, S. 2017. Diel variation of grazing of the dinoflagellate Lepidodinium sp. and ciliate Euplotes sp. on algal prey: the effect of prey cell properties. *J Plankton Res,* 39**,** 450-462.

NOT, F., LATASA, M., SCHAREK, R., VIPREY, M., KARLESKIND, P., BALAGUÉ, V., ONTORIA-OVIEDO, I., CUMINO, A., GOETZE, E., VAULOT, D. & MASSANA, R. 2008. Protistan assemblages across the Indian Ocean, with a specific emphasis on the picoeukaryotes. *Deep Sea Res I: Oceanogr Res Pap,* 55**,** 1456-1473.

O'DONNELL, B. V., TEW, D. G., JONES, O. T. & ENGLAND, P. J. 1993. Studies on the inhibitory mechanism of iodonium compounds with special reference to neutrophil NADPH oxidase. *Biochem J,* 290 (Pt 1)**,** 41-49.

ODA, T., ISHIMATSU, A., SHIMADA, M., TAKESHITA, S. & MURAMATSU, T. 1992. Oxygen-radical-mediated toxic effects of the red tide flagellate *Chattonella marina* on *Vibrio alginolyticus*. *Mar Biol,* 112**,** 505-509.

ODA, T., MORITOMI, J., KAWANO, I., HAMAGUCHI, S., ISHIMATSU, A. & MURAMATSU, T. 1995. Catalase- and superoxide dismutase-induced morphological changes and growth inhibition in the red tide phytoplankton *Chattonella marina*. *Biosci Biotechnol Biochem,* 59**,** 2044-2048.

ODA, T., NAKAMURA, A., OKAMOTO, T., ISHIMATSU, A. & MURAMATSU, T. 1998. Lectin-induced enhancement of superoxide anion production by red tide phytoplankton. *Mar Biol,* 131**,** 383-390.

ODA, T., NAKAMURA, A., SHIKAYAMA, M., KAWANO, I., ISHIMATSU, A. & MURAMATSU, T. 1997. Generation of reactive oxygen species by raphidophycean phytoplankton. *Biosci Biotechnol Biochem,* 61**,** 1658-62.

OMAR, N. M., PRASIL, O., MCCAIN, J. S. P. & CAMPBELL, D. A. 2022. Diffusional Interactions among Marine Phytoplankton and Bacterioplankton: Modelling H2O2 as a Case Study. *Microorganisms,* 10**,** 821.

OSHIKAWA, J., URAO, N., KIM, H. W., KAPLAN, N., RAZVI, M., MCKINNEY, R., POOLE, L. B., FUKAI, T. & USHIO-FUKAI, M. 2010. Extracellular SOD-derived H2O2 promotes VEGF signaling in caveolae/lipid rafts and post-ischemic angiogenesis in mice. *PLoS One,* 5**,** e10189.

PAASCHE, E. 2002. A review of the coccolithophorid Emiliania huxleyi (Prymnesiophyceae), with particular reference to growth, coccolith formation, and calcification-photosynthesis interactions (Phycological Reviews 20). *Phycologia,* 40**,** 503-529.

PALENIK, B., ZAFIRIOU, O. C. & MOREL, F. M. M. 1987. Hydrogen peroxide production by a marine phytoplankter1. *Limnol Oceanogr,* 32**,** 1365-1369.

PARK, S. Y., CHOI, E. S., HWANG, J., KIM, D., RYU, T. K. & LEE, T.-K. 2009. Physiological and biochemical responses of Prorocentrum minimum to high light stress. *Ocean Sci J,* 44**,** 199-204.

PLATT, T., GALLEGOS C.L., HARRISON W.G. 1980. Photoinhibition of photosynthesis in natural assemblages of marine phytoplankton. *J Mar Res,* 38**,** 687-701.

PLUMMER, S., TAYLOR, A. E., HARVEY, E. L., HANSEL, C. M. & DIAZ, J. M. 2019. Dynamic regulation of extracellular superoxide production by the coccolithophore *Emiliania huxleyi* (CCMP 374). *Front Microbiol,* 10**,** 1546.

PORTUNE, K. J., CARY, S. C. & WARNER, M. E. 2010. Antioxidant enzyme response and reactive oxygen species production in marine Raphidophytes. *J Phycol,* 46**,** 1161-1171.

POULSON-ELLESTAD, K. L., HARVEY, E. L., JOHNSON, M. D. & MINCER, T. J. 2016. Evidence for Strain-Specific Exometabolomic Responses of the Coccolithophore Emiliania huxleyi to Grazing by the Dinoflagellate Oxyrrhis marina. *Front Mar Sci,* 3.

POWERS, L. C., BABCOCK-ADAMS, L. C., ENRIGHT, J. K. & MILLER, W. L. 2015. Probing the photochemical reactivity of deep ocean refractory carbon (DORC): Lessons from hydrogen peroxide and superoxide kinetics. *Mar Chem,* 177**,** 306-317.

POWERS, L. C. & MILLER, W. L. 2016. Apparent quantum efficiency spectra for superoxide photoproduction and its formation of hydrogen peroxide in natural waters. *Front Mar Sci,* 3.

ROACH, T., NA, C. S. & KRIEGER-LISZKAY, A. 2015. High light-induced hydrogen peroxide production in *Chlamydomonas reinhardtii* is increased by high CO_2 availability. *Plant J,* 81**,** 759-66.

ROE, K. L. & BARBEAU, K. A. 2014. Uptake mechanisms for inorganic iron and ferric citrate in *Trichodesmium erythraeum* IMS101. *Metallomics,* 6**,** 2042-2051.

ROE, K. L., SCHNEIDER, R. J., HANSEL, C. M. & VOELKER, B. M. 2016. Measurement of dark, particle-generated superoxide and hydrogen peroxide production and decay in the subtropical and temperate North Pacific Ocean. *Deep Sea Res I: Oceanogr Res Pap,* 107**,** 59-69.

ROSE, A. L. 2012. The influence of extracellular superoxide on iron redox chemistry and bioavailability to aquatic microorganisms. *Front Microbiol,* 3**,** 124.

ROSE, A. L., SALMON, T. P., LUKONDEH, T., NEILAN, B. A. & WAITE, T. D. 2005. Use of Superoxide as an Electron Shuttle for Iron Acquisition by the Marine Cyanobacterium *Lyngbya majuscula*. *Environ Sci Technol,* 39**,** 3708-3715.

ROSE, A. L., WEBB, E. A., WAITE, T. D. & MOFFETT, J. W. 2008. Measurement and implications of nonphotochemically generated superoxide in the equatorial Pacific Ocean. *Environ Sci Technol,* 42**,** 2387-93.

ROSSI, D. C. P., GLEASON, J. E., SANCHEZ, H., SCHATZMAN, S. S., CULBERTSON, E. M., JOHNSON, C. J., MCNEES, C. A., COELHO, C., NETT, J. E., ANDES, D. R., CORMACK, B. P. & CULOTTA, V. C. 2017. *Candida albicans* FRE8 encodes a member of the NADPH oxidase family that produces a burst of ROS during fungal morphogenesis. *PLoS Pathog,* 13**,** e1006763.

SARAGOSTI, E., TCHERNOV, D., KATSIR, A. & SHAKED, Y. 2010. Extracellular production and degradation of superoxide in the coral *Stylophora pistillata* and cultured *Symbiodinium*. *PLoS One,* 5**,** e12508.

SARAN, M. 2003. To what end does nature produce superoxide? NADPH oxidase as an autocrine modifier of membrane phospholipids generating paracrine lipid messengers. *Free Radic Res,* 37**,** 1045-59.

SCHAREK, R., LATASA, M., KARL, D. M. & BIDIGARE, R. R. 1999. Temporal variations in diatom abundance and downward vertical flux in the oligotrophic North Pacific gyre. *Deep-Sea Res I: Oceanogr Res Pap,* 46**,** 1051-1075.

SCHNEIDER, R. J., ROE, K. L., HANSEL, C. M. & VOELKER, B. M. 2016. Species-level variability in extracellular production rates of reactive oxygen species by diatoms. *Front Chem,* 4**,** 5.

SHAPIGUZOV, A., VAINONEN, J., WRZACZEK, M. & KANGASJÄRVI, J. 2012. ROS-talk – how the apoplast, the chloroplast, and the nucleus get the message through. *Front Plant Sci,* 3.

SICILIANO, S. D., O'DRISCOLL, N. J. & LEAN, D. R. 2002. Microbial reduction and oxidation of mercury in freshwater lakes. *Environ Sci Technol,* 36**,** 3064-8.

SIES, H. & JONES, D. P. 2020. Reactive oxygen species (ROS) as pleiotropic physiological signalling agents. *Nat Rev Mol Cell Biol,* 21**,** 363-383.

STRICKLAND, J. D. H., PARSONS, T.R. 1972. *A Practical Handbook of Seawater Analysis,* Ottawa, ON, Fisheries Research Board of Canada.

STROM, S., WOLFE, G., HOLMES, J., STECHER, H., SHIMENECK, C., LAMBERT, S. & MORENO, E. 2003. Chemical defense in the microplankton I: Feeding and growth rates of heterotrophic protists on the DMS-producing phytoplankter Emiliania huxleyi. *Limnol Oceanogr,* 48**,** 217-229.

STROM, S. L. & BRIGHT, K. J. 2009. Inter-strain differences in nitrogen use by the coccolithophore Emiliania huxleyi, and consequences for predation by a planktonic ciliate. *Harmful Algae,* 8**,** 811-816.

SUGGETT, D. J., LE FLOC'H, E., HARRIS, G. N., LEONARDOS, N. & GEIDER, R. J. 2007. Different strategies of photoacclimation by two strains ofEmiliania huxleyi(Haptophyta)1. *J Phycol,* 43**,** 1209-1222.

SUNDA, W. G. & HARDISON, D. R. 2010. Evolutionary tradeoffs among nutrient acquisition, cell size, and grazing defense in marine phytoplankton promote ecosystem stability. *Mar Ecol Prog,* 401**,** 63-76.

SUTHERLAND, K. M., COE, A., GAST, R. J., PLUMMER, S., SUFFRIDGE, C. P., DIAZ, J. M., BOWMAN, J. S., WANKEL, S. D. & HANSEL, C. M. 2019. Extracellular superoxide production by key microbes in the global ocean. *Limnol Oceanogr,* 64**,** 2679-2693.

SUTHERLAND, K. M., WANKEL, S. D. & HANSEL, C. M. 2020. Dark biological superoxide production as a significant flux and sink of marine dissolved oxygen. *Proc Natl Acad Sci USA,* 117**,** 3433-3439.

TANAKA, K., YOSHIMATSU, S. & SHIMADA, M. 1992. Generation of superoxide anions by *Chattonella antiqua*: Possible causes for fish death caused by 'Red Tide'. *Experientia,* 48**,** 888-890.

VARDI, A., HARAMATY, L., VAN MOOY, B. A., FREDRICKS, H. F., KIMMANCE, S. A., LARSEN, A. & BIDLE, K. D. 2012. Host-virus dynamics and subcellular controls of cell fate in a natural coccolithophore population. *Proc Natl Acad Sci USA,* 109**,** 19327-32.

VERMILYEA, A. W., DIXON, T. C. & VOELKER, B. M. 2010a. Use of $H_2{}^{18}O_2$ to measure absolute rates of dark H_2O_2 production in freshwater systems. *Environ Sci Technol,* 44**,** 3066-3072.

VERMILYEA, A. W., HANSARD, S. P. & VOELKER, B. M. 2010b. Dark production of hydrogen peroxide in the Gulf of Alaska. *Limnol Oceanogr,* 55**,** 580-588.

WATERBURY, J. B. 1987. Biological and ecological characterization of the marine unicellular Cyanobacterium Synechococcus. *Photosynthetic picoplankton Canadian Bulletin of Fisheries Aquatic Sciences,* 214**,** 71-120.

WEINBERGER, F. 2007. Pathogen-induced defense and innate immunity in macroalgae. *Biol Bull,* 213**,** 290-302.

WESTBROEK, P., YOUNG, J. R. & LINSCHOOTEN, K. 1989. Coccolith Production (Biomineralization) in the Marine Alga *Emiliania huxleyi*. *J Protozool,* 36**,** 368-373.

WOOTTON, E. C., ZUBKOV, M. V., JONES, D. H., JONES, R. H., MARTEL, C. M., THORNTON, C. A. & ROBERTS, E. C. 2007. Biochemical prey recognition by planktonic protozoa. *Environ Microbiol,* 9**,** 216-22.

WU, S., HUANG, A., ZHANG, B., HUAN, L., ZHAO, P., LIN, A. & WANG, G. 2015. Enzyme activity highlights the importance of the oxidative pentose phosphate pathway in lipid accumulation and growth of Phaeodactylum tricornutum under CO_2 concentration. *Biotechnol Biofuels,* 8**,** 78.

WUTTIG, K., HELLER, M. I. & CROOT, P. L. 2013. Reactivity of inorganic Mn and Mn desferrioxamine B with O_2, $O_2(^-)$, and H_2O_2 in seawater. *Environ Sci Technol,* 47**,** 10257-65.

YANG, C. Z., ALBRIGHT, L. J. & YOUSIF, A. N. 1995. Oxygen-Radical-Mediated Effects of the Toxic Phytoplankter Heterosigma-Carterae on Juvenile Rainbow-Trout Oncorhynchus-Mykiss. *Dis Aquat Org,* 23**,** 101-108.

YUASA, K., SHIKATA, T., KITATSUJI, S., YAMASAKI, Y. & NISHIYAMA, Y. 2020a. Extracellular secretion of superoxide is regulated by photosynthetic electron transport in the noxious red-tide-forming raphidophyte Chattonella antiqua. *J Photochem Photobiol B: Biol,* 205**,** 111839.

YUASA, K., SHIKATA, T., ICHIKAWA, T., TAMURA, Y. & NISHIYAMA, Y. 2020b. Nutrient deficiency stimulates the production of superoxide in the noxious red-tide-forming raphidophyte Chattonella antiqua. *Harmful Algae,* 99**,** 101938.

ZHANG, T., DIAZ, J. M., BRIGHI, C., PARSONS, R. J., MCNALLY, S., APPRILL, A. & HANSEL, C. M. 2016a. Dark Production of Extracellular Superoxide by the Coral *Porites astreoides* and Representative Symbionts. *Front Mar Sci,* 3.

ZHANG, T., HANSEL, C. M., VOELKER, B. M. & LAMBORG, C. H. 2016b. Extensive dark biological production of reactive oxygen species in brackish and freshwater ponds. *Environ Sci Technol,* 50**,** 2983-93.

ZINSER, E. R. 2018. The microbial contribution to reactive oxygen species dynamics in marine ecosystems. *Environ Microbiol Rep,* 10**,** 412-427.

ŽUNIĆ, J., HIROTA, K. & ROSIN, P. L. 2010. A Hu moment invariant as a shape circularity measure. *Pattern Recognit,* 43**,** 47-57.